ADMEt Evaluation of Anti-tuberculosis Compounds and New Methodologies Development

BY

Yang Song
B.S., China Pharmaceutical University, China, 2003
M.S., Peking Union Medical College, China, 2006

DISSERTATION

Submitted as partial fulfillment of the requirements
for the degree of Doctor of Philosophy in Pharmacognosy
in the Graduate College of the
University of Illinois at Chicago, 2011

Chicago, Illinois

Defense Committee:

Scott G. Franzblau, Chair and Advisor

Richard van Breemen, Co-Advisor

Larry Klein

Larry Danziger, Pharmacy Practice

Hyun-Young Jeong, Pharmacy Practice

This dissertation is dedicated to my husband Yang Tian and my parents for their consistent support for my studies.

ACKNOWLEDGEMENTS

I first and foremost would like to thank my advisor, Dr. Scott G. Franzblau and Dr. Richard van Breemen for being wonderful mentors. Dr. Franzblau has provided guidance throughout my entire graduate career and has been always available and helpful in discussing experiments and in providing new stimulating ideas on how to pursue my research. Dr. van Breemen is always there coaching and polishing my skills on mass spectrometry and drug metabolism study. I would also like to acknowledge my committee members Dr. Larry Klein, Dr. Hyun-Young Jeong, and Dr. Larry Denziger for all the kind advices during the preliminary examination and in writing the dissertation. Special thanks to Dr. Hyun-Young Jeong for supervision on HepaRG cell related research. Special thanks to Dr. Kuan-wei Peng and Nan Zhang for helping in all aspects of my experiments. They have been a great help during the difficult times while working on the TB related experiments.

I would also like to acknowledge all the present and past members of Institute for Tuberculosis Research, for providing each day an incredibly fun environment. In particular, I am grateful to Dr. Larry Klein, for being always available and patient in discussing experiments, and for being a dear friend during these years. Also, I would like to thank Dr. Yuehong Wang and Baojie Wan who have been my lab mates since the beginning and with whom I shared “joys and griefs” during the entire graduate school; Changhua Hwang, Valentina Petukhova, Yeun Kim, Minjee Kim, Geping Cai, Wei Gao, Hiten Gutka for making the lab work a wonderful experience, for being always available in helping out with experiments.

ACKNOWLEDGEMENTS (continued)

This work was funded by grants from the TB Alliance.

YS

TABLE OF CONTENTS

CHAPTER PAGE

1. INTRODUCTION....1
   1.1. Introduction to *Mycobacterium tuberculosis* 1
   1.2. Global urgencies of discovering new drugs for TB treatment....2
   1.3. Liability of current anti-TB drugs informs the discovery strategies for 'next generation' anti-TB drugs 3
   1.4. Optimization of ADMEt properties is essential for the discovery of 'next generation' anti-TB drugs 4
      1.4.1. Overview of our understanding of the metabolism of existing anti-TB drugs 5
      1.4.2. Overview of known active/toxic metabolites of existing anti-TB drugs 7
      1.4.3. Current drug metabolism studies on established anti-TB drugs....9
      1.4.4. Drug metabolism and pharmacokinetics of lead compounds in internal anti-TB drug discovery programs....11
   1.5. Methods in drug metabolism and pharmacokinetics as applied to anti-TB lead discovery and optimization....13
      1.5.1. Metabolic stability 13
      1.5.2. Structure determination of drug metabolites 13
      1.5.3. Plasma protein binding 14
      1.5.4. CYP P450 inhibition assay....14
      1.5.5. CYP P450 induction assay 15
   1.6. In vitro bioassays for the measurement of anti-TB activity of test compounds....16
   1.7. Objective and overall research strategies 18

2. MATERIALS AND METHODS (ADMEt ASSAY)....22
   2.1. Chemicals and biological matrices 22
   2.2. Metabolic stability assay 22
   2.3. Protein binding 25
   2.4. Plasma stability 26
   2.5. Gastric fluid stability 27
   2.6. Simultaneous quantitation of metabolites of multiple cytochrome P450 substrates 29

TABLE OF CONTENTS (continued)

CHAPTER PAGE

2.7. Cytochrome P450 inhibition assay 30
2.8. Cytochrome P450 induction assay 32
2.9. Multiplex toxicity assay 36
2.10. Metabolite toxicity assay using HepaRG cells 38

3. DRUG METABOLISM AND ANALYTICAL STUDY OF ESTABLISHED ANTI-TB DRUGS 40
3.1. Introduction 40
3.2. Materials and methods 42
3.2.1. Chemicals and biological matrices 42
3.2.2. Instrumentation 42
3.2.3. Standard solutions 42
3.2.4. Sample preparation procedures 44
3.2.5. Liquid chromatography 44
3.2.6. Mass spectrometry 45
3.2.7. Method validation 45
3.2.7.1. Accuracy, precision, lower limit of detection, lower limit of quantitation 46
3.2.7.2. Recovery and matrix effects 46
3.2.7.3. Linearity and selectivity 47
3.2.7.4. Stability evaluation 47
3.2.8. Metabolite identification of LL3858 48
3.3. Results 50
3.3.1. Chromatography of 15 established and experimental drugs in human plasma 50
3.3.2. Method validation 50
3.3.3. Metabolic stability of established and experimental anti-TB drugs 54
3.3.4. Metabolite identification of LL3858 55
3.4. Discussion 64

4. METABOLISM-GUIDED HIT-TO-LEAD OPTIMIZATION IN ANTI-TB DRUG DISCOVERY 67
4.1. Introduction 67
4.2. Materials and methods 69
4.2.1. Chemicals and reagents. 69
4.2.2. MABA 69

TABLE OF CONTENTS (continued)

CHAPTER PAGE

4.2.3. LORA....70
4.2.4. Cytotoxicity Assay....70
4.2.5. Macrophages and culture conditions....71
4.2.6. Time dependent and concentration dependent killing assay....72
4.2.7. Determination of MIC for single-drug-resistant strains of *M. tuberculosis*....72
4.2.8. Mutation frequency....73
4.2.9. Dosing and in vivo sample collection....73
4.2.10. Pharmacokinetics of compound XIII....74
4.2.11. Metabolite identification of compound 1....74
4.2.12. LC-MS-MS quantitation of isoxazole series....75
4.2.13. Metabolite characterization of compound I from tetrahydroindazole series....76
4.2.14. LC-MS-MS method for quantitation of tetrahydroindzole series....77
4.3. Drug metabolism-guided hit-to-lead optimization of isoxazole series....79
4.3.1. Metabolism of compound 1....82
4.3.2. Major metabolites of compound 1....83
4.3.3. Metabolite activity and toxicity....87
4.3.4. Selecting lead compounds based on metabolism profiles....87
4.3.5. Metabolism study of compound 8a....88
4.3.6. Time dependent and concentration dependent killing effects of compound 8a....89
4.3.7. Pharmacokinetics of compound 8a in mice....90
4.3.8. Biological profiling of compound 8a....92
4.3.8.1. Confirmation of intracellular concentration of compound 8a....92
4.3.8.2. Mutation frequency of compound 8a....93
4.3.9. In vivo efficacy of compound 8a....93
4.3.10. Discussion....95
4.4. Tetrahydroindazole series....97
4.4.1. Metabolism of compound I....98
4.4.2. Metabolite identification of compound I....98
4.4.3. Anti-TB activity of M1....102

TABLE OF CONTENTS (continued)

CHAPTER PAGE

4.4.4. Metabolism of synthesized analogs 102
4.4.5. Pharmacokinetics of compound XIII 104
4.4.6. Intracellular anti-TB activity determination of compound XIII (by DR. Yuehong Wang) 105
4.4.7. Activity of compound XIII against single-drug-resistant strains of *M. tuberculosis* and against non-mycobacteria (by Dr. Sanghyun Cho) 106
4.5. Discussion 108

5. HARNESSING HepaRG CELLS FOR CYTOCHROME P450 INDUCTION STUDIES 109
5.1. Introduction 109
5.2. Materials and methods 111
5.2.1. Chemicals and reagents. 111
5.2.2. Culturing of HepaRG cells in customized medium for induction study 111
5.2.3. Establish methods to evaluate CYP activity and expression in HepaRG cells 112
5.2.3.1. Functional assay 113
5.2.3.2. RT-qPCR method 113
5.2.4. Time course of cytochrome P450 induction by rifampin 114
5.2.5. Method to assess effect of medium composition on CYP activity 115
5.2.6. Medium composition effect on CYP induction potential by rifampin 115
5.2.7. Effect of DMSO on CYP induction 115
5.2.8. Assay validation using benchmark inducers 116
5.3. Results 117
5.3.1. Effects of DMSO on CYP expression 117
5.3.2. Effect of DMSO on CYP induction 118
5.3.3. Kinetics of CYP P450 induction by rifampin 121
5.3.4. Optimization of culture medium for maximum CYP P450 expression. 122

TABLE OF CONTENTS (continued)

CHAPTER PAGE

5.3.4.1. Effects of hydrocortisone on CYP P450 expression 123
5.3.4.2. Effects of hydrocortisone on induction potential 124
5.3.4.3. Effects of human insulin on CYP P450 expression 125
5.3.4.4. Effects of insulin on induction potential 127
5.3.4.5. Effect of FCS concentration on CYP expression 127
5.3.4.6. Effect of FCS on CYP induction potential 128
5.3.5. Optimized culture medium for CYP induction assay using HepaRG cells 128
5.3.6. Induction assay validation by benchmark inducers 129
5.3.7. Concentration-dependent induction of CYPs by rifampin in DMSO-free medium 133
5.4. Discussion 134

6. DEVELOPMENT OF ACTIVE METABOLITE-BASED BIOASSAY SYSTEM TO STUDY ANTI-TB ACTIVITY OF COMPOUND METABOLITE 137
6.1. Introduction 137
6.1.1. Deficiencies in contemporary drug discovery algorithms 138
6.1.2. Importance of pharmacologically active metabolite(s) 139
6.1.3. Novelty of this approach 140
6.2. Materials and methods 141
6.2.1. Materials 141
6.2.2. Interference of Microsomes and NADPH on MABA 141
6.2.3. Microsome and NADPH effects on *M. tuberculosis* growth 141
6.2.4. Eliminating interference from microsomes and NADPH in the assay 142
6.3. Results 143
6.3.1. Interference of Microsome and NADPH on MABA 143
6.3.2. Effects of microsome and NADPH on the growth of *M. tuberculosis* 144
6.3.3. A pilot experiment with metabolically stable and unstable compounds 145
6.4. Discussion 149

TABLE OF CONTENTS (continued)

CHAPTER PAGE

6.4.1. Searching for control compounds with active metabolites to validate the assay 149
6.4.2. Eliminating interference from microsomes and NADPH 151
6.4.3. Development of HTS assay to identify prodrugs (Type 4 compounds) 151

CITED LITERATURE 153

VITA 161

LIST OF TABLES

TABLE		PAGE
TABLE I.	ESTABLISHED ANTI-TB DRUGS WITH ACTIVE OR TOXIC METABOLITES*	8
TABLE II.	SRM TRANSITIONS AND LOQ OF METABOLITES	30
TABLE III.	TOXIC COMPOUNDS AND RESPECTIVE MECHANISMS USED FOR ASSAY VALIDATION.	38
TABLE IV.	CC_{50} OF TOXIC COMPOUNDS IN THE MULTIPLEX ASSAY.	38
TABLE V.	SRM TRANSITION TABLE OF ANTI-TB DRUGS AND INTERNAL STANDARDS	45
TABLE VI.	LINEAR RANGE, LOQ, LOD, ACCURACY, INTERDAY/INTRADAY PRECISION, MATRIX EFFECT AND RECOVERY OF THE ESTABLISHED AND EXPERIMENTAL ANTI-TB DRUGS*	52
TABLE VII.	RECOVERY, MATRIX EFFECT, LONG TERM, FREEZE & THAW, ROOM TEMPERATURE, STOCK SOLUTION STABILITY OF ESTABLISHED AND EXPERIMENTAL ANTI-TB DRUGS	53
TABLE VIII.	LIVER MICROSOME METABOLIC STABILITY OF THE ESTABLISHED AND EXPERIMENTAL ANTI-TB DRUGS	54
TABLE IX.	METABOLIC STABILITY AND MABA MIC VALUES FOR HITS OBTAINED FROM A HTS OF AN ASINEX DIVERSE LIBRARY	68
TABLE X.	SRMS AND RETENTION TIMES OF COMPOUNDS 1, 6o, 8a	75
TABLE XI.	SRMS AND RETENTION TIMES OF COMPOUND 6g	76
TABLE XII.	SELECTED REACTION MONITORING (SRM TRANSITIONS) AND RETENTION TIMES OF ANALOGS	78
TABLE XIII.	IN VITRO ACTIVITY (μM) OF ISOXAZOLE ANALOGS – ARYL MODIFICATIONS*	80
TABLE XIV.	IN VITRO ACTIVITY (μM) OF ISOXAZOLE ANALOGS – AMINE MODIFICATIONS*	81
TABLE XV.	METABOLIC STABILITY PARAMETERS OF COMPOUND 1 IN MOUSE	

LIST OF TABLES (continued)

TABLE		PAGE
	MICROSOMES	83
TABLE XVI.	ACCURATE MASS OF COMP.1, M1, AND M2	84
TABLE XVII.	METABOLIC STABILITY PARAMETERS OF COMPOUND 8a IN MOUSE AND HUMAN MICROSOMES.	89
TABLE XVIII.	PHARMACOKINETIC PARAMETERS OF COMPOUND 8a IN MICE.	92
TABLE XIX.	METABOLIC STABILITY PARAMETERS OF COMPOUND I IN MOUSE MICROSOMES.	98
TABLE XX.	METABOLIC STABILITY AND IN VITRO ANTI-TB ACTIVITY OF TETRAHYDROINDAZOLE SERIES.	103
TABLE XXI.	PHARMACOKINETIC PARAMETERS OF COMPOUND XIII AT A DOSAGE OF 100MG/KG*	105
TABLE XXII.	COMPARATIVE MICS (μM) OF COMPOUND XIII *	107
TABLE XXIII.	MIC (μM) OF COMPOUND XIII AGAINST *M. TUBERCULOSIS* STRAINS RESISTANT TO SINGLE TB DRUGS*	107
TABLE XXIV.	PRIMER PAIRS FOR EACH TRANSCRIPT.	114
TABLE XXV.	HYDROCORTISONE CONCENTRATION-DEPENDENCE OF CYP ENZYME INDUCTION IN HEPARG CELLS.	125
TABLE XXVI.	EFFECT OF INSULIN CONCENTRATION ON INDUCTION OF CYP ENZYMES IN HepaRG CELLS.	127
TABLE XXVII.	EFFECT OF FCS CONCENTRATION ON CYP ACTIVITY OF HepaRG CELLS	128
TABLE XXVIII.	EFFECT OF FCS CONCENTRATION ON INDUCTION OF CYP ENZYMES IN HepaRG CELLS	128
TABLE XXIX.	CLINICAL AND EXPERIMENTAL ANTI-TB DRUGS WITH KNOWN OR SUSPECTED ACTIVE METABOLITES.	140
TABLE XXX.	ANTI-INFECTIVE DRUGS TESTED AND THEIR METABOLITE(S)	149

LIST OF FIGURES

FIGURE		PAGE
Figure 1.	Structures of existing anti-TB drugs and experimental drugs in clinical trials.	7
Figure 2.	Simulated metabolic stability of compounds.	24
Figure 3.	Plasma stability of disulfiram after 3hr incubation.	27
Figure 4.	Experimental design of gastric fluid stability assay.	28
Figure 5.	Simulated gastric fluid stability of clarithromycin (A) and erythromycin (B).	29
Figure 6.	Chromatography of metabolites of eight CYP substrates and internal standard phenacetin.	30
Figure 7.	Validation of cytochrome P450 inhibition assay.	32
Figure 8.	A flow chart showing the culture of HepaRG cells in commercial medium.	34
Figure 9.	Validation of induction assay in commercial medium by rifampin and phenobarbital.	35
Figure 10.	Experimental design of the multiplex toxicity assay.	37
Figure 11.	Comparative cytotoxicity dose-response of aflatoxin B1 in HepaRG and HepG2 cells.	39
Figure 12.	LC/positive ion electrospray total ion chromatrography of fifteen TB established ,experimental drugs and internal standards.	50
Figure 13.	Summary of proposed hydroxylation metabolites structures of LL3858.	55
Figure 14.	Spectrum of in-source fragmentation of LL3858.	56
Figure 15.	Major hydroxylation metabolites of LL3858 in human microsomes.	57
Figure 16.	Fragmentation pattern of in-source fragments m/z 290 and 231	58
Figure 17.	Tandem mass spectrometry of m/z 231 ion and 247 ions from LL3858 and M1.	60
Figure 18.	Tandem mass spectrometry of m/z 290 ion and 306 ion from LL3858 and M2, M3, M4.	62

LIST OF FIGURES (continued)

FIGURE		PAGE
Figure 19.	Scheme of metabolism-guided hit-to-lead optimization.	69
Figure 20.	Structure of compound 1.	79
Figure 21.	*In vitro* metabolism of compound 1 by mouse liver microsomes.	83
Figure 22.	LC-MS chromatograms for the positive ion electrospray LC-MS analysis of metabolites of compound 1	84
Figure 23.	Tandem mass spectram of compound 1 (A) and M1 (B) under collision energy of 50eV.	85
Figure 24.	The fragmentation pathway of compound 1.	86
Figure 25.	Time dependent and concentration dependent killing of *M. tuberculosis* by compound 8a.	90
Figure 26.	Pharmacokinetics of compound 8a in mice at 75mg/kg po (BID, second dose at 8 hours).	91
Figure 27.	Lung tissue concentration of compound 8a at 16 hours after the second daily dose.	92
Figure 28.	Compound 8a versus *M. tuberculosis* in J775A.1 macrophages.	93
Figure 29.	Compound 1 *vs. M. tuberculosis* Erdman in Balb/c mice	94
Figure 30.	Compound 8a *vs M.tuberculosis* Erdman in Balb/c mice	95
Figure 31.	Structure of lead compound I.	97
Figure 32.	LC-MS chromatograms for the positive ion electrospray LC-MS analysis of metabolites of compound I.	100
Figure 33.	Positive ion electrospray tandem mass spectra of the key fragment ions of compound I (A) and M1 (B).	101
Figure 34.	Fragmentation pattern of compound I.	102
Figure 35.	Plasma concentrations of compound XIII in Balb/c mice following a single oral dose of 100mg/kg	104

LIST OF FIGURES (continued)

FIGURE PAGE

Figure 36. Compound XIII versus *M. tuberculosis* in J774.2 macrophages. 106

Figure 37. Cell culture of HepaRG cells in customized medium..... 112

Figure 38. Effects of DMSO on CYP P450 activity of HepaRG cells..... 118

Figure 39. The induction potential of three inducers on CYP enzymes of HepaRG cells in the presence and absence of 1% DMSO. 120

Figure 40. Time course of CYP P450 induction by rifampin using HepaRG cell model..... 122

Figure 41. Effects of hydrocortisone on CYP P450 activity of HepaRG cells. 124

Figure 42. Effects of insulin concentration on CYP activity of HepaRG cells. 126

Figure 43. CYP induction by multiple inducers using functional assay readouts..... 131

Figure 44. CYP induction by multiple inducers using mRNA readout..... 132

Figure 45. Rifampin concentration-dependent induction on CYP3A4 in HepaRG cells grown in customized DMSO-free medium..... 133

Figure 46. Four types of compounds with metabolites. 138

Figure 47. Optimization of TAMA 143

Figure 48. Interference of microsome (A) and NADPH (B) on MABA readout. 144

Figure 49. Effect of liver microsomes and NADPH on *M. tuberculosis* growth/viability as determined by cfu. 145

Figure 50. Work flow of pilot experiments..... 147

Figure 51. Comparison of bacterial growth inhibition effects of PA824, ITR306 between reaction and control groups. 147

Figure 52. Candidate Type 3 or Type 4 controls and their metabolites..... 149

Figure 53. Projected data scheme of TAMA..... 152

LIST OF ABBREVIATIONS

3-MC	3-methylcholanthrene
AcHZ	acetylhydrazine
ADMEt	adsorption, deposition, metabolism, excretion, and toxicity
AhR	aryl hydrocarbon receptor
AK	adenylate kinase
ATCC	American Type Culture Collection
AUC	area under the curve
AUC	area under curve
CAR	constitutive androstane receptor
CC_{50}	cytotoxicity concentration 50
CCCP	carbonylcyanide-3-chlorophenylhydrazone
CFU	colony forming unit
CITCO	6-(4-chlorophenyl)imidazo[2,1-b][1,3]thiazole-5-carbaldehyde O-(3,4-dichlorobenzyl)oxime
CL'_{int}	intrinsic clearance
CL_h	hepatic plasma clearance
CTG	Celltiter Glo
CYP	cytochrome
DETC	diethyldithiocarbamate

LIST OF ABBREVIATIONS (continued)

DMEM	Dulbecco's Modified Eagle Medium
DMPK	drug metabolism and pharmacokinetics
DMTD	detection of multiple TB drugs
DOTS	directly Observed Treatment, Short-course
FCS	fetal calf serum
FDA	Food and drug administration
FTICR	fourier transform ion cyclotron resonance
GFPMA	green fluorescent protein microplate assay
GST	glutathiontransferase
HTS	high throughput screening
HTS	high-throughput screening
HZ	hydrazine
IC_{50}	half maximal inhibitory concentration
LC-MS	liquid chromatography mass spectrometry
LC-MS-MS	liquid chromatography/tandem mass spectrometry
LOD	limit of detection
LOQ	limit of quantitation
LORA	low oxygen recovery assay
MABA	microplate Alamar Blue assay
MABA	microtiter plate alamar blue assay

LIST OF ABBREVIATIONS (continued)

MDR-TB	multidrug-resistant tuberculosis
MGS	metabolite generation system
MIC	minimum inhibitory concentration
NAT	N-acetyltransferase
NMR	Nuclear magnetic resonance
PAS	p-aminosalicylic acid
PDTC	pyrrolidine dithiocarbamat
PXR	pregnane X receptor
QC	quality Control
$Q_{p,h}$	hepatic plasma clearance
RED	rapid equilibrium dialysis
RT-qPCR	reverse transcriptase-quanitative PCR
SAR	structure activity relationship
SAR	structure-activity relationships
SI	selectivity index
SIF	simulated gastric fluid
SRM	single reaction monitoring
$T_{1/2}$	half life
TAMA	TB active metabolite assay
TB	tuberculosis

USP	United States Pharmacopeia
XDR-TB	extensively drug-resistant tuberculosis

SUMMARY

Tuberculosis (TB) is among the top three life-threatening infectious diseases in developing countries. The treatment program recommended by the WHO, Directly Observed Treatment, Short-course (DOTS), relies upon a multiple drug regimen that requires frequent dosing over six months. This often results in patient noncompliance, which may result in treatment failure and the emergence of resistant strains. With the emergence of multidrug-resistant tuberculosis (MDR-TB) and extensively drug-resistant tuberculosis (XDR-TB), effective new therapeutic agents against all forms of this disease are critically important for global healthcare. Therefore, there is a great need to discover and develop novel anti-TB drugs.

The discovery and development of 'next-generation' anti-TB drugs should focus on overcoming the drawbacks of existing TB drugs. While a novel mechanism of action is required to effectively treat existing resistant strains, future anti-TB drugs should also have better adsorption, distribution, metabolism, excretion, and toxicity (ADMEt) properties than those of existing drugs. An ideal new anti-TB drug should have a long half-life in the patient's body to simplify dosing, which should increase patient compliance and suppress the emergence of resistance strains. Minimum induction and inhibition of human liver enzymes would avoid unfavorable interactions with other drugs such as antiviral agents, and a reduction in side effects and toxicity, even after a long period of usage, would reduce the negative side effects that continue to result from current TB drug regimens. Overcoming these challenges requires extensive and

thorough optimization of ADMEt properties in the discovery and development of any new anti-TB drugs, especially at the early discovery stage.

The current dissertation research focused on overcoming three of the challenges mentioned above: drug metabolism, induction of liver enzymes, and toxicity. Drug metabolism assays were used to study existing anti-TB drugs and to extend the half-life of experimental anti-TB compounds in internal drug discovery projects. A new cell model using HepaRG cells was developed and validated to study the induction potential of an experimental compound on liver enzymes. A multiplexed cytotoxicity assay was developed and validated with HepG2 cells to monitor three toxicity markers from the same culture. Finally, research was initiated to develop a novel TB active metabolite assay (TAMA) for monitoring the anti-TB activity of drug metabolites without the need for structural identification and synthesis.

Initial work involved the establishment of a panel of ADMEt assays. This panel assessed microsome stability, protein binding, plasma stability, gastric acid stability, cytochrome (CYP) P450 inhibition and induction, multiplexed cytotoxicity using HepG2 cells and metabolite toxicity using HepaRG cells. All of the assays were developed and validated in 96-well format in order to increase the throughput.

Of particular interest was the development and validation of a LC-MS-based quantitation method to detect eight CYP P450 substrates (based on FDA guidelines) for eight CYP P450 enzymes simultaneously in one run. This quantitation method was

used in a liver microsome-based assay to measure CYP P450 inhibition, and in a HepaRG cell-based assay to measure CYP P450 induction. The simultaneous detection of eight substrates greatly increased the throughput of those assays.

This panel of ADMEt assays was then applied to retrospective drug metabolism studies on existing anti-TB drugs. A bio-analytical method to detect TB drugs was developed and validated, which could simultaneously quantitate 15 existing anti-TB drugs from human serum plasma samples in one run. The method was given a name of 'detection of multiple TB drugs' (DMTD). The development and validation of DMTD followed FDA guidelines and appeared to be the first bio-analytical method that could detect more than 10 drugs in one run for anti-tuberculosis drugs. Compared with a previously reported method, which could simultaneously quantitate four anti-TB drugs in one run, DMTD gave an equal, or up to 10-fold lower, limit of quantitation (LOQ). Therefore, DMTD offered higher throughput and greater sensitivity than the previously published method.

DMTD can be applied in pharmacokinetics and drug-drug interaction studies of a majority of existing anti-TB drugs. It has potential applications in both the pharmaceutical industry and in hospital clinical laboratories. However, the instability of ethionamide and OPC-67683 at room temperature, -20 °C, or following three freeze-thaw cycles might limit application of this bio-analytical method in the quantitation of these two drugs, especially when plasma samples require long distance transportation

and/or long-term storage. Further experiments are required to test additional stabilizing reagents in plasma to stabilize those two drugs.

DMTD was then applied in the assessment of the in vitro stability for all 15 established and experimental anti-TB drugs in both mouse and human microsomes. Five drugs were relatively unstable in both mouse and human microsomes; four of those drugs had previously been reported to be metabolically unstable and to have active metabolites. An extensive literature search failed to reveal any reports of metabolic stability for LL3858, which is in Phase I clinical trial for the treatment of TB. The experimental data, however, showed that LL3858 was metabolically unstable, and its metabolites were identified. This lays the groundwork for improving the drug-like properties of this series including the determination of the anti-TB activity of the (synthesized) metabolites.

Metabolic studies were used to guide 'hit-to-lead' optimization of two anti-TB series emanating from high-throughput screening (HTS) of a parallel synthetic library for growth inhibition of *M. tuberculosis*. The first series of compounds contained an isoxazole ring core structure. Since the original screening hit had a half-life of only 1.5 minutes in mouse microsomes, subsequent chemical modifications were directed toward both enhanced anti-TB activity and metabolic stability. Two major metabolites were identified in mouse liver microsome incubations, leading to identification of the metabolic "soft-spots". Through iterative, metabolism-guided, chemical modification, a

lead compound was discovered that exhibited excellent anti-TB activity at sub-micromolar concentrations, with a 10-fold increase in in-vitro metabolic stability. Further pharmacokinetic studies of this lead compound in mice ultimately led to an optimized dosing regimen in the mouse model for TB.

The second series was based on a tetrahydroindazole template with a low micromolar minimum inhibitory concentration (MIC). Similar compounds have been previously reported to have promising anti-TB activity but to be relatively unstable in liver microsomes. However, the metabolites of this type of compound have yet to be identified. Through metabolite identification, the tert-butyl group of tetrahydroindazole was identified as the major metabolism site for hydroxylation. The metabolites were then synthesized but showed little anti-TB activity. Guided by microsomal stability data, a series of compounds were designed to block the metabolism site. A new lead compound, with a trifluoromethoxy group replacing the tert-butyl group, showed the best drug-like profile among all analogs synthesized with a 5-fold increase in microsomal stability, and similar anti-TB activity to the original screening hit. When administered orally to mice, plasma concentrations exceeded the MIC for more than 24 hours. Further research confirmed the compound to be active in inhibiting the growth of intracellular *M. tuberculosis* and to be effective against strains resistant to individual established TB drugs.

In summary, two successful cases of 'hit-to-lead' optimization demonstrated the effectiveness of using drug metabolism studies to guide analoging efforts aimed at improving the drug-like properties of anti-TB compounds. Currently, mouse and human liver microsome assays have been incorporated into the "hit-to-lead" process in all of our internal drug discovery projects in order to discover potential anti-TB lead compounds with longer half-lives.

Liver enzyme induction can cause undesirable drug-drug interactions as well as drug metabolite-induced liver toxicity. Both can be especially problematic in treating diseases such as TB that require long term administration of drug combinations. Historically, liver enzyme-induction, drug-drug interactions, and toxicity were often revealed only when a drug entered clinical trials. In order to overcome this drawback at the early discovery stage, it was necessary to establish an in vitro assay system to determine rapidly the induction potential of test compounds on CYP P450 enzymes and the toxicity of the resulting metabolites. The novel HepaRG cell line expresses CYP P450 enzymes at levels similar to primary hepatocytes. Therefore this cell line was chosen to develop an assay system to assess P450 induction and metabolite-based toxicity. An expensive commercial culture medium was required for HepaRG cells to express CYP P450 enzymes at levels observed in primary hepatocytes, preventing the use of this cell model to screen large numbers of compounds. Therefore, this project began with customizing in-house culture media that could match the performance of

commercial product for inductioin assay. Various concentrations of four key components of this medium were tested for their effects on the P450 expression and induction potentials in HepaRG cells. Through iterative optimization, the final formula of this culture medium could induce the expression of P450 enzymes in HepaRG cells in a manner similar to the commercial culture medium but at 8-fold lower cost. Compared with the cost of primary hepatocytes-based induction assay, this induction assay reduced the cost 50-fold. The study further reduced the leading cell culture time from 4 weeks (published induction protocol) to 2 weeks before the treatment with inducers. With the modified protocol and customized medium, both experimental time and assay costs were dramatically reduced, thus increasing throughput. A 96-well-based HepaRG induction assay was developed and validated using six known CYP 450 inducers. The validation results were comparable to those reported from primary hepatocytes-based induction assays. With a 96-well format, this induction assay could support a throughput of 50 compounds per run with a turnaround time of 3 days. This assay is currently being evaluated with a larger panel of known inducers and non-inducers and is expected to be of great value in detecting compounds with potential liver induction liabilities early in the drug discovery process.

Current algorithms for HTS-based drug discovery of anti-TB agents fail to account for the possibility of active metabolites early in the drug discovery process. In order to overcome this drawback, attempts were made to establish in vitro assays to

rapidly detect the anti-TB activity of liver enzyme-derived metabolites. These TB-active metabolite assays should obviate the need for metabolite ID and synthesis to confirm the presence or absence of an active metabolite. A novel method to evaluate metabolite activity was developed by combining a mouse microsome assay with a microtiter plate alamar blue assay (MABA) to test anti-TB activity. The microsome assay system interfered with both the MABA fluorescence readout and the growth rate of *M. tuberculosis* (determined by CFU counting, the gold standard growth rate assay). A detailed assay protocol was designed to normalize those assay interferences. In a proof of concept pilot experiment, this assay unequivocally differentiated active compounds that were metabolically stable from active compounds that were metabolically unstable but had inactive metabolites. Currently, a benchmark inactive parent compound with active metabolites is being prepared; this compound will be used to benchmark the capability of this assay in detecting prodrugs. Once fully developed, this novel assay will have many applications. It will serve to increase compound libraries' chemical diversity and to consider revisiting previously screened libraries. To distinguish active metabolites of active parent compounds from metabolically stable, active parent compounds, concurrent LC-MS analysis of parent compound stability is required along with optimized data analysis. The ability to detect active metabolites by this method early in the drug discovery process will allow for the further progression of some active

compounds with poor metabolic stability that otherwise would be deprioritized using only LC-MS based stability assays.

In summary, this dissertation included a series of projects to create innovative ADMEt methods to facilitate the discovery of new anti-TB drugs that can overcome the drawbacks of existing drugs. These assays were developed to overcome challenges in three aspects of anti-TB drug discovery: drug metabolism, liver enzyme induction and toxicity. All assays were validated in 96-well format using known benchmark compounds and the results were comparable to literature reported values. This panel of assays has been successfully used to provide new insights for existing anti-TB drugs and also used to guide medicinal chemistry efforts to optimize screening hits into leads. Currently, all methodologies developed in this dissertation are being used in the anti-TB drug discovery projects at the Institute for Tuberculosis Research at the University of Illinois at Chicago and will soon become available to the global tuberculosis research community to facilitate discovery and development of ‘next generation’ anti-TB drugs.

1. INTRODUCTION

1.1. Introduction to *Mycobacterium tuberculosis*

The genus *Mycobacterium* is composed of about 100 species *(1)*, one of which, *Mycobacterium tuberculosis* is the causive agent of most human tuberculosis (TB). *M. tuberculosis* is a rod-shaped bacillus, 2-4 μm in length and 0.2-0.5 μm in width. Although classified as gram-positive, it stains weakly when a gram stain is performed due to the high lipid and mycolic acid content of its cell wall which prevents the retention of the gram stain. *M. tuberculosis* is an aerobe, or facultative anaerobe. The genome of *M. tuberculosis* strain H37Rv has been sequenced and contains about 4000 genes. One striking discovery related to its genome is that about 8% of its genes are related to lipid metabolism, suggesting the importance of lipid metabolism in its life cycle (*2*). Indeed, the cell wall of *M. tuberculosis* is high in lipid content and this high lipid content is essential for its virulence (*3*).

The primary route of infection for *M. tuberculosis* is through inhalation of airborne bacilli, originating from TB patients' coughing, shouting and sneezing. Inhaled bacilli multiply to an extent that triggers an initial host immune response, the local lesion termed the Ghon focus. As a result, macrophages will migrate to the site of infection and cause the formation of tubercles (*4*). This host immune response may last from days to months. *M. tuberculosis* bacilli that survive the host immune response may enter into dormant states which are difficult to treat by anti-TB drugs. Depending on the strength of host immune response, the disease can be suppressed permanently or enter into a late stage (*5*). In the late stage of TB, the spread of macrophages into

peripheral lymph nodes may carry surviving bacilli into other tissues and organs such as spleen, liver and bones (*5*).

1.2. Global urgencies of discovering new drugs for TB treatment

M. tuberculosis infection is a severe and old disease that can be traced back to the early 17th century (*6-7*). There is an estimate that one third of the world population is infected with *M. tuberculosis*, resulting in about 2-3 million deaths per year (*8*). Most of the first line and second line anti-TB drugs except quinolone analogs were discovered during the 1950s and 1960s (*9*). Directly Observed Treatment, Short-course (DOTS) is a TB control program promoted by the WHO which utilizes 2 months treatment with 3-4 drugs followed by 4 months treatment with 2 drugs. DOTS, when practiced in a setting with adequate health care infrastructure, can have a cure rate up to 95% (*10*). Despite the significant side effects encountered with a 6-month, multidrug regimen, for many years TB was considered as a disease on the way to being eradicated.

Beginning in the 1980s, with the emergence of multiple-drug resistant (MDR) strains (resistant to at least isoniazid and rifampin) and HIV co-infections, there was a trend of resurgence of *M. tuberculosis* infections and a great demand for the discovery of new anti-TB drugs to treat MDR strains and avoid side effects (*11*). It is estimated that about 50 million people worldwide are infected with *M. tuberculosis* strains that are resistant to at least one approved anti-TB drug. Of particular concern is the emergence of MDR, and the recent recognition of extensively-drug-resistant TB (XDR-TB), which is resistant to the most effective anti-TB drugs (including rifampin, isoniazid and quinolone family of drugs) (*12*). Despite the pressing medical need, there was two decades

(1970s-1990s) of silence with respect to TB drug discovery with only a few drugs entering clinical trials (*1*). The reasons for the lack of interest of the pharmaceutical industry to invest in anti-TB drug discovery include 1) the increasing cost for the discovery of new anti-TB drugs; 2) the lack of financial reward since the majority of the TB patients are in developing countries and 3) the risk of patent violation since intellectual property is less respected in developing countries where the majority of the anti-TB drugs will be manufactured and used. Facing a resurgence of TB, more organizations, especially nonprofit organizations and institutes, are involved or starting to be involved in anti-TB drug discovery. Not only are numerous compounds with novel structures being studied in drug discovery programs, but drugs used in the treatment of other diseases are also being assessed for their anti-TB activity (*13*).

1.3. Liability of current anti-TB drugs informs the discovery strategies for 'next generation' anti-TB drugs

The regimen used in DOTS starts with two months' daily treatment of four drugs – rifampin isoniazid, pyrazinamide and ethambutal or streptomycin, followed by four to six months (daily) of a combination of rifampin and isoniazid. Adherence to the treatment schedule is required to achieve high cure rate in the DOTS program. One of the drawbacks of DOTS is the lengthy treatment duration, which can cause high rates of noncompliance and result in treatment failure, the progression of TB symptoms, and the emergence of resistant strains.

With the increase of HIV/TB coinfections, many patients need to take both anti-TB drugs and antiviral drugs. Several drugs (rifampin and isoniazid) in DOTS have liver

enzyme induction and inhibition properties (*14-15*), which may interfere with antiviral drugs and cause reduced antiviral efficacy or liver toxicity.

1.4. Optimization of ADMEt properties is essential for the discovery of 'next generation' anti-TB drugs

The discovery of new anti-TB drugs should focus on overcoming the drawbacks of existing TB drugs. In addition to novel mechanisms of action compared to currently approved drugs, optimum ADMEt properties are very important for the discovery and development of new anti-TB drugs. Currently, anti-TB drug discovery is mainly focused on extensive screening of chemical libraries against various drug targets or whole cells to identify new compounds, both synthetic and natural, as novel drugs. Unfortunately, this approach has yielded very few successes in the field of anti-TB drug discovery (*16*). One of the reasons for this low success rate is that potency is always the major, if not the only, property pursued during the drug discovery process, especially at an early discovery stage. It is tempting to assume that a potent compound with a novel mechanism of action will overcome all drawbacks of existing drugs and therefore offer better anti-TB treatment. However, more formidable is the requirement for optimum ADMEt properties in order to achieve efficacy in small animal disease models as well as clinical trials.

In order to overcome the these drawbacks, an ideal anti-TB drug should have a long half-life in patient's body to increase treatment efficacy and allow decreased dosing frequency, which would increase patient compliance and help to suppress the emergence of resistance strains. Minimum induction and inhibition of liver enzymes are

required to avoid unfavorable drug-drug interactions with other drugs such as antivirals. Furthermore, some drugs used in current DOTS still have significant side effects, especially after a long period of treatment (*17-18*). Therefore, a reduction in toxicity will be desirable for new anti-TB drugs. Overcoming the above challenges requires an extensive and through optimization of a drug's ADMEt properties, preferably at an early discovery stage.

Performing ADMEt studies and optimization on current anti-TB drugs can provide us with opportunities to discover new drugs. The majority of existing anti-TB drugs was discovered during the 1950s, when today's ADMEt methods were not available. Therefore, their ADMEt properties, especially the metabolism properties, for most of the existing anti-TB drugs were not studied and are not in the public domain. It is meaningful to do retrospective ADMEt studies for existing drugs, which will provide the following insights to help in the discovery of new drugs. First, a detailed study of drug metabolism of existing drugs will help us to understand whether their metabolites have anti-TB activities or not. Once active metabolites from existing drugs are discovered, they can become promising new leads since it is not uncommon that drug metabolites have better ADMEt properties than their parent drugs (*19-20*). Second, although several existing anti-TB drugs have significant side effects, their mechanism of toxicity is still unknown (*21-22*). A detailed understanding of their toxicity profile can help us discover new drugs with better safety profiles.

1.4.1. Overview of our understanding of the metabolism of existing anti-TB drugs

Examples of existing anti-TB drugs and experimental drugs in clinical trials are listed in Figure 1. Among those approved anti-TB drugs, rifampin (1966), isoniazid (1952), ethambutol (1961), pyrazinamide (1952), streptomycin (1946), para-aminosalicylic acid (1948) and ethionamide(1965), are the grandfathered drugs that were discovered before FDA published the rules for new drug approval (Figure 1). There are only a few retrospective studies on their in vitro metabolism properties (*21*).

First line drugs:

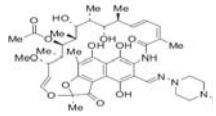

Rifampin (1966)

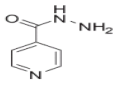

Isoniazid (1952)

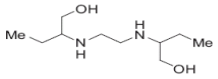

Ethambutol (1961)

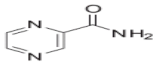

Pyrazinamide (1952)

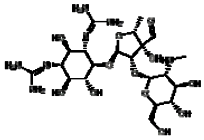

Streptomycin (1943)

Second line drugs:

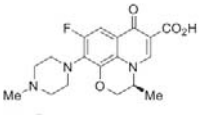

Levofloxacin (2004)

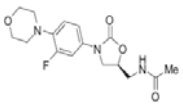

Linezolid (2000)

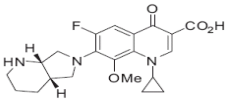

Moxifloxacin (2008)

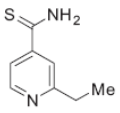

Ethionamide (1965)

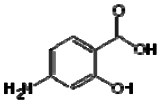

p-aminosalcylic acid (1948)

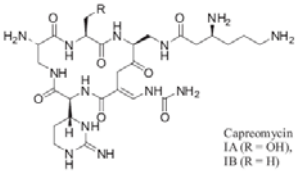

Capreomycin (1971)

Third line drugs:

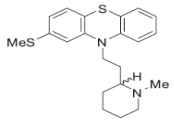

Thioridazine (1985)

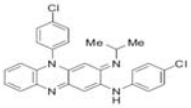

Clofazimine (1986)

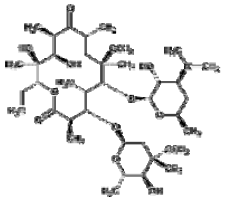

Clarithromycin (2005)

Drugs in clinical trials:

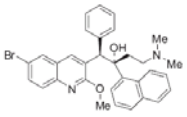

TMC-207
(Phase II)

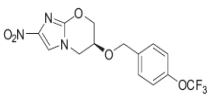

PA-824
(Phase II)

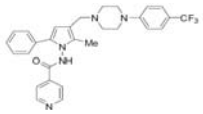

LL3858
(Phase I)

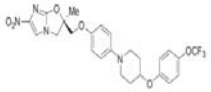

OPC67683
(Phase II)

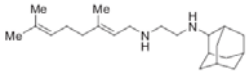

SQ109(Phase II)

Figure 1. Structures of existing anti-TB drugs and experimental drugs in clinical trials.

1.4.2. Overview of known active/toxic metabolites of existing anti-TB drugs

Metabolite activity/toxicity information is only available for a limited number of existing anti-TB drugs (TABLE I). There are a total of 18 marketed drugs and 5 compounds (PA824, OPC67683, TMC207, SQ109 and LL3858) at various stages of clinical trials for the treatment of TB. Out of these 23 anti-TB drugs entering the clinic,

only 10 were studied for active metabolites, five of which were positive. Eight of the 23 were studied for metabolite toxicity (*23-30*), of which 3 were found to have toxic metabolites. This further confirms that active metabolites and toxic metabolites can be found for current anti-TB drugs and are very likely to be found associated with experimental compounds at various stages of the discovery pipeline.

TABLE I. ESTABLISHED ANTI-TB DRUGS WITH ACTIVE OR TOXIC METABOLITES*

Drug	Active metabolite	Toxic metabolite	Drug	Active metabolite	Toxic metabolite
Rifampin	25-deacetyl rifampicin(esterase)	NA	**Moxifloxacin**	NA	NA
Isoniazid	NA	AcHZ,Hydrazine (MFO,CYP2E1)	**Metronidazole**	NA	NA
Pyrazinamide	Pyrazinoic acid (xanthine oxidase)	NA	**Gatiloxacin**	NA	NA
Ethambutol.2HCl	NA	NA	**Thioridazine**	Mesoridazine(CYP2C19,CYP2D6)	NA
Steptomycin	No major metabolite indentified	No major metabolite indentified	**Capreomycin**	NA	NA
Kanamycin	NA	NA	**Clarithromycin**	14-hydroxy Clarithromycin(CYP3A4)	NA
p-Aminosalicylic acid	NA	N-acetylated PAS(NAT1)	**PA824**	No major metabolite indentified	No major metabolites identified
Cycloserine	No major metabolite indentified	No major metabolite indentified	**OPC67683**	No major metabolite indentified	No major metabolites identified
Ethionamide	S-oxide Ethionamide(FMO)	S-oxide Ethionamide(FMO)	**TMC207**	NA	NA
Ciprofloxacin.HCl	NA	NA	**SQ109**	NA	NA
Ofloxacin	NA	NA	**LL3858**	NA	NA
Linezolid	Inactive metabolite	Inactive metabolite	/	/	/

*NA refers to no study has been performed

Although it is very important to study drug metabolites, methodologies used in those studies are still low in throughput since they require time-consuming chemical synthesis of drug metabolites. Therefore, there is an urgent need to develop simple and high-throughput *in vitro* assays to study the activity and toxicity of metabolites of large numbers of compounds.

1.4.3. Current drug metabolism studies on established anti-TB drugs

This section will provide a more detailed review on the drug metabolism studies.. Five metabolites were identified for rifampin: mono-oxygenated rifampin, desacetylrifampin, rifampin quinine, demethylrifampin, and rifampin glucuronide. The deacetylated form was the only rifampin metabolite studied for activity against *M. tuberculosis*, and the result was positive (*31*). Isoniazid is biotransformed into multiple metabolites by hydroxylation, mono-oxidation, and a reaction mediated by *N*-acetyltransferase (NAT). Hydrazine (HZ) and acetylhydrazine (AcHZ) were considered to be the metabolites that partially contribute to the toxicity of isoniazid (*24*). Pyrazinamide is metabolized to its anti-TB active metabolite pyrazinoic acid by xanthine oxidase in the liver (*32*). The major metabolite of p-aminosalicylic acid (PAS) in human plasma is *N*-acetylated PAS. It was reported that the *S*-oxide metabolite of ethionamide had equivalent activity and toxicity as its parent compound (*26*).

With respect to drug-drug interactions, rifampin is a well known inducer of a variety of drug metabolism enzymes such as CYP3A, CYP1A2, CYP2C, glucuronosyl transferase, sulfotransferase, isoniazide hydrolase as well as a PgP transporter (*33*). Caution should be taken when combining rifampin with other drugs since the former

could possibly reduce the efficacy of the latter or enhance the production of toxic metabolite(s). Isoniazid is metabolized by type 2 NAT. It also inhibits CYP1A, 2C9, 2C19, 2E1, 3A4 and 2D6 activity (*22, 34*). Pyrazinamide inhibits CYP2B, 2C, 2E1 and 3A in rats while showing no inhibition of human CYPs (*35*). Ethionamide may inhibit the acetylation of isoniazid and result in increasing levels of isoniazid and cycloserine (*35*). Capreomycin is a peptide drug that can only be dosed parentally. It has no inhibition or induction effect for clinically significant CYP enzymes (*36*). Linezolid is metabolized into its only metabolite hydroxylinezolid (*37*). It has no inhibition nor induction for clinically significant CYP enzymes (*37*). The fluoroquinolones (moxifloxacin and levofloxacin) are not subject to significant metabolism and have no inhibition nor induction of major CYP enzymes (*38*). There are three major metabolites identified for clofazimine although the anti-TB activities of its metabolites are still not confirmed (*39*). 14-Hydroxyclarithromycin is the active metabolite of clarithromycin. Clarithromycin has significant inhibition effects on CYP3A4 and PgP. Ethionamide inhibits the activity of CYP1A2 and CYP3A4 (*40*). There are two major metabolites of thioridazine of which mesoridazine is known to be anti-TB active (*41*).

Currently there are several experimental anti-TB drugs at different stages of clinical trials for the treatment of TB (Figure 1), some with active metabolite(s). TMC207 was found to be biotransformed by CYP3A4 to an active *N*-demethyl metabolite that has a 2-3 fold higher exposure in humans than in dogs and rats (*42*). SQ-109 is subject to extensive hepatic clearance with multiple metabolites generated by liver enzymes CYP2D6 and CYP2C19 (*43*). OPC-67683 was found not to be subject to hepatic clearance (*27*).

1.4.4. Drug metabolism and pharmacokinetics of lead compounds in internal anti-TB drug discovery programs

From 2006 to 2010, various anti-TB drug discovery projects were performed in the ITR at UIC. A series of lead compounds were identified either from chemical optimization of known anti-TB compounds or from chemical library screening against whole cell *M. tuberculosis*. These included macrolides, dicarbonates, mefloquine analogs, isoxazoles, pyrazines and tetrahydroindazoles.

Macrolides have been used as antibiotics for a long time. However this series of compounds has shown limited activity against TB (*44*). About 300 macrolide analogs were synthesized and tested for anti-TB activity at the ITR. The results showed novel structure-activity relationships (SAR) which can help improve the potency of this series of compounds against TB (*45*). Preliminary in vitro metabolic studies showed that they were not subject to phase I metabolism. However, several analogs were found to be unstable in simulated gastric fluid. Lead compounds from this series were active in vitro but not in mouse models (*45*). Retrospective pharmacokinetics studies of representative compounds in this series would be necessary to understand whether in vivo exposures were inadequate.

The dicarbonate series included pyrrolidine dithiocarbamate (PDTC), disulfiram and diethyldithiocarbamate (DETC). These compounds showed potent in vitro activity against TB (*46*). Disulfiram was stable in the GI tract but it was unstable and converted to active metabolites in human microsomes and plasma. The metabolic profile of DETC and PDTC required further study.

A series of hybrid esters of mefloquine and isoxazole substructure showed potent anti-TB activity in vitro (*47*). However, they were converted very quickly in plasma and microsomes to inactive acid forms (*47*). Further study showed that the ester substructure was the crucial pharmacophore for this series of compounds. The metabolic stability of this series of compounds needs to be optimized further.

An isoxazole-based series was identified from the HTS of a parallel synthetic library for growth inhibition of *M. tuberculosis*. Screening hits were subject to extensive hepatic metabolism study. However, the good potency and selectivity of the analogs in this series was accompanied by poor metabolic stability thus this series requires further optimization.

Compounds in the pyrazine series showed potent in vitro activity against TB and were metabolically stable. In vivo pharmacokinetic studies showed good lung tissue exposure in mice. However, this series of compounds failed to show in vivo anti-TB activity. Interestingly, they were also found to be potent CYP2B6, 2D6 and 3A4 inhibitors (manuscript in preparation). Further metabolic and pharmacokinetic studies were required to explain its lack of activity in vivo.

The tetrahydroindazole series was discovered through a whole-cell based screening of a chemical library. The original screening hit showed low metabolic stability, precluding anti-TB activity in vivo. Through iterative in vitro metabolic stability assay guided chemical modification, the ‘soft spots’ of metabolism were blocked. More stable analogs were thus synthesized. The optimized lead compound showed low systemic clearance and high plasma concentration with potent anti-TB activity (*48*).

1.5. Methods in drug metabolism and pharmacokinetics as applied to anti-TB lead discovery and optimization

The drug metabolism studies in this dissertation include measurements of metabolic stability, metabolism enzyme phenotyping, metabolite activity and toxicity. Pharmacokinetics was limited to pre-clinical evaluations. A brief review of these methods is provided below.

1.5.1. Metabolic stability

The metabolic stability assay is an enzymatic assay with concentrated phase I enzymes to predict compound clearance by the liver. The substrate concentrations of 1 μM to 10 μM are close to those obtained in vivo; the enzyme concentrations range from 0.1 to 2 mg/ml; the NADPH cofactor is either added directly or supplied via a NADPH regeneration system (*49*). Metabolic stability data could be used to predict hepatic clearance for compounds undergoing extensive phase I metabolism. With the increasing demands to know drug liabilities during the discovery stage, more and more high-throughput applications have been integrated with metabolic stability assays. Compounds that fail to pass the metabolic stability filters are usually deprioritized in development and subject to chemistry modification to make more stable analogs.

1.5.2. Structure determination of drug metabolites

LC-MS is widely used in identification and structure elucidation of drug metabolites. Using tandem mass spectrometry (MS_n), sites of metabolism (soft spots) and structures of metabolites can be proposed and elucidated. With the technique of

accurate mass determination, the elemental composition of drug metabolites can be determined by comparing the accurate mass of the metabolite to the theoretical mass with accuracy within 1ppm. However, LC-MS methods cannot unambiguously confirm the structures of the metabolites without authentic compound standards. Nuclear magnetic resonance (NMR) can precisely characterize the structure and stereochemistry of metabolites by monitoring the $^{1}H/^{13}C$ resonance of different functional groups. However the throughput for NMR is relatively low.

1.5.3. Plasma protein binding

The majority of anti-TB drugs are distributed to target tissues through the bloodstream. Blood plasma can bind a significant proportion of drug molecules and only the free portion, unbound by plasma protein, can be distributed into the target tissue and exert a therapeutic effect. Plasma protein binding assays determine the free drug fraction in plasma obtained from the peripheral circulation. There are multiple methods for measuring plasma protein binding such as equilibrium dialysis, ultrafiltration and ultracentrifugation. Rapid equilibrium dialysis is regarded as the gold standard for determination of plasma protein binding (*50*).

1.5.4. CYP P450 inhibition assay

CYP P450 inhibition is a major cause of liver toxicity in anti-TB therapy (*33*). Therefore, CYP450 inhibition should be determined during the lead discovery and optimization process. CYP P450 inhibition assays can also be used to predict in vivo drug-drug interactions (*51*). Microsomes and recombinant enzymes both can be used to

assess CYP 450 inhibition. There are three types of CYP P450 inhibition: 1) direct inhibition, 2) metabolite-based inhibition and 3) time-dependant inhibition. Different assay protocols are applied to differentiate these three types of inhibition. Because of the differences of protein binding amoung these assays, the EC_{50} from each assay can be different. In general, the lower the protein concentration, the lower EC_{50} measured (*52*).

1.5.5. CYP P450 induction assay

There are two mechanisms for CYP P450 inductions. Most CYP induction, e.g. CYP3A4, 2B6, and 1A2, start with receptor-activation by inducing compounds, followed by translocation of transcription factors into the nucleus and then increased transcription of specific CYP P450 genes. The other mechanism (CYP2E1) is through stabilizing translation or inhibiting the protein degradation pathway of CYP P450 enzymes (*53*).

The major CYPs with induction concerns are CYP3A4, 2B6 and 1A2. By evaluating compound-mediated induction of CYP3A4, 2B6 and 1A2, the potential for activation of the pregnane X receptor (PXR), the constitutive androstane receptor (CAR), and the aryl hydrocarbon receptor (AhR) can be determined. The other CYPs, including CYP2Cs, are proportionally induced as CYP3A4 through PXR (*54*).

In vitro models of induction include the use of primary hepatocytes, engineered cell lines and reporter genes with the former regarded as the gold standard. However, 1) the supply of primary hepatocytes is very limited, 2) the half-life of cytochrome P450 enzymes in primary cells is very short, and 3) there are significant differences in cytochrome P450 expression levels among hepatocyte donors. Reporter gene assays

for PXR can increase the throughput for screening for CYP3A4 induction but this method is not available for other receptors and corresponding CYP enzymes (*55*).

Engineered cell lines with overexpression of one or multiple CYP enzymes can be used for induction studies. However, those cell lines have an incomplete gene expression spectrum relative to that which occurs in vivo. As a result, the in vitro-in vivo correlation is poor using this cellular model (*55*).

The HepaRG cell line is a newly developed carcinoma cell line isolated from a female cancer patient. This cell line expresses an entire panel of cytochrome P450 enzymes at levels that are very close to those observed in vivo thus making it a suitable model for cytochrome P450 induction studies (*56*). A detailed study using this cell line to assess induction is presented in Chapter 5.

1.6. In vitro bioassays for the measurement of anti-TB activity of test compounds

Many bioassays have been developed for the screening of anti-TB compounds; most often used with *M. tuberculosis* strain H37Rv. However, three types of assays are most commonly used: redox dye-based, reporter gene-based and intracellular ATP-based (*57*).

Alamar blue, resazurin and tetrazolium are the three most commonly used dyes in redox-based assays for quantitative measurement of the proliferation of bacterial and fungal cells as well as various human and animal cells (*58-59*). If the organisms are metabolic active, the intercellular redox enzymes can use the co-factors NADH or NADPH in the living organisms to transform those dyes into reduced products (resorufin

or formazans), which have specific UV absorbance or fluorescence peaks. MABA utilizes the alamar blue dye as the indicator of bacterial viability and is the most cited assay for the measurement of anti-TB activity of testing compounds. Compared with other assays, redox-based assays are low in cost, easy to apply, robust and accurate. However, because of the nature of the assay, compounds with reducing abilities or fluorescent properties could potentially interfere with the assay readout and need to be checked by an alternate assay or their interferences need to be subtracted using a proper control reaction.

In the reporter gene-based assay, a reporter gene (usually GFP gene or luciferase gene) is introduced into *M. tuberculosis* either on an autonomously replicating plasmid or as a chromosomally integrated gene. Under a given physiological condition, the reporter gene products are proportional to the number of live bacteria in culture. As a result, growth and inhibition can be monitored by measuring either the fluorescence signal from GFP or other fluorescent proteins or the luminescence signal from the luciferase (*60-61*). The green fluorescent protein microplate assay (GFPMA) can monitor the kinetics of bacterial growth or inhibition because there is no need to add extra reagents. Most luciferase-based assays require the addition of the luciferase substrate luciferin and ATP (for firefly luciferase) or the cofactor n-decanal (for *Vibrio harvyeii* luciferase) in order to generate a luminescence signal. These are end point assays and could be used in high-throughput format. However, the signal-to-background ratio of fluorescent protein reporter gene-based assay is relatively low, possibly leading to high standard errors for the readout of this assay.

Luciferase-based assays to measure intracellular ATP level have been used more and more widely to monitor bacteria growth in culture. In this type of assays, excess amount of luciferase and its substrates (without ATP) are mixed with bacteria cell lysis buffer and added into bacteria culture. Lysed bacteria cells release intracellular ATP into the mixture which can be used by luciferase to produce luminescence signal. The amount of assay signal is proportional to the amount of bacteria cells in the culture. This assay is simple and very sensitive (can detect as low as 1500 cells per well with a signal/background ratio higher than 100) (*62*). However, this type of assay provides end-point measurements of bacteria growth and cannot be used to monitor the kinetics of bacteria growth. The cost of this type of assay is slightly higher than MABA since it requires the purchase of commercial luciferase assay reagents.

In this dissertation research, MABA was chosen as the assay format to measure anti-TB activity of test compounds due to its low cost. Also in the development of a novel assay to measure the anti-TB activity of drug metabolites, MABA can be combined with a mouse microsome metabolite generation system for the measurement of the anti-TB activity of drug metabolites (see Chapter 6 for details). The interference from fluorescent compounds or reducing agents on the readout of the MABA can be dealt with by subtracting the readout of control reactions or by re-testing the compound in an alternative assay, e.g. the luciferase reporter gene assay.

1.7. Objective and overall research strategies

Our long-term goal is to discover new small molecule therapeutics against TB that can overcome the drawbacks of existing drugs. I started my dissertation research in

the ITR at UIC on June, 2007. The current dissertation research focused on overcoming three challenges mentioned above: metabolism, induction of liver enzymes, and toxicity. A total of five aims were achieved in this dissertation. The rationales behind those aims are described as the following:

Aim 1. Establish a panel of ADMEt assays for anti-TB drug discovery

In 2007, very few ADMEt assays were established in the ITR to evaluate the screening hits and leads. Serious disconnections between in vitro activity and in vivo efficacy were common. Various anti-TB drug discovery projects experienced metabolic stability problems. To bridge this disconnection, my initial efforts focused on establishing a panel of ADMEt assays for anti-TB drug discovery (Chapter 2).

Aim 2. Bioanalysis method establishment and retrospective metabolism study of existing anti-TB drugs

From drug metabolism and bioanalysis perspectives, there are still many unknowns to be studied for the established anti-TB drugs. We proposed to develop a simultaneous LC-MS-MS method to quantify the existing anti-TB drugs in human plasma. The metabolic stabilities of these compounds were also evaluated to retrospectively see how these ‘old’ drugs behave in these new assays. This study resulted in the first identification of possible active metabolites of LL3858 (Chapter 3).

Aim 3. Drug metabolism-guided drug discovery using the established ADMEt methods

From 2006 to 2008, three compound libraries were screened for growth inhibition of *M. tuberculosis*. However, extensive metabolism-related problems existed in the screening hits. Metabolite profiling for those hits was carried out to find 'soft-spots' for further chemistry modifications. New lead compounds were synthesized with better DMPK profiles and drug-like properties, and these compounds were subjected to additional biological and metabolic evaluations to attain a more comprehensive understanding of their drug potential (Chapter 4).

Aim 4. Develop and validate an *in vitro* induction assay using HepaRG cells

Anti-TB drugs are usually used in combination with each other and with antiviral drugs. Induction effects of one drug on liver enzymes can reduce the efficacy of another drug, causing undesirable drug-drug interaction or even metabolite-related liver toxicity. Historically, the liver enzyme induction potential of drug candidates was only evaluated after they entered clinical trials. Late stage failures can cause patient suffering and financial loss. In order to overcome this drawback, we proposed to develop a faster and cost effective method using HepaRG cells to establish an in vitro induction model to predict induction potential of test compounds on liver enzymes in vivo (Chapter 5).

Aim 5. Develop and validate an assay to measure the anti-TB activity of drug metabolites

Current algorithms for high-throughput screening-based drug discovery for anti-TB agents fail to account for the possibility of active metabolites early in the drug discovery process. In order to overcome this drawback in our screening efforts for novel

anti-TB drugs, we attempted to develop *in vitro* assays to detect the anti-TB activity of liver enzyme-derived metabolites. These TB-active metabolite assays (TAMA) can obviate the need for metabolite ID and synthesis to confirm the presence or absence of an active metabolite. A novel method to evaluate metabolite activity was developed by combining a liver enzyme metabolite generation system (MGS) with an anti-TB assay (Chapter 6).

2. MATERIALS AND METHODS (ADMEt ASSAY)

2.1. Chemicals and biological matrices

Pooled mouse and human liver microsomes (20 mg/mL protein) were purchased from XenoTech (Lenexa, KS). All chemicals were purchased from Sigma Aldrich (St. Louis, MO). All solvents were HPLC grade and purchased from Fisher Scientific (Hanover Park, IL). The rapid equilibrium dialysis device was purchased from Pierce (Thermo Scientific) (*58*). Human plasma and serum were purchased from Bioreclamation (Westbury, NY).

2.2. Metabolic stability assay

General method. Compound stock solutions were prepared in DMSO. The final concentration of DMSO in the incubation media was less than 0.2% (v/v). The stability of compounds in microsomes was determined in triplicate after their incubation with liver microsomes in 50 mM potassium phosphate buffer (pH 7.4) at 37 °C. Total incubation volume was 50 µL. The reaction mixture was prewarmed at 37 °C for 5 minutes before adding NADPH (1 mM). Reactions were quenched by adding acetonitrile (150 µL) containing internal standard at 0.01 µM. Samples were centrifuged at 4000 g for 30 minutes before liquid chromatography/tandem mass spectrometry (LC-MS-MS) analysis of the parent compound. For control experiments, NADPH was omitted from these incubations.

Substrate and microsome concentration. Compound concentrations were based on their respective ionization efficiencies/sensitivities of detection. In general, 10 µM compounds were added to 1 mg/mL microsomes or 1 µM compounds were added

to 0.5 mg/mL microsomes. Thus the concentration of the substrate and enzymes in the incubation was close to the physiological condition.

Multiple time points *vs* single time point. Li and coworkers from Wyeth Research Lab have previously published comparisons of microsomal stability data of 41 established drugs with 39 in-house compounds. Their data have shown that single-time-point experiment results have excellent correlation with multiple-time-point experiment results, regardless of approved drugs or in-house compounds (*63-64*). In this dissertation, both single time point and multiple time points were used. In high-throughput screening, the half-life ($T_{1/2}$) from a single time point assay is calculated by the following equation:

$$t_{1/2} = -\frac{\ln 2 \times (\text{incubation time})}{\ln(\%\text{remaining}/100)} \qquad (1)$$

For multiple time point assays, the half-life ($T_{1/2}$) of the compound in liver microsomes was calculated using the following equation from simulated data in Figure 2.

$$t_{1/2} = \ln 2 / -k_{el} \quad (1) \qquad (2)$$

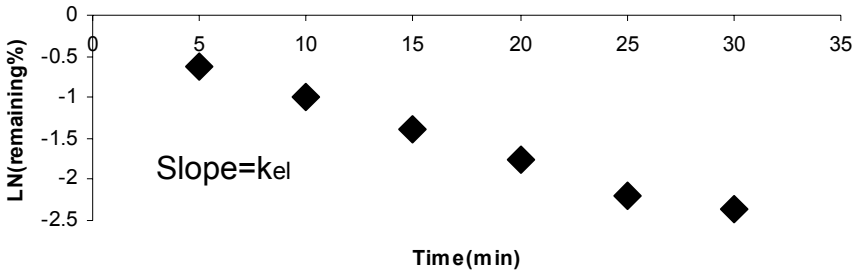

Figure 2. Simulated metabolic stability of compounds.
The Y axis represents the natural log of the percentage remaining of parent compound in liver microsomes. The X axis reprents the corresponding incubation time.

Extrapolate Cl_{int} and $Cl_{in\ vivo,h,p}$ from metabolic stability data. For those compounds with phase I hepatic metabolism as the primary elimination route from the body, metabolic stability data from microsome incubations could be used to predict the in vivo clearance of the compounds.

Various hepatic clearance models have been developed to integrate other factors such as the protein binding, transporters, and liver enzyme activities into the prediction. Two commonly used models are the “well-stirred” model and the “parallel tube” model. The “well-stirred” model views the liver as a compartment with the same concentration of drug in the liver as in the blood circulation (*65-66*). The “parallel tube” model regards the liver as a series of parallel tubes with declining tube length but with the same enzyme concentration in each tube (*67*). All the calculations in this dissertation are based on the well-stirred model which hypothesizes that compounds disperse very quickly throughout the liver. The following equations were used:

$$CL_{int} = (\ln(2)/t_{1/2}) \times (\text{g liver weight / kg body weight}) \times (\text{ml incubation / mg microsomal protein}) \times (45\ \text{mg microsomal protein / g liver weight}) \quad (3)$$

$$Cl_{H,b} = (Q \times Cl_{int} \times f_u)/(Q + Cl_{int} \times f_u)$$

($CL_{H,b}$: Hepatic clearance; Cl_{int} : intrinsic clearance; f_u : fraction unbound)

$$E = Cl_{H,b}/Q \quad (4)$$

(E : Extraction ratio; Q : Blood flow)

In this dissertation, all the calculations for clearance prediction are based on multiple time point metabolic stability data; the single time point experiment design is only used in high-throughput evaluations of screening hits and leads.

Assay Validation: The assay is validated by control compounds propranolol and midazolam in human and mouse microsomes.

2.3. Protein binding

General Method. This assay was carried out using a Rapid Equilibrium Dialysis (RED) device from Thermo Co (Rockford, IL). Briefly, 200 µL of human plasma with 10 µM compound was added to one side of the dialysis chamber and 350 µL PBS buffer was added in the other side of the chamber. A total of 48 chambers can be placed in one 96-well plate. The plate was then covered with a gas-permeable membrane and shaken at approximately 100-200 rpm in a water bath at 37°C for four hours. Upon

removal of the seal, 50 µL was transferred from the plasma and buffer chambers to new tubes. Fifty microliters of fresh plasma or PBS was added to the samples removed from the buffer chamber and and plasma chamber, respectively before addition of three volumes of cold acetonitrile. After centrifuging at 10,000 g for 30 minutes, compound contained in supernatants was then quantified using mass spectrometry. The protein binding was calculated using the following equation:

$$\%Bound = 100 - \frac{C_{buffer} \times 100}{C_{buffer} + C_{plasma}} \qquad (5)$$

where C_{buffer} is the compound concentration in the buffer chamber; C_{plasma} is the compound concentration in the plasma chamber.

Assay Validation: Propranolol showed 77.59±0.72% binding to human plasma protein binding, which is consistent with the literature reported value (*68*).

2.4. Plasma stability

General Method. Compounds at 50 µM were incubated with human plasma over a time course. After precipitation of the proteins using acetonitrile and centrifugation, the supernatant was transferred and analyzed by LC-MS-MS. Stability was calculated as the percentage of parent compound remaing compared to a control reaction quenched at time zero.

Method Validation. The method was validated using an unstable compound disulfiram. The compound degrades after only three hours incubation in human plasma (Figure 3).

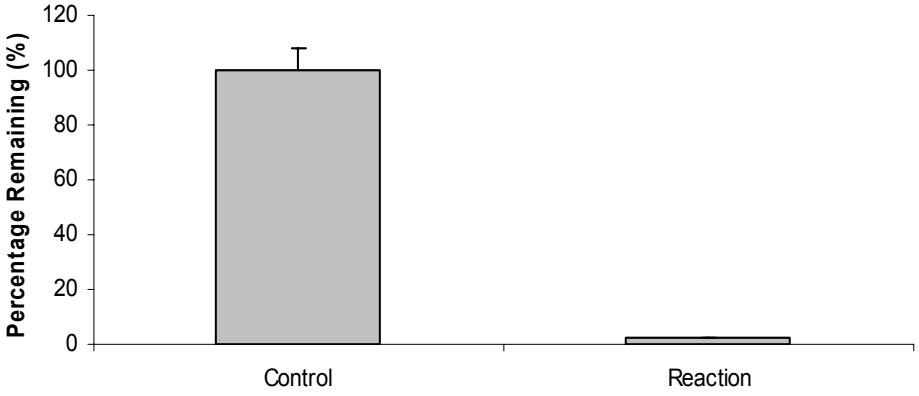

Figure 3. Plasma stability of disulfiram after 3hr incubation.

2.5. Gastric fluid stability

Genearal Method. Simulated gastric fluid was prepared according to the United States Pharmacopeia (USP) description: “Dissolve 2.0 g of sodium chloride and 3.2 g of purified pepsin, which is derived from porcine stomach mucosa, with an activity of 800 to 2500 units per mg of protein, in 7.0 mL of hydrochloric acid and sufficient water to make 1000 mL”. The solution has a pH of 1.2. The assay was carried out as depicted in Figure 4. Briefly, 3.2 mg pepsin was added to 1 ml semi-prepared simulated gastric fluid (SIF) (Fisher scientific, Pittsburg, PA). 10 μM compound was spiked into SIF and quenched by adding a 50-fold volume of base to neutralize the acid at different time intervals. The control was the reaction with compound directly spiked into PBS solution.

The stability was calculated by comparing the percentage remaining of parent compound relative to control reactions.

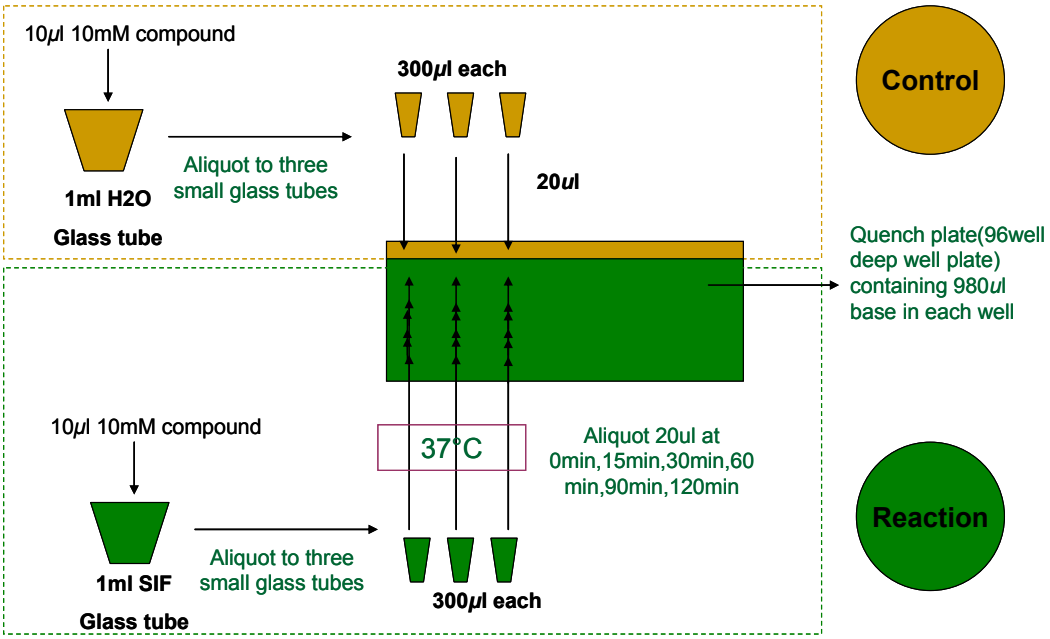

Figure 4. Experimental design of gastric fluid stability assay.

Assay Validation: The method was validated with erythromycin and clarithromycin using multiple time points (Figure 5).

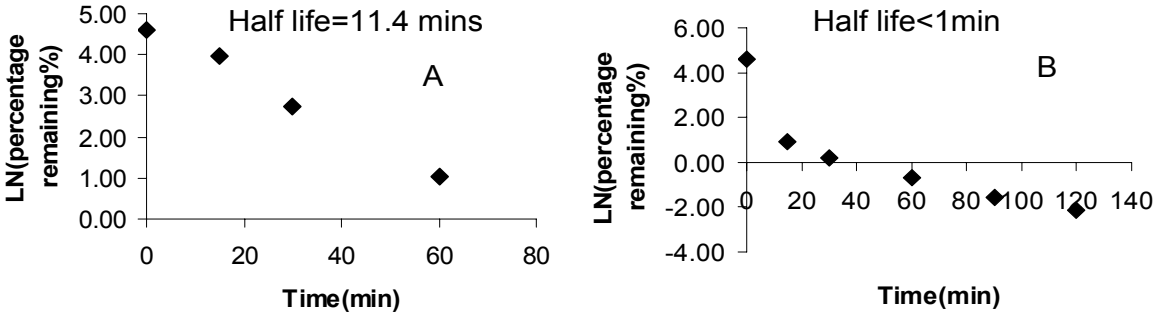

Figure 5. **Simulated gastric fluid stability of clarithromycin (A) and erythromycin (B).**

2.6. Simultaneous quantitation of metabolites of multiple cytochrome P450 substrates

The cocktail of substrates contained melatonin (CYP1A1/2), coumarin (CYP2A6,), bupropion (CYP2B6), amodiaquine (CYP2C8), tolbutamide (CYP2C9), omeprazole (CYP2C19), dextromethorphan (CYP2D6), and midazolam (CYP3A4).

LC-MS condition. Quantitative analysis of probe substrate metabolites were carried out using LC-MS-MS with an Agilent 1200 series HPLC system interfaced to an Agilent 6410 triple quadrupole mass spectrometer. Aliquots (5 μL) of each sample were analyzed using a Waters XTerra MS C18 (50 × 2.1 mm, 2.5 μm) reversed-phase column with a linear gradient from 0.1% formic acid in water (solvent A) to methanol (solvent B): 5 to 30% B over 1 min; and 30 to 70% B over the next 6 min. The flow rate was 0.4 mL/min. Positive ion electrospray was used for the measurement of each metabolite. The selected reaction monitoring (SRM) transitions for each analyte and limit of quantitation (LOQ) are listed in TABLE II. The eight metabolites and internal standard were well separated by chromatography (Figure 6).

TABLE II. SRM TRANSITIONS AND LOQ OF METABOLITES

Metabolites	Retention time (min)	Transition	Fragmentor	CE	LOQ(μM)
6-hydroxymelatonin(CYP1A1/2)	4.0	249.1-->190	115	9	0.3
7-hydroxycoumarin (CYP2A6)	4.6	163-->107	130	25	0.01
hydroxybupropion(CYP2B6)	3.8	256.1-->238.1	85	9	0.001
desethylamodiaquine(CYP2C8)	1.6	328-->283	125	16	0.04
5-hydroxyomeprazole(CYP2C9)	5.6	362.1-->264	100	9	0.002
hydroxytolbutamide(CYP2C19)	5.3	287.1-->89	115	45	0.002
dextrophan(CYP2D6)	3.8	258.2-->199.1	130	25	0.0005
1'-hydroxymidazolam (CYP3A4)	5.4	342.1-->324	150	17	0.002
phenacetin(Internal standard)	5.1	180.1-->110.1	130	21	/

LOQ:limit of quantitation

SRM: Selected reaction monitoring

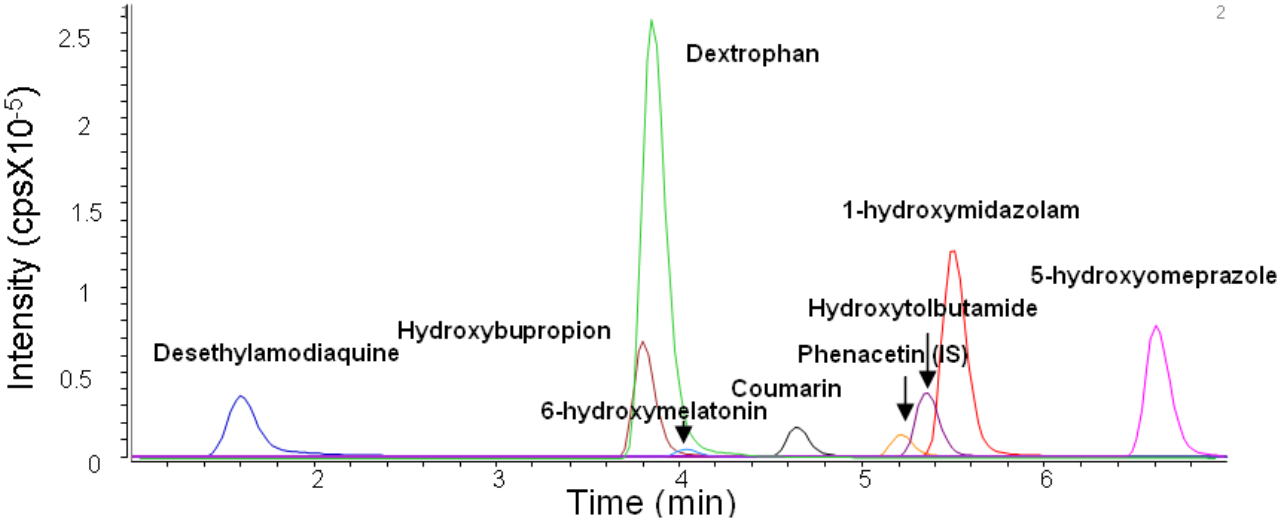

Figure 6. Chromatography of metabolites of eight CYP substrates and internal standard phenacetin.

2.7. Cytochrome P450 inhibition assay

Cocktail substrates concentration. Melatonin (CYP1A1/2) and tolbutamide (CYP2C9) were tested at 4 μM. Coumarin (CYP2A6), amodiaquine (CYP2C8) and

omeprazole (CYP2C19) were tested at 2 μM. Buproprion (CYP2B6), midazolam (CYP3A4) and dextromethorphan (CYP2D6) were tested at 1, 0.4 and 0.2 μM, respectively

General method. Compounds (25 μL) were serially diluted in PBS buffer and the same volume was preincubated with 25 μL liver microsomes (0.1 mg/ml protein) for 2 minutes at 37 °C. Then 25 μL NADPH and 25 μL substrate cocktail were added to initiate the reaction. After 20 minutes incubation at 37 °C, the reaction was quenched by adding a 3-fold volume of acetonitrile containing the internal starandard phenacetin. After centrifuging at 10,000 g for 30 minutes, the supernatants were injected into LC-MS/MS for analyisis.

Method validation. Multiple inhibitors for corresponding CYP enzymes were selected according to FDA guidance for drug-drug interactions. The experimental IC_{50} values were comparable to the literature reported values thus validating the assay (Figure 7).

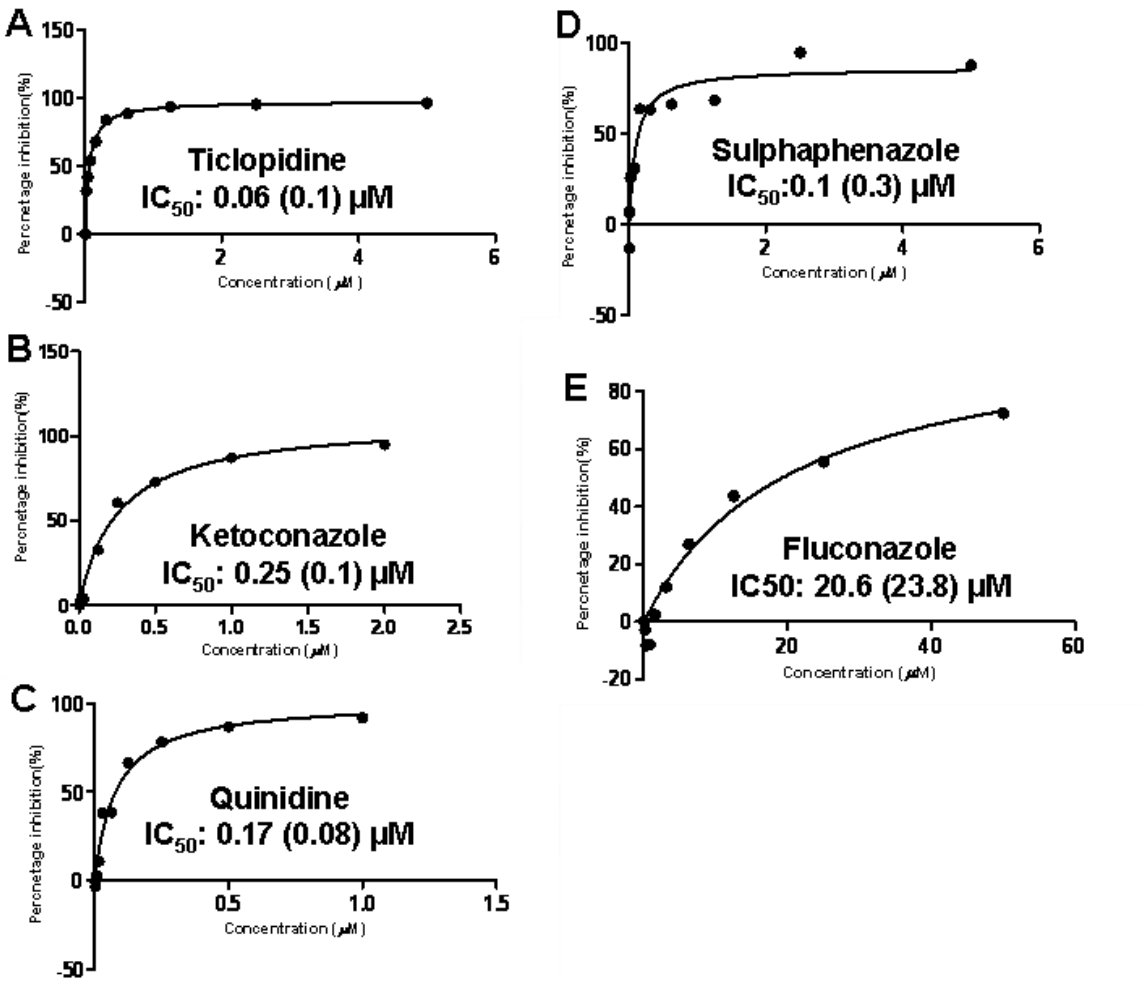

Figure 7. Validation of cytochrome P450 inhibition assay.
Cytochrome P450 inhibition of CYP2B6 (A), CYP3A4 (B), CYP2D6(C), CYP2C9 (D), CYP2C19(E) by ticlopidine, ketoconazole, quinidine, sulphaphenazole, fluconazole, respectively. The experimental IC_{50} values are very similar to literature reported values (in parentheses).

2.8. Cytochrome P450 induction assay

Cocktail substrates concentration. Cocktail substrate mixture contained chlorzoxazone (CYP2E1) at 60 µM; melatonin (CYP1A1/2) and tolbutamide (CYP2C9) at 40 µM; coumarin (CYP2A6), amodiaquine (CYP2C8) and omeprazole (CYP2C19) at 20 µM; bupropion (CYP2B6) and testosterone (CYP3A4) at 10 µM; midazolam

(CYP3A4) and dextromethorphan (CYP2D6) at 4 μM and 2 μM, respectively. All substrates were dissolved in low serum medium (2% FCS, 100 units/ml penicillin, 100 μg/ml streptomycin, 0.5 μg/ml insulin, 2 mM glutamine, and 5×10^{-5} M hydrocortisone).

General method. For general maintenance of cell cultures, HepaRG cells were seeded in 25 cm^2 flasks with a starting density of 2.6×10^4 cells/cm^2 in the growth medium (Biopredict ® Rennes, France; documented composition: Williams' E medium supplemented with 10% FCS, 100 units/ml penicillin, 100 *μ*g/ml streptomycin, 5 *μ*g/ml insulin, 2 mM glutamine, and 5×10^{-5} M hydrocortisone). The medium was replenished every two or three days. The cells continued proliferating until reaching confluence after two weeks. The cells were then trypsinized and passaged (Figure 8).

Low density culturing protocol. Cells were seeded and maintained according to the general maintenance protocol except cells were cultured in 12/96 well supports. After two weeks, cultures attaining confluence were shifted to differentiation medium (Biopredict ® Rennes, France; the same as growing culture medium except being supplemented with 2% DMSO) for two more weeks in order to obtain differentiated cells for induction assay (Figure 8).

High density culturing protocol. Cells were seeded and maintained according to the general maintenance protocol in T25 flasks for two weeks before being shifted to differentiation medium (Biopredict ® Rennes, France, the same as growing culture medium except being supplemented with 2% DMSO) for another two weeks. The cells were then trypsinized and passaged to fresh supports for induction assay (Figure 8).

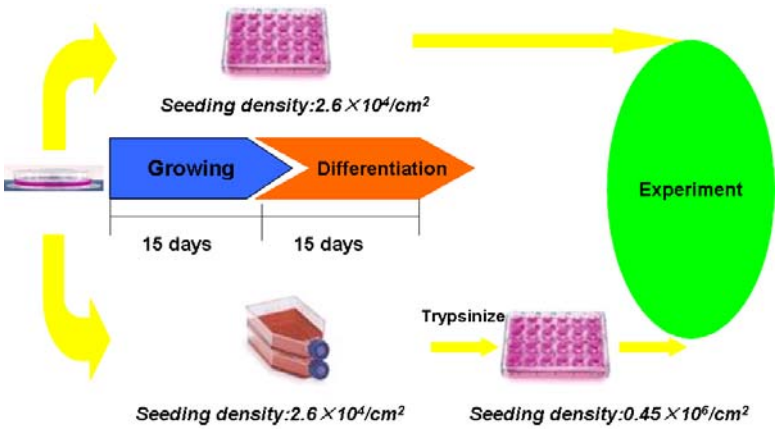

Figure 8. **A flow chart showing the culture of HepaRG cells in commercial medium.**

Induction assay. HepaRG cells were seeded and maintained in 96-well plates following low density culturing protocol. After four weeks, media (100 µL) with different concentrations of inducers were added into testing wells with differentiated HepaRG cells. After incubation for 72 h, 100 µL substrate cocktail in medium was added to each well. The induction of CYP1A1/2, CYP2B6, CYP2C9, CYP2C19, and CYP3A4 activity by each inducer was determined simultaneously by measuring the metabolite concentration of each probe substrate using LC-MS-MS (section 2.6).

Functional assay. Cells were incubated in substrate cocktail medium for 24 hours. The medium was transferred in a 96-well plate and mixed with a two-fold volume of acetonitrile. The sample was then centrifuged at 10000 g for 30 minutes. The supernatant was injected to LC-MS-MS. CYP1A1/2, CYP2B6, CYP2C9, CYP2C19, and CYP3A4 activity were determined simultaneously by measuring the metabolite concentration of each probe substrate (section 2.6).

Method validation: this assay was validated using the benchmark compounds rifampin and phenobarbital dissolved in commercial medium. Medium (100 µL) with different concentrations of inducers was added to the testing wells containing differentiated HepaRG cells. After incubation for 72 h, 100 µL substrate cocktail medium was added to each well. The induction of CYP1A1/2, CYP2B6, CYP2C9, CYP2C19, and CYP3A4 activity by each compound was determined simultaneously by measuring the metabolite concentration of each probe substrate using LC-MS-MS (Figure 9).

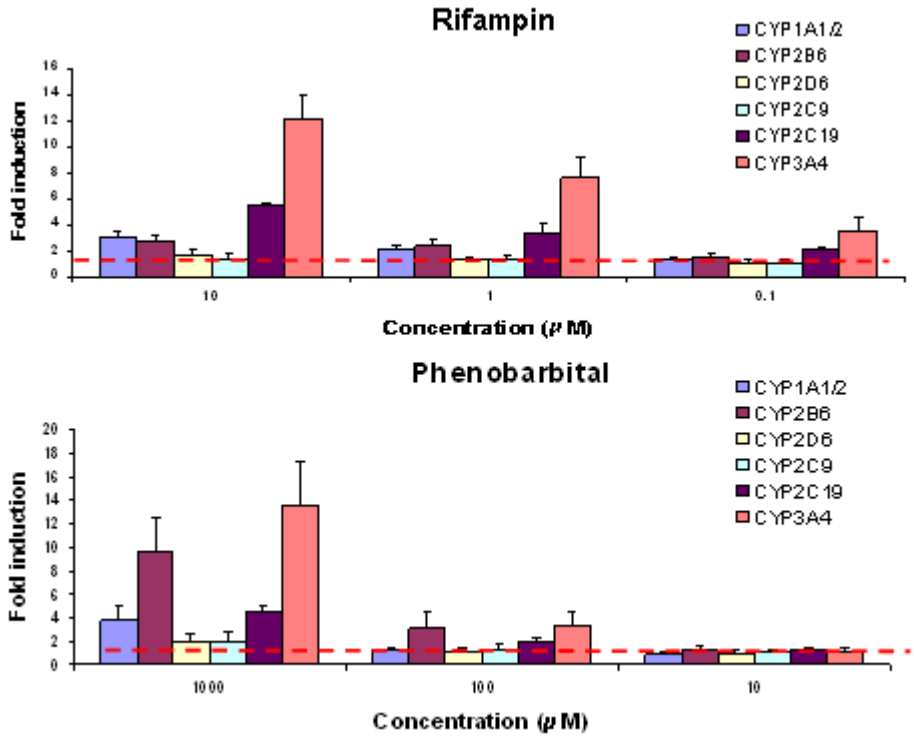

Figure 9. Validation of induction assay in commercial medium by rifampin and phenobarbital.
Both rifampin and phenobabital can induce selected liver enzymes in a dose response manner.

2.9. Multiplex toxicity assay

General Method. Toxicity was assessed by measuring four parameters (assays): intracellular ATP content (Cell Titer Glo), cellular necrosis (via adenylate kinase activity; ToxiLight), intracellular esterase activity and cell membrane integrity, the latter two measured in a single assay (Calcein-AM). Briefly, HepG2 cells were seeded in 96-well plate with a density of 5000 cells/well (in 50 µl medium). After 3 hours culture, 50 µL test compounds were then added to the wells (DMSO concentration<0.2%). After three days incubation, three assays were performed to test the cytotoxicity of compounds from the same plate (Figure 10).

1) ToxiLight. 10 µL medium was transferred from the cell culture plates into another plate and mixed with 50 µL reconstituted ToxiLight assay reagent in luminescence-compatible plates. After 5 minutes incubation, luminescence signal was measured using a Victor plate reader (Perkin Elmer, Waltham, MA).
2) Calcein-AM. Medium was removed and cells washed in PBS three times. 100 µL of assay reagent containing 400 nM calcein-AM was added to each well and incubated at 37 °C for at least 30 minutes. Fluorescence was measured at excitation and emission wavelengths of 490 nm 510 nm, respectively, using a Victor plate reader (Perkin Elmer, Waltham, MA).
3) Celltiter Glo: After the calcein-AM assay, the calcein-AM assay reagent was removed and the cells were rinsed with PBS. 50 µl PBS and 50 µl Celltiter Glo assay reagent was added to each well and mixed for for 2 minutes. After 15 minutes of incubation, the mixture was transfered to white opaque plates and

luminescence measured using a Victor plate reader (Perkin Elmer, Waltham, MA).

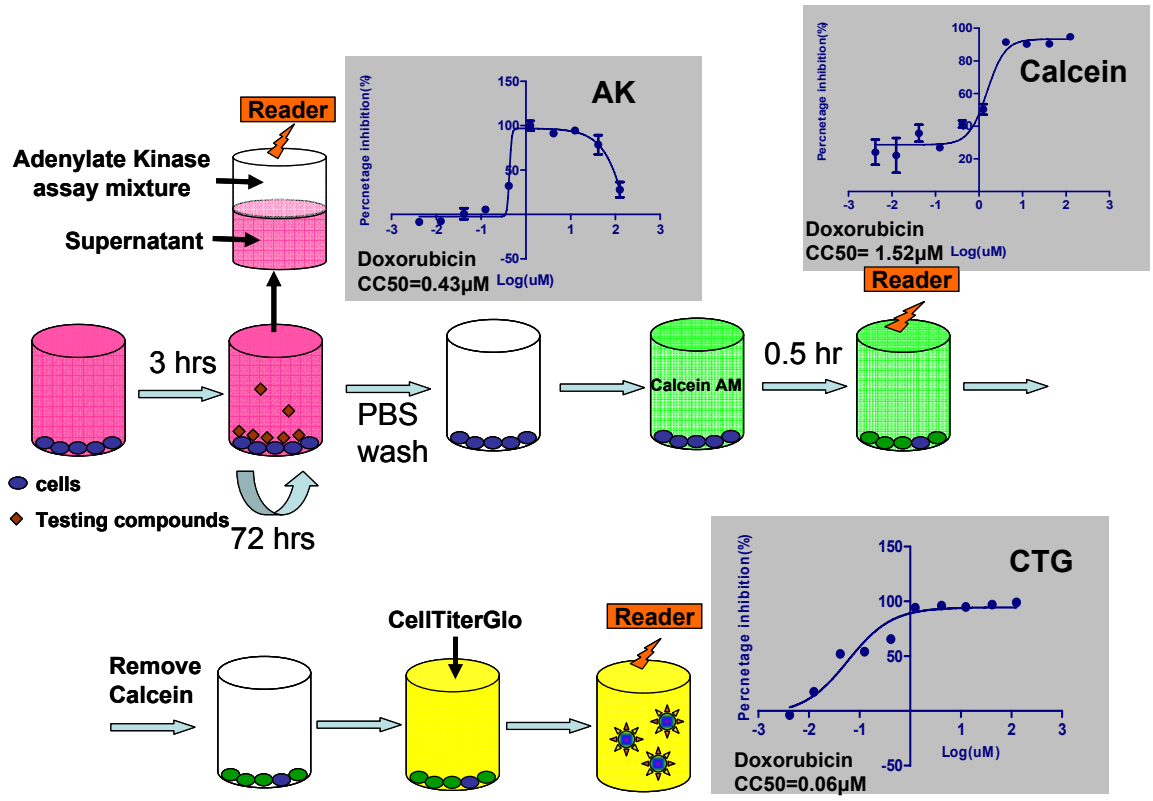

Figure 10. Experimental design of the multiplex toxicity assay.
The cytotoxicity dose response curves of doxorubicin are shown for three parameters. AK, adenylate kinase activity was measured by ToxiLight; Calcein, intercellular esterase activity and membrane integrity were measured by calcein-AM stain; CTG, intracellular ATP content was measured by Celltiter Glo.

Assay Validation. This three-parameter cytotoxicity assay was performed with a panel of seven toxic compounds, each with a different mechanism of toxicity (TABLE

III). For each compound, cytotoxicity (CC_{50}) by all three parameters was determined after 72 hours exposure (TABLE IV).

TABLE III. TOXIC COMPOUNDS AND RESPECTIVE MECHANISMS USED FOR ASSAY VALIDATION.

Compounds	Toxicology
Doxorubicin	Intercalate DNA
Podophyllotoxin	Microtublin inhibitor
Rotenone	Mitochondria inhibitor
Vinblastine	Microtublin inhibitor
Puromycin	Ribosome inhibitor
CCCP	Mitochondria inhibitor
Valinomycin	Ionophore; Potassium transporter

TABLE IV. CC_{50} OF TOXIC COMPOUNDS IN THE MULTIPLEX ASSAY.

Compounds	Adenylate Kinase (μM)	Calcein-AM (μM)	CellTiter Glo (μM)
Doxorubicin	0.43	1.52	0.06
Podophyllotoxin	>125	0.02	0.02
Rotenone	11.54	16.76	0.01
Vinblastine	83.56	<0.004	<0.004
Puromycin	1.23	0.91	0.43
CCCP	14.93	7.46	3.31
Valinomycin	22.37	1.19	<0.004

2.10. Metabolite toxicity assay using HepaRG cells

General Method. Briefly, HepG2 cells were seeded at $5X10^3$ cells/well in 96-well plates before co-incubation with compounds for 72 hours. HepaRG cells were seeded with a density of 2.6×10^4 cells/cm^2 in 96-well supports and cultured under the low density protocol (section 2.8) for 4 weeks before adding compounds previously

dissolved in growing medium. After 72 hours incubation cell viability was evaluated following the Celltiter Glo assay protocol described above.

Assay Validation. The cytotoxicity of aflatoxin B1 is mediated by CYP1A2 and CYP3A4-generated metabolites (*69*). The dose-response curves of aflatoxin B1 for HepG2 and HepaRG cells suggested the latter to be more sensitive (Figure 11), presumably due to the generation of a toxic metabolites by CYP enzymes in HepaRG cells. For the compounds with toxic metabolite(s), HepaRG is a model superior to HepG2 model.

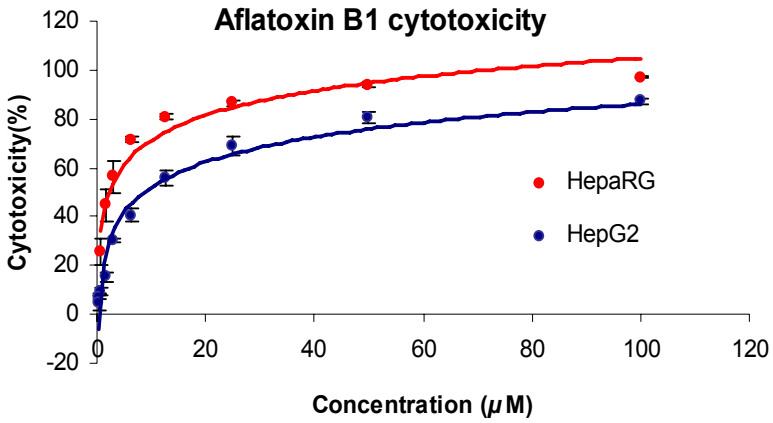

Figure 11. Comparative cytotoxicity dose-response of aflatoxin B1 in HepaRG and HepG2 cells.

3. DRUG METABOLISM AND ANALYTICAL STUDY OF ESTABLISHED ANTI-TB DRUGS

3.1. Introduction

As mentioned in Chapter 1 (section 1.4), most existing anti-TB drugs were discovered and developed before today's in vitro ADMEt methods were available. As a result, ADMEt properties of most existing drugs were studied through clinical trials and there were few ADMEt studies using in vitro methods. The lack of in vitro ADMEt data prevents the establishment of in vitro-in vivo correlations which are essential to build predictive in vitro models for TB drug discovery. In this chapter, we performed retrospective in vitro ADMEt studies on existing anti-TB drugs, specifically using drug metabolism methods. For existing drugs that have been studied neither by in vivo nor in vitro ADMEt methods, this research represented the first attempt to understand their ADMEt properties. For existing drugs that have been studied using in vivo ADMEt methods, the in vitro ADMEt data presented here can complement our current understanding. With the application of established metabolism methods (Chapter 2) and mass spectrometry technologies, two major goals were proposed.

Anti-TB drugs are typically used in combinations in order to avoid the emergence of drug-resistant strains. However, there are few analytical methods to detect multiple TB drugs simultaneously within a single run from clinical plasma samples. In 2005, Chen and colleagues developed a method for simultaneous measurement of isoniazid and ethambutol with LOQs of 10 ng/ml for both drugs (*70*). In 2007, Song and colleagues reported a LC-MS-MS based method to quantify four first-line TB drugs simultaneously (*71*). However, this method was not fully validated for drug stability and

interday precision variability. The LOQ of this method was relatively high for rifampin (100 ng/ml), isoniazid (50 ng/ml), ethambutol (50 ng/ml) and pyrazinamide (1000 ng/ml) (*71*), preventing this method from being useful for plasma samples that have low drug concentrations. Therefore, the first goal was to develop and validate a more sensitive method for analysis of more than four anti-TB drugs in clinical research setting.

Most of the first-line and second-line anti-TB drugs were discovered in the 1950s to 1960s. There was a lack of published data on their in vitro metabolic stability. It would be beneficial to the scientific community to investigate and document the metabolic characteristics of these established drugs and compare their stability data to those of screening hits derived from large scale anti-TB compound screens. Therefore, the second goal was to study the in vitro metabolic stability of existing TB drugs.

This chapter presents, 1) a LC-MS-MS-based quantification method that can quantify 15 anti-TB drugs in human plasma simultaneously with improved detection sensitivity compared with the previously published method (*71*). These TB drugs include moxifloxacin, ethambutol, isoniazid, levofloxacin, pyrazinamide, linezolid, LL3858, PA-824, rifampin, ethionamide, thioridazine, TMC 207, clarithromycin, clofazimine and OPC 67683; 2) the metabolic stability of fifteen TB drugs evaluated in human and mouse microsomes using this new method; and 3) the major metabolites of unstable anti-TB candidate drug LL3858 were characterized by tandem mass spectrometry for the first time.

3.2. Materials and methods

3.2.1. Chemicals and biological matrices

Rifampin, isoniazid, pyrazinamide, ethambutol, 6-aminonicotinamide, thiocetazone, rifaximin, and ethionamide were purchased from Sigma (St. Louis, MO). Levofloxacin was purchased from Fluka, Inc. (St. Louis, MO). Moxifloxacin, linezolid, LL3858, PA-824, TMC207, clarithromycin, clofazimine and OPC 67683 were obtained from Southern Research Institute (Birmingham, AL). Acetonitrile and HPLC grade water were purchased from Sigma (St. Louis, MO). The quantitative data processing was carried out using Analyst software (AB SCIEX, Foster City, CA).

3.2.2. Instrumentation

Quantitative analysis of established drugs was performed using LC-MS-MS with a Shimadzu Prominence HPLC interfaced to an Applied Biosystems (Foster City, CA) SCIEX 4000 QTrap mass spectrometer.

3.2.3. Standard solutions

Ten milligram per milliliter stock solutions of moxifloxacin, ethambutol, isoniazid, levofloxacin, and pyrazinamide were prepared in 50% v/v methanol and those of linezolid, PA-824, and rifampin were prepared in 100% methanol. Stock solutions of 1 mg/ml ethionamide, thioridazine, and TMC 207 were prepared in 50% v/v and those of clarithromycin, clofazimine, and LL3858 were prepared in 100% methanol. A stock solution of OPC 67683 was prepared at 200 µg/ml in 100% methanol. All stock solutions were stored in -80°C. All stock solutions were subsequently serially diluted in 75% methanol to produce working solutions of moxifloxacin, ethambutol, isoniazid,

levofloxacin, pyrazinamide, linezolid, PA-824, rifampin at 500, 200,100, 50, 20, 10, 5, 2, 1, 0.5, 0.2, 0.1, 0.05, 0.02, 0.01, 0.005, 0.002, and 0.001 µg/ml; of ethionamide, thioridazine, TMC 207, clarithromycin, clofazimine, LL3858 at 50, 20,10, 5, 2, 1, 0.5, 0.2, 0.1, 0.05, 0.02, 0.01, 0.005, 0.002, and 0.001 µg/ml; and of OPC 67683 at 10, 5, 2, 1, 0.5, 0.2, 0.1, 0.05, 0.02, 0.01, 0.005, 0.002, 0.001, 0.0005, and 0.0002 µg/ml. Calibration standards were prepared by adding 5 µl of each working solution to 45 µl human plasma. Final standard concentrations in plasma were 50, 20,10, 5, 2, 1, 0.5, 0.2, 0.1, 0.05, 0.02, 0.01, 0.005, 0.002, and 0.001 µg/ml for moxifloxacin, ethambutol, isoniazid, levofloxacin, pyrazinamide, linezolid, PA-824, and rifampin; 5, 2, 1, 0.5, 0.2, 0.1, 0.05, 0.02, 0.01, 0.005, 0.002, 0.001, 0.0005, 0.0002, and 0.0001 µg/ml for ethionamide, thioridazine, TMC 207, clarithromycin, clofazimine, and LL3858; and 1, 0.5, 0.2, 0.1, 0.05, 0.02, 0.01, 0.005, 0.002, 0.001, 0.0005, 0.0002, 0.0001, 0.00005, and 0.00002 µg/ml for OPC 67683 .

The stock solutions for quality control (QC) were prepared by separately weighing each individual compound and dissolving in 75% methanol. The concentrations of moxifloxacin, ethambutol, isoniazid, levofloxacin, pyrazinamide, linezolid, PA-824, and rifampin were 500 µg/mL; the concentrations of ethionamide, thioridazine, TMC 207, clarithromycin, clofazimine, and LL3858 were 50 µg/mL; and the concentration of OPC 67683 was 10 µg/mL. QC samples were prepared at three levels: 10, 1, and 0.1 µg/mL for moxifloxacin, ethambutol, isoniazid, levofloxacin, pyrazinamide, linezolid, PA-824, and rifampin; 1, 0.1 and 0.01 µg/mL for ethionamide, thioridazine, TMC 207, clarithromycin, and clofazimine, and 0.2, 0.02 and 0.02µg/mL for OPC

67683. The calibration standards and QC samples were stored in -80°C. Samples were thawed at room temperature before use.

Three internal standards were applied in the quantitation method. Stock solutions of rifaximin and thiacetazone were prepared in methanol at 5 mg/mL and 2.5 mg/mL, respectively, and a stock solution of 6-aminonicotinic acid was prepared in water at 500 µg/mL. Stock solutions were further diluted with acetonitrile to obtain working internal standard solutions of 62.5 ng/mL, 125 ng/mL, 625 ng/mL of rifaximin, thiacetazone, and 6-aminonicotinic acid, respectively.

3.2.4. Sample preparation procedures

Ice cold acetonitrile containing internal standard (200 µl) was added to plasma samples (50µL). The samples were then centrifuged at 10,000 g for 30 min to remove protein precipitates. The final sample solution (1 µL) was injected for LC-MS-MS analysis.

3.2.5. Liquid chromatography

Chromatographic separation was carried out on an Agilent (Santa Clara,CA) aqueous SB Aq (50 × 2.1 mm, 1.8 µm) column. The column oven temperature was controlled at 40°C. Processed samples were kept in an auto-sampler at 4°C. A linear gradient from 0.1% formic acid in water (solvent A) to acetonitrile (solvent B) was used as follows: 5-35% B for the first 1.5 minutes; 35%-75% for the next 1.5 minutes; and 75%-95% for another 2 minutes. The flow rate was 0.5 mL/min and the injection volume was 1 µL.

3.2.6. Mass spectrometry

Parameters for mass spectrometry were as follows: GS1, 60 psi; GS2, 40 psi; curtain gas, 20 psi; temperature, 500 °C; curtain gas: 20 psi; and needle voltage, +5.5 kV. The selected reaction monitoring (SRM) and retention times for all the compounds and internal standards are listed in TABLE V.

TABLE V. SRM TRANSITION TABLE OF ANTI-TB DRUGS AND INTERNAL STANDARDS

Compd.	SRM ion pairs (m/z)	Dwell time (ms)	DP (Volts)	CE (Volts)	CXP(Volts)	RT (min)
Clarithromycin	748.61-->590.05	50	126	25	8	3.8
Clofazimine	473.12-->431.10	50	181	49	12	4.43
Ethambutol	205.21-->116.00	50	71	21	6	0.98
Ethionamide	167.13-->107.10	50	96	37	6	2.65
Isoniazid	138.04-->121.00	50	81	21	6	1.38
Levofloxacin	362.15-->318.10	50	116	27	8	3.07
Linezolid	338.15-->296.23	50	126	27	8	3.76
LL3858	520.40-->290.00	50	101	23	8	3.96
Moxifloxacin	402.20-->384.24	50	126	31	10	3.37
OPC67683	535.18-->352.10	50	121	37	8	4.38
PA-824	360.13-->175.10	50	126	35	12	4.55
Pyrazinamide	124.00-->81.10	50	51	24	14	2.69
Rifampin	823.50-->791.40	50	146	27	12	4.13
Thioridazine	371.20-->126.14	50	116	33	8	3.96
TMC-207	557.20-->539.20	50	106	27	8	4.36
6-aminonicotinic acid (IS1)	139.10-->93.00	50	86	29	6	1.37
TAC (IS2)	237.00-->220.1	50	76	17	14	3.5
Rifaximin (IS3)	786.39-->754.20	50	146	31	22	4.78

3.2.7. Method validation

Method validation followed the “Bioanalytical Method Validation” guidance provided by FDA (72). The following parameters were evaluated: accuracy, linearity, selectivity, intra and interday precision, recovery, matrix effect and stability.

3.2.7.1. Accuracy, precision, lower limit of detection, lower limit of quantitation

These analyses were all evaluated at three concentrations with five replicates. The accuracy was calculated as the percentage of calculated concentration over the nominal concentration of each sample. The bias percentage should be within 15% of samples at three concentrations. Intraday precision was calculated by analyzing five different samples in the same batch within the same day. Interday precision was calculated by analyzing samples prepared on five different days. The acceptable precision should be within 15% for samples at three concentrations. LOQ is the lowest concentration that is within the linear range of regression and has a signal-to-noise ratio higher than 10. LOD is the detection limit with signal to noise ratio higher than 3.

3.2.7.2. Recovery and matrix effects

Three sets of samples were prepared to calculate recovery and matrix effects. The first set was regularly prepared samples as quality controls with three concentrations. The second set was the same concentration of compounds spiked in organic solvent instead of plasma. The third set consisted of spike-after-extraction samples. Blank human plasma was processed the same as regular samples by protein precipitation with acetonitrile containing internal standard. High, medium, and low concentrations of samples were prepared by spiking the compounds into the supernatants.

The recoveries were calculated by comparing mean concentrations of samples from the first set at low, medium, and high QC concentrations with the mean

concentrations of spike-after-extraction samples from the third set, which represented 100% recovery.

The matrix effects were calculated by comparing the mean concentration of spike-after-extraction samples from the third set with the mean concentrations of samples from the second set in organic solvent, which represented zero matrix effects.

3.2.7.3. Linearity and selectivity

On each day during a five day period, a single calibration curve was obtained. Linear regression was applied to achieve a linear calibration curve with appropriate weighting factor. Selectivity was evaluated by processing and analyzing six different sources of blank human plasma samples and comparing with the peak of each compound at its LOD.

3.2.7.4. Stability evaluation

Four stability tests were performed according to the requirements of the FDA guidance (*72*). These tests include long term storage stability, freeze & thaw stability, room temperature stability, and stock solution stability.

Long term storage stability. Samples were freshly prepared and stored at -20 °C for 28 days. The samples were then prepared by protein precipitation and compared with freshly prepared QCs as 100% stable standards.

Freeze & thaw stability. Samples were freshly prepared and stored at -80°C. Samples were thawed to room temperature and frozen again on each day. After three

such freeze-thaw cycles, samples were then prepared by protein precipitation and compared with freshly prepared QCs as 100% stable standards.

Room temperature stability. Spiked samples were freshly prepared and left at room temperature for 24 hours before being analyzed. Freshly prepared QCs were used as 100% stable controls.

Stock solution stability. Compound stock solutions were freshly prepared and held for 24 hours at room temperature before being diluted and analyzed. Freshly prepared stock solutions were used as 100% stable controls.

3.2.8. Metabolite identification of LL3858

LL3858 stock solutions were prepared in DMSO. The final concentration of DMSO in the incubation buffer was 0.2% (v/v). The 50 μM test compound solutions were incubated with 1 mg/ml mouse microsomes and 1 mM NADPH for 60 minutes at 37 °C. The reaction was quenched with three-fold ice-cold acetonitrile before centrifuging at 10000 g for 30 minutes. Samples were dried under cold nitrogen flow. The reconstituted sample was injected in LC-MS-MS for analysis.

Metabolite identification of LL3858 was carried out with an Applied Biosystems Q-trap 4000 mass spectrometer. Aliquots of 5 μL of each sample were analyzed using a Waters XTerra MS C18 (100 × 2.1 mm, 3.5 μm) reverse-phase column. A linear gradient from 0.1% formic acid in water (solvent A) to 0.1% formic acid in acetonitrile (solvent B) was used as follows: 5-65% B for 65 minutes. The flow rate was 0.2 mL/min. Positive ion electrospray was used for the detection of LL3858 and its metabolite. The

column temperature was 40 °C, and the autosampler was maintained at 4°C. The electrospray voltage was 4 kV, and the capillary temperature was 300°C.

3.3. Results

3.3.1. Chromatography of 15 established and experimental drugs in human plasma

Fifteen established and experimental anti-TB drugs were well separated within a 5 minute gradient. The retention times of the low, medium and high polarity standards spanned the retention times observed with 15 drugs (Figure 12).

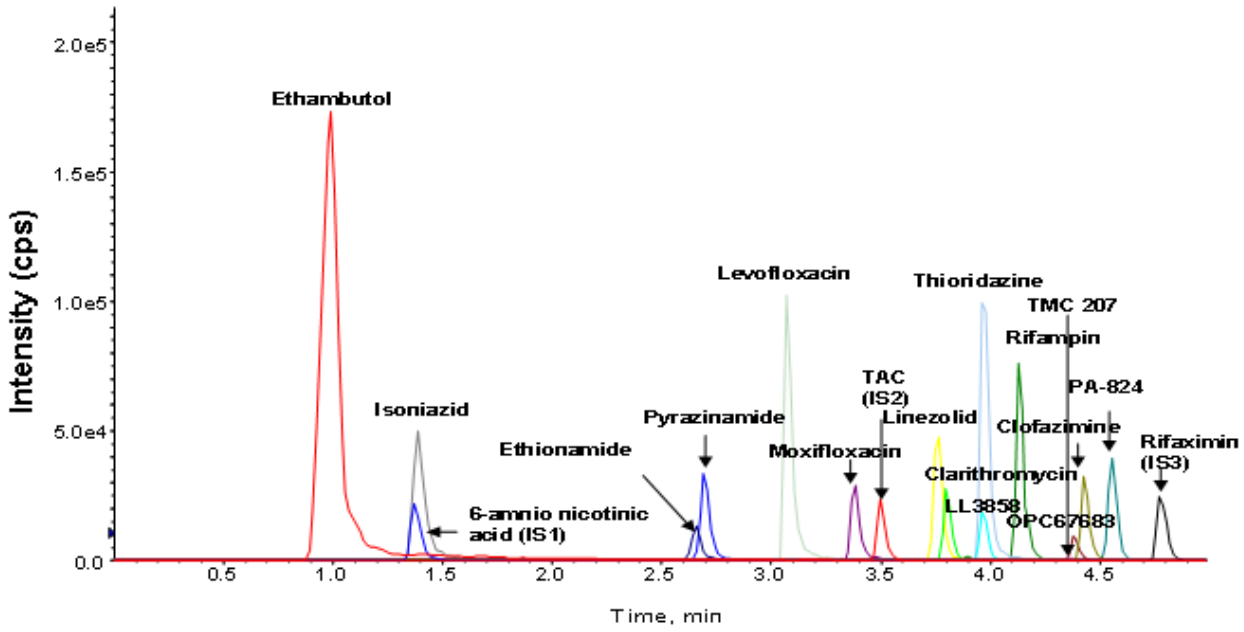

Figure 12. LC/positive ion electrospray total ion chromatrography of 15 TB established ,experimental drugs and internal standards.

3.3.2. Method validation

The method was validated for simultaneous quantitation of 15 anti-TB established and experimental drugs in human plasma (TABLE VI and TABLE VII). The

LOD of each compound was lower than the MIC. C_{max} values of 14 drugs were within their corresponding linear range except for PA824, which needed additional dilution. The linear ranges of TMC207 and LL3858 were relatively narrow as compared with other drugs. The in-source fragmentation of LL3858 could possibly explain the narrow linear range of this compound (section 3.3.4). Of particular interest was that the quality control and calibration standards of ethionamide and OPC67683 must be freshly prepared in parallel in order to achieve more accurate and consistent data. This is presumably due to instability (TABLE VII) .The recovery was not 100% for all the drugs. However, the recovery of internal standards was consistent during the analysis of all samples in the batch. There was no obvious matrix effect on those drugs over their corresponding retention times.

Ethionamide was found to be unstable at room temperature or after freeze-thaw cycles that could possily be explained by the oxidation of the sulfur atom. OPC67683 was found to be unstable after either long-term storage at -20°C, room temperature storge or three freeze–thaw cycles. These samples must be analyzed with fresh material and avoiding freeze-thaw cycles. Those compounds should also be analyzed as quickly as possible to avoid degradation. All other compounds showed excellent stability under the experimental conditions.

TABLE VI. LINEAR RANGE, LOQ, LOD, ACCURACY, INTERDAY/INTRADAY PRECISION, MATRIX EFFECT AND RECOVERY OF THE ESTABLISHED AND EXPERIMENTAL ANTI-TB DRUGS*

			Calibration curves		Precision , (CV%)					
Drugs	C_{max} (ng/ml)	MIC (ng/ml)	Linear range (ng/ml)	IS	QC (ng/ml)	Accuracy (%)	Intraday (n=5)	Interday (n=5)	LLOQ (ng/ml)	LLOD (ng/ml)
Pyrazinamide	40000	6000~50000	50~50000	IS1	10000	108.3%	3.3%	4.5%	50	20
					1000	102.6%	1.4%	4.4%		
					100	95.2%	7.4%	3.5%		
Ethambutol	5000	100	20~10000	IS1	10000	96.1%	2.6%	4.8%	20	2
					1000	108.9%	2.9%	3.5%		
					100	102.1%	6.1%	2.5%		
Rifampin	15000	400	10~50000	IS3	10000	108.0%	5.0%	3.5%	10	5
					1000	101.1%	6.3%	2.8%		
					100	93.2%	3.7%	9.4%		
Isoniazid	7000	25	50~50000	IS1	10000	107.7%	0.9%	3.0%	50	20
					1000	110.1%	1.1%	1.8%		
					100	107.9%	8.4%	5.8%		
Thioridazine	150	10000	1~5000	IS2	1000	95.6%	4.3%	3.1%	1	0.1
					100	102.5%	3.9%	5.4%		
					10	105.8%	1.6%	5.5%		
TMC-207	1000	60	100~2000	IS2	1000	101.3%	5.0%	4.2%	100	50
					100	80.7%	5.1%	13.0%		
PA-824	25000	12	20~5000	IS3	1000	96.4%	1.4%	3.0%	20	10
					100	95.9%	3.8%	6.7%		
Moxifloxacin	3000	500	50~50000	IS2	10000	112.9%	2.1%	3.8%	50	5
					1000	96.5%	1.1%	2.4%		
					100	96.1%	5.2%	10.2%		
LL3858	NA	25~120	20~500	IS3	100	110.3%	8.4%	13.7%	20	5
Linezolid	13000	250	20~50000	IS1	10000	96.1%	3.2%	5.3%	20	5
					1000	99.5%	6.6%	5.0%		
					100	97.0%	6.4%	4.7%		
Levofloxacin	12000	500	10~10000	IS1	10000	100.1%	6.6%	2.4%	20	10
					1000	108.6%	4.8%	2.6%		
					100	105.9%	4.6%	4.1%		
Clarithromycin	1000	8000	2~1000	IS3	1000	99.0%	5.7%	3.1%	2	0.5
					100	112.4%	3.8%	2.7%		
					10	114.7%	4.4%	4.2%		
Ethionamide	2000	250	10~5000	IS1	1000	113.4%	5.1%	4.6%	10	5
					100	108.1%	5.8%	5.4%		
					10	88.5%	12.3%	8.9%		
OPC67683	500	12	10~1000	IS3	1000	22.6%	2.3%	4.2%	10	5
					100	22.3%	2.3%	3.4%		
Clofazimine	150	100	5~1000	IS3	1000	102.3%	2.8%	3.6%	5	0.5
					100	103.9%	3.6%	3.5%		
					10	104.3%	4.8%	7.4%		

***C_{max} values were obtained from reference (*25*).**

TABLE VII. RECOVERY, MATRIX EFFECT, LONG TERM, FREEZE & THAW, ROOM TEMPERATURE, STOCK SOLUTION STABILITY OF ESTABLISHED AND EXPERIMENTAL ANTI-TB DRUGS

Drugs	QC (ng/ml)	Recovery	Matrix Effects	Long term -20°C storage stability (28days)	Three Freeze&Thaw Cycles stability	Room Temperat-ure 24hour stabiliy	Room Temperature Stock solution 24hour stabiliy
Pyrazinamide	10000	80%	No	97%	104%	102%	101%
	1000	76%	No	107%	108%	106%	99%
	100	78%	No	98%	107%	97%	102%
Ethambutol	10000	81%	No	91%	98%	99%	95%
	1000	63%	78%	97%	100%	104%	104%
	100	60%	71%	97%	97%	91%	110%
Rifampin	10000	108%	73%	74%	102%	95%	91%
	1000	92%	No	107%	97%	101%	92%
	100	82%	No	74%	107%	74%	85%
Isoniazid	10000	73%	No	76%	87%	86%	100%
	1000	69%	No	96%	98%	104%	100%
	100	71%	No	45%	96%	76%	105%
Thioridazine	1000	106%	No	98%	99%	98%	94%
	100	90%	No	108%	100%	102%	87%
	10	93%	No	101%	108%	98%	77%
TMC-207	1000	55%	78%	101%	87%	92%	94%
	100	43%	80%	102%	90%	95%	92%
PA-824	1000	105%	78%	120%	106%	102%	95%
	100	104%	84%	111%	120%	105%	112%
Moxifloxacin	10000	92%	No	96%	99%	97%	100%
	1000	84%	No	107%	101%	98%	101%
	100	87%	No	117%	107%	96%	98%
LL3858	100	112%	71%	121%	104%	106%	96%
Linezolid	10000	75%	No	98%	103%	103%	101%
	1000	69%	No	101%	105%	107%	97%
	100	66%	No	98%	101%	98%	104%
Levofloxacin	10000	82%	No	93%	100%	99%	97%
	1000	68%	No	98%	103%	102%	95%
	100	70%	No	107%	98%	93%	114%
Clarithromycin	1000	100%	80%	95%	99%	100%	96%
	100	99%	80%	116%	101%	106%	102%
	10	95%	90%	109%	116%	95%	111%
Ethionamide	1000	94%	No	63%	63%	59%	106%
	100	93%	No	96%	101%	102%	102%
	10	94%	No	75%	96%	63%	114%
OPC67683	1000	83%	84%	14%	3%	2%	91%
	100	85%	84%	33%	25%	28%	88%
Clofazimine	1000	79%	68%	96%	92%	90%	89%
	100	66%	79%	117%	94%	97%	96%
	10	63%	91%	102%	117%	96%	91%

3.3.3. Metabolic stability of established and experimental anti-TB drugs

The metabolic stabilities of 15 existing and experimental anti-TB drugs were determined in human microsomes and rank ordered (TABLE VIII). Among the top five unstable drugs, four (ethionamide, thioridazine, isoniazid, TMC207) have been previously reported to have active metabolites (*25-26*). LL3858, was found to be relatively unstable in both mouse and human liver microsomes. Despite an extensive literature search, no reports were found regarding the metabolic stability of LL3858.

TABLE VIII. LIVER MICROSOME METABOLIC STABILITY OF THE ESTABLISHED AND EXPERIMENTAL ANTI-TB DRUGS

Drugs	Half life (mins)	
	Mouse	Human
Ethionamide	31	6
Thioridazine	35	18
LL3858	40	36
Isoniazid	262	59
TMC-207	193	63
PA-824	67	79
OPC67683	92	103
Rifampin	62	171
Linezolid	50	172
Pyrazinamide	>300	221
Ethambutol	>300	280
Clofazimine	>300	281
Clarithromycin	89	287
Moxifloxacin	>300	287
Levofloxacin	>300	>300

3.3.4. Metabolite identification of LL3858

A total of four hydroxylated metabolites were characterized for LL3858 (Figure 13). LL3858 fragmented in-source to form abuandant ions of *m/z* 231 and *m/z* 290 with dissociation of the methylene bond (Figure 14).

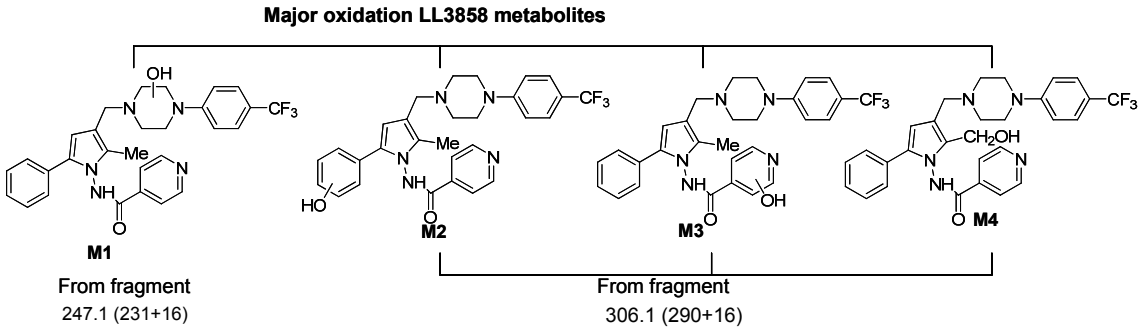

Figure 13. Summary of proposed hydroxylation metabolites structures of LL3858.

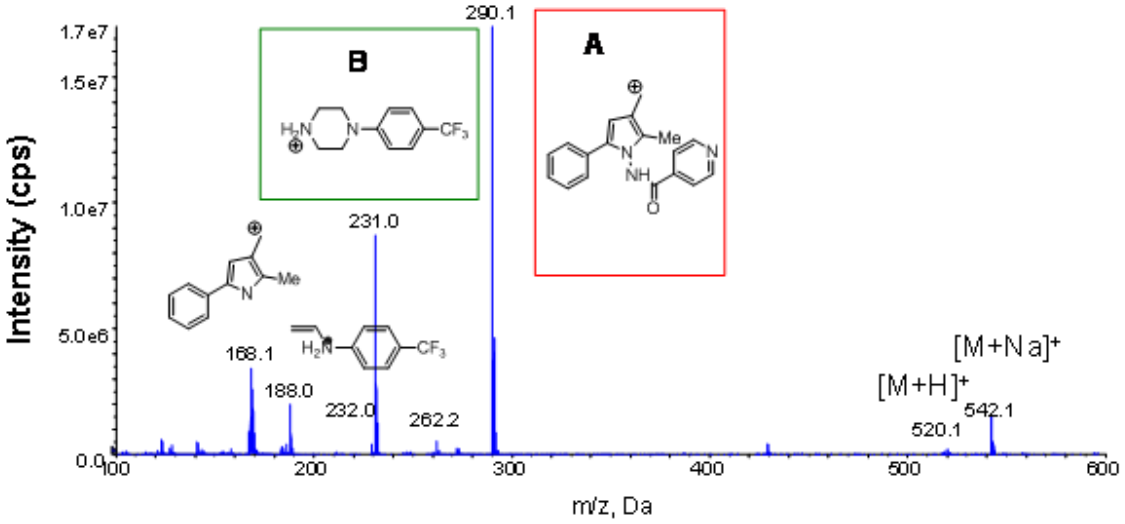

Figure 14. Spectrum of in-source fragmentation of LL3858.
Two major fragments were detected as m/z 290 (A) and m/z 231 (B) with the dissociation of the methylene linker.

Four major hydroxylation metabolites (**M1, M2, M3, and M4**) of *m/z* 538 were detected following incubation with human microsomes (Figure 15). **M1** showed hydroxylation on the m/z 231 fragment; and the ion of *m/z* 290 of **M2, M3, M4** with 16 unit higher than the corresponding ion of *m/z* 290 indicating addition of oxygen. The fragmentation pathways of m/z 231 and m/z 290 were elucidated (Figure 16).

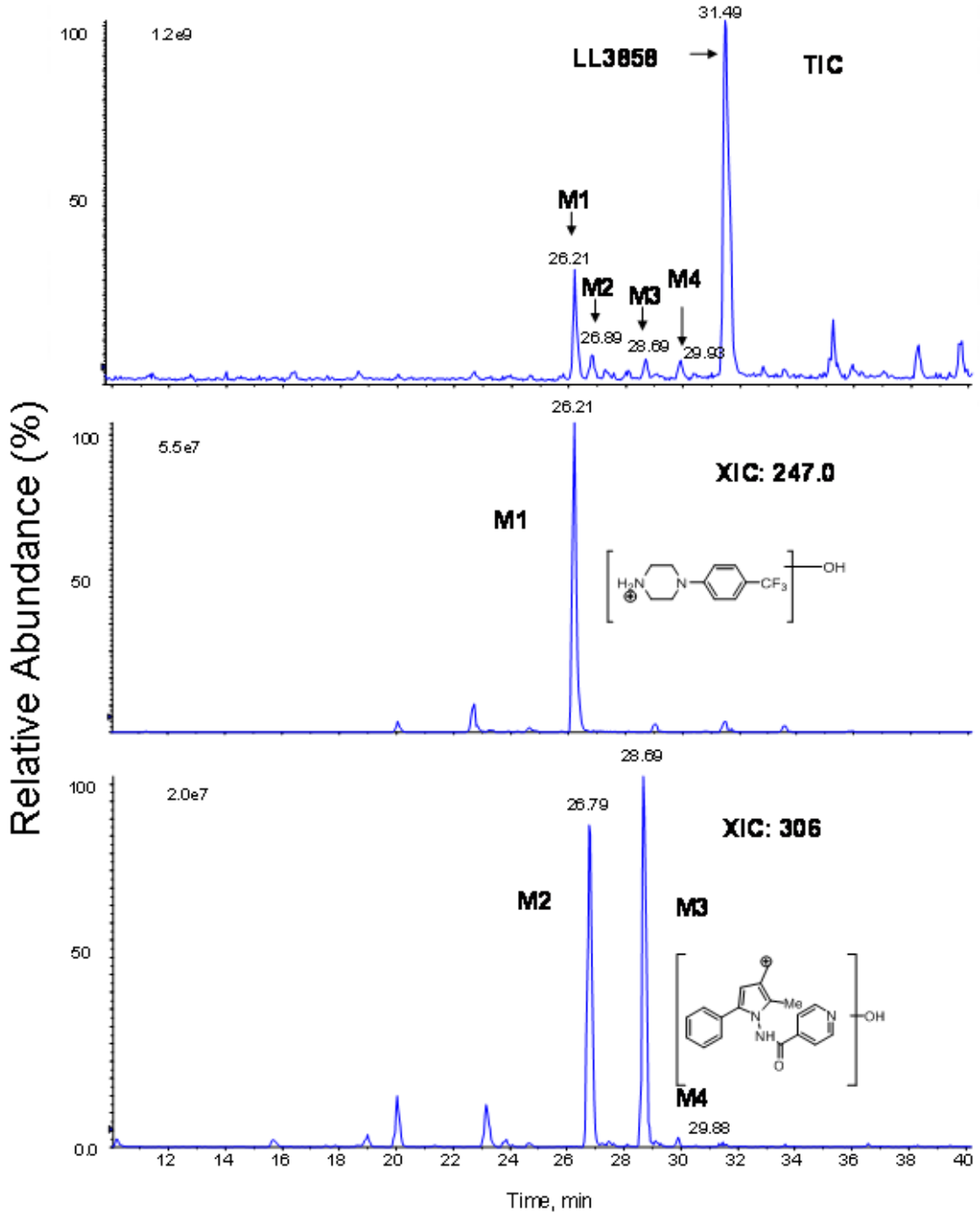

Figure 15. **Major hydroxylation metabolites of LL3858 in human microsomes.**

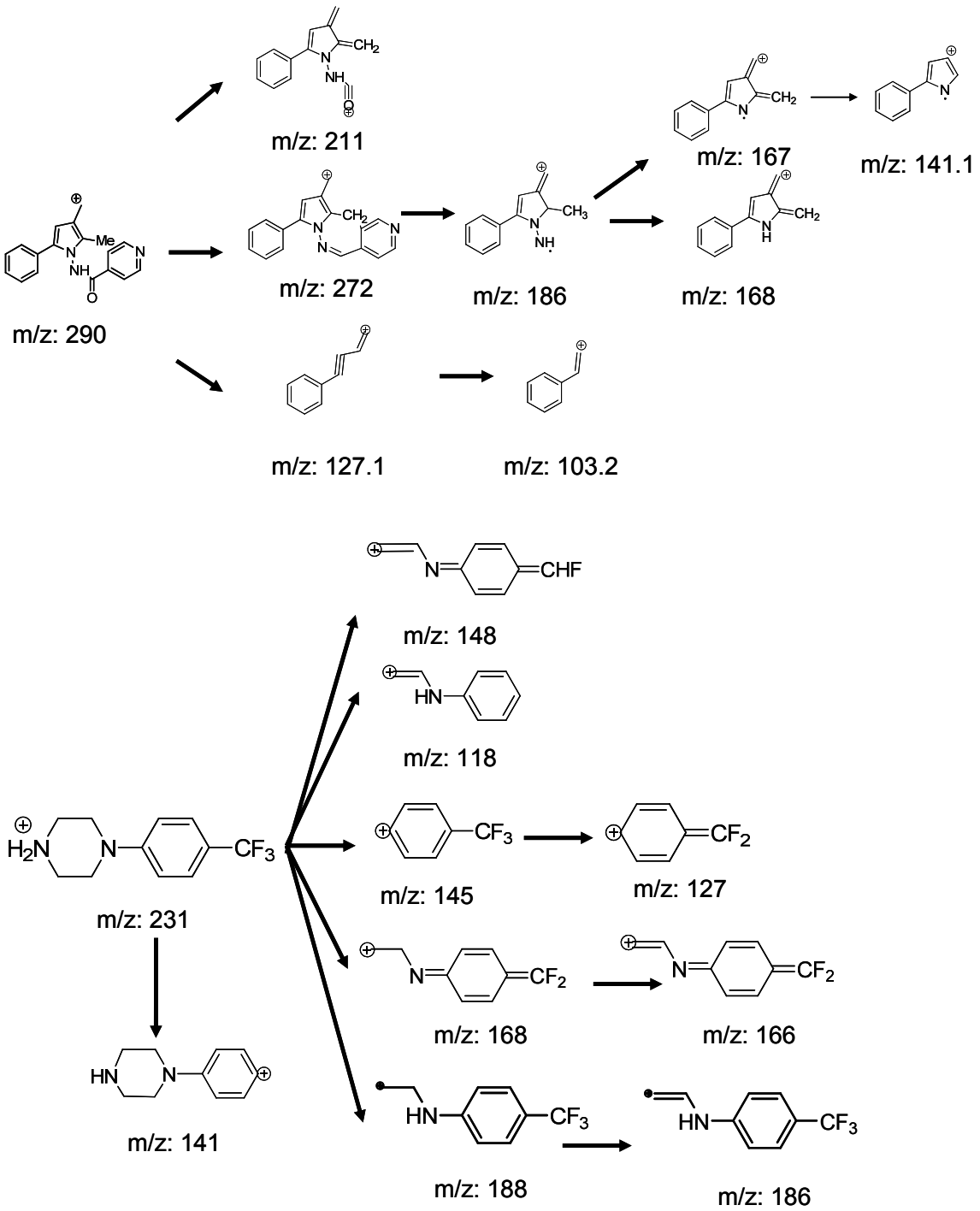

Figure 16. **Proposed in-source fragmentation of *m/z* 290 and *m/z* 231 from LL3858.**

Structure elucidation of **M1** (Figure 17): Comparing the tandem mass spectra of in-source fragment ions of *m/z* 231 from LL3858 and *m/z* 247 from **M1**, the structure of **M1** was proposed. The same *m/z* 127 ion was detected in the spectra of both LL3858 and **M1**, indicating that hydroxylation was not on the phenyl ring of the structure. The other ions shared by the two spectra had *m/z* of 166 and 188, indicating half of the piperazine ring and the phenyl ring remained unchanged. However, there were 16 unit mass shifts from fragments *m/z* 118, 168 and 186 to *m/z* 134, 184, 202 respectively, which suggested that the hydroxylation reaction occurred on the other symmetric half of the piperazine ring (Figure 16).

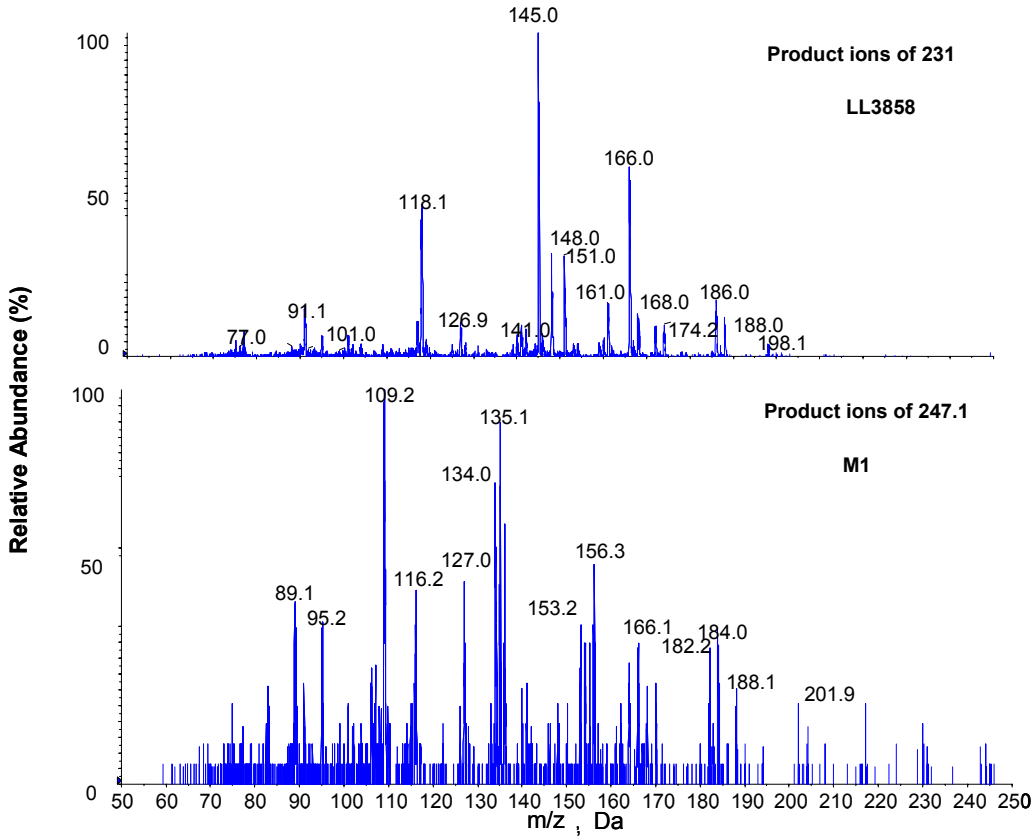

Figure 17. Positive ion electrospray tandem mass spectrometrya of in source fragmentation of *m/z* 231 ion and *m/z* 247 ions from LL3858 and M1.

Structure elucidation of **M2** (Figure 18): comparing the tandem mass spectra of in-source fragment ions of m/z 290 from LL3858 and *m/z* 306 from **M2**, the structure of **M2** was proposed. There was a 16 unit mass shift for fragments *m/z* 167, and 168 to 183 and 184 which suggested that the hydroxylation was on the 5-methyl-2-phenyl-3H-pyrrole substructure. The 16 unit mass shift of fragment *m/z* 103 to *m/z* 119 suggested reaction sites on the phenyl ring and the C-5 methyl group of the pyrrole ring. The observed quantum fragment of LL3858 and **M2** indicates a 16 unit shift from

phenylammonium (*m/z* 104) to hydroxyl- phenylammonium (*m/z* 120) which indicates the location of hydroxylation sites on the phenyl ring and the C-5 carbon of the pyrrole ring (unpublished data). Since there were no unsaturated electron pairs on the C-5 carbon of the pyrrole ring, the hydroxylation site was proposed to be on the 2-phenyl ring.

Structure elucidation of **M3** (Figure 18): comparing the tandem mass spectra of in-source fragment ions of *m/z* 290 from LL3858 and m/z 306 from **M3**, the structure of **M3** was proposed. The *m/z* of 211 remained unchanged in the **M3** spectrum which suggested that the N-(2-methyl-5-phenyl-pyrrole) substructure was not hydroxylated. Therefore, the 16 unit shift from m/z 290 to m/z 306 indicated that the hydroxylation site of **M3** was on the pyridine ring.

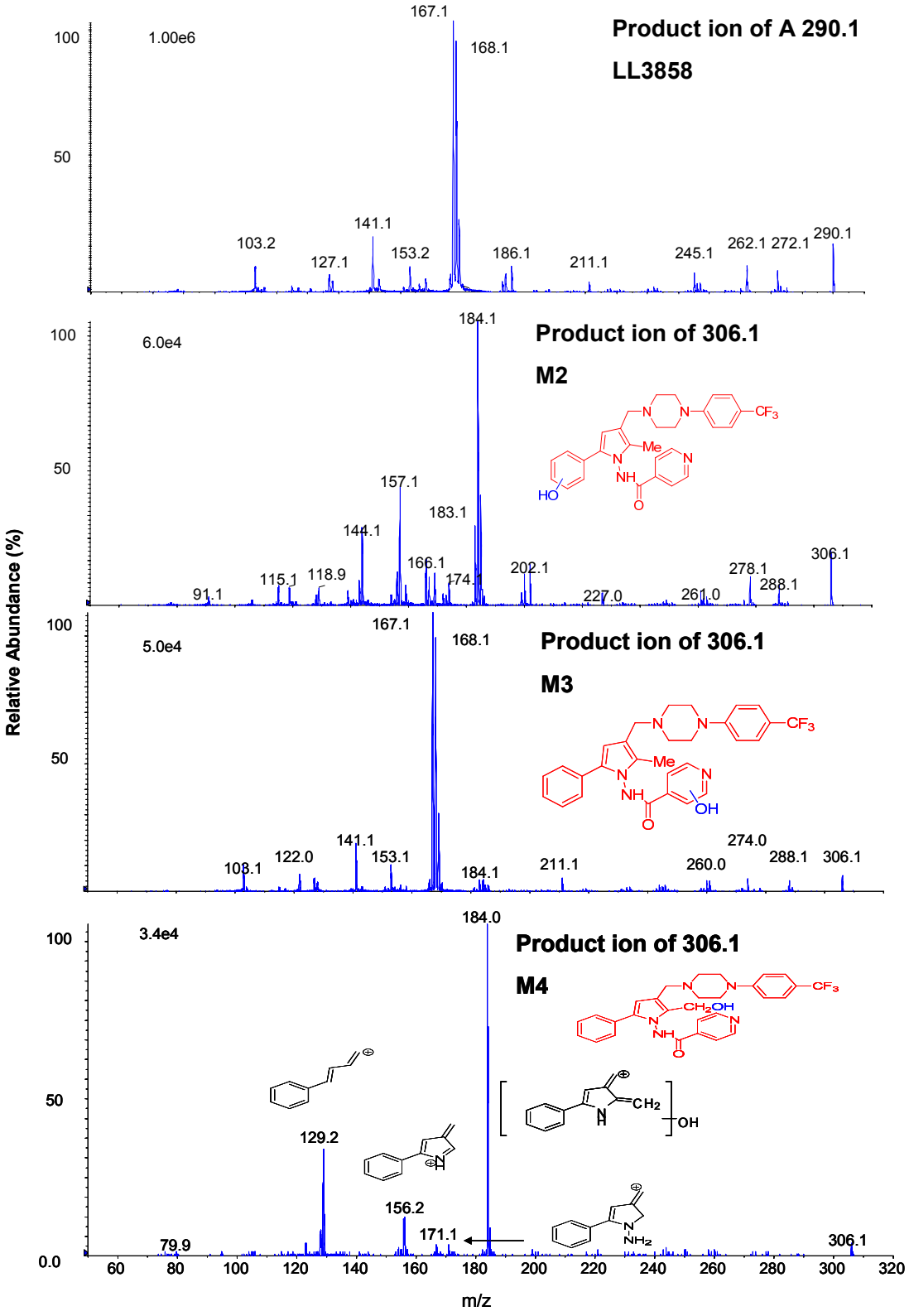

Figure 18. Tandem mass spectrometry of in source fragment ion *m/z* 290 ion from LL3858 and *m/z* 306 ions from M2, M3 and M4.

Structure characterization of **M4** (Figure 18): comparing the tandem mass spectra of in-source fragment ions of *m/z* 290 from LL3858 and *m/z* 306 from **M4**, the structure of **M4** was proposed. The fragments of **M4** showed a unique pattern that was different from those of LL3858. The fragment ion of *m/z* 129 suggested that hydroxylation was not on the buta-1,3-dienylbenzene following the dissociation of the pyrrole ring. The fragment ion of *m/z* 156 and *m/z* 171 suggested that the hydroxylation was not on the pyrrole ring, the phenyl ring or the methylene linker. Instead, the 16 unit mass shift of the ion of *m/z* 168 to m/z 184 suggested that the hydroxylation site of **M4** was on the C-2 methyl substituent of the pyrrole ring.

3.4. Discussion

In this chapter, retrospective drug metabolism studies were performed on 15 existing anti-TB drugs. An analytical method was developed and validated, which could simultaneously quantitate 15 existing and experimental anti-TB drugs from human plasma samples in one run. This appears to be the first bio-analytical method that is capable of quantitating more than four anti-TB drugs simultaneously in one run. Compared with a previously reported method, which could simultaneously quantitate four anti-TB drugs in one run, the method presented here gave an equal, or up to 10-fold lower, limit of quantitation (LOQ) (*71*). Therefore, this research method offers higher throughput and more sensitivity than the previous published method.

Out of a total of 23 established and experimental anti-TB drugs, 15 were selected in this bioanalysis method development. Eight drugs were not included either due to availability problems or poor ionization during LC-MS-MS analysis.

In general, the most appropriate internal standard for the analysis of clinical samples should have similar structure and polarity with analytes and have a wider linear range with less matrix effect. In selecting the internal standard compounds, 6-amnionicotinic acid (similar structure to isoniazid) and thiacetazone were chosen because they are rarely used as clinical drugs. Therefore although their LC and ionization properties are similar to some anti-TB drugs, they are less likely to exist in patient plasma samples. Likewise, rifaximin, a clinical drug for gastrointestinal infections with a structure that is similar to the anti-TB drug rifampin, is not orally absorbed, making it an ideal internal standard for rifampin.

The assay development and validation process followed FDA guiance. The described method could be applied in pharmacokinetic and drug-drug interaction studies of the majority of existing anti-TB drugs. This method has potential applications in both the pharmaceutical industry and in clinical studies. However, ethionamide and OPC 67683 were not stable after storage at room temperature, -20 °C, or three freeze-thaw cycles. This problem would eventually limite the wider application of this method in the quantitation of these two drugs, especially if the plasma samples required long distance transportation and/or long-term storage. Stabilizing reagents could be considered for addition to the plasma.

The next step was to determine the in vitro stability for all 15 anti-TB drugs in both mouse and human microsomes. Five drugs were relatively unstable in both mouse and human microsomes; four of those drugs had previously been reported to be metabolically unstable and to have active metabolites. To the best of our knowledge, this is the first comprehensive study of in vitro metabolic stability covering the majority of the existing anti-TB drugs. This data set suggested that a good anti-TB drug should either be stable in microsomes or have anti-TB active metabolites.

There appears to be no reports, published or unpublished, regarding the metabolic stability of LL3858 which is in Phase I clinical trial for the treatment of TB. The experimental data, however, showed that LL3858 was metabolically unstable and the structures of its metabolites were subsequently elucidated. This finding greatly improved our understanding of this anti-TB drug candidate. Further efforts should focus on synthesis of the proposed metabolites to test their activity against *M. tuberculosis*. If the

metabolites exhibit in vitro activity, they could be evaluated as anti-TB drugs with possibly superior PK properties and less toxicity.

The metabolic stability data of 15 established and experimental anti-TB drugs suggests that active metabolites are not rare among this group of agents. Therefore, further study of the metabolites of both existing anti-TB drugs and experimental anti-TB compounds may be of value. Likewise it may not be wise to triage metabolically unstable hits which arise in drug discovery screening programs prior to assessing their anti-TB activity.

4. METABOLISM-GUIDED HIT-TO-LEAD OPTIMIZATION IN ANTI-TB DRUG DISCOVERY

4.1. Introduction

The search for new drugs to combat *M. tuberculosis* was the focus of our efforts in this chapter. Toward this end, we utilized a high-throughput screening (HTS) protocol based upon whole-cell anti-TB activity in both replicating and non-replicating TB cultures (*58*). From year 2006 to 2010, three combinatory libraries ('NOVACore' library, Analyticon library and Asinex library) were screened to find new chemical scaffolds for 'next generation' of anti-TB drugs.

Multiple screening hits emerging from the HTS campaigns were classified to different series according to the chemical structures. Metabolic stability of these hits was evaluated. A very high percentage of hits was subjected to extensive metabolic biotransformation. In one of those screening compaigns, a 50K compound library (Asinex, Moscow, Russia) was screened for activity against replicating *M. tuberculosis* using MABA (*58*). Eighteen structurally diverse compounds with MIC lower than 3 μM were selected and tested for their metabolic stability (TABLE IX). Unexpectedly 17 of the 18 compounds had a half-life shorter than 45 minutes (the predicted hepatic plasma clearance was proportional to 75% of *in vivo* plasma flow) in mouse microsomes and 6 of the 18 compounds had a half-life shorter than 15 minutes (the predicted plasma clearance was proportional to 75% of *in vivo* plasma flow) in human microsomes. Metabolism-guided hit-to-lead optimization was thus carried out to block the metabolic 'soft-spots' in order to create more stable lead compounds (Figure 19). In this chapter,

two case studies of metabolism-guided hit-to-lead optimization are presented, one involving isoxazoles and the other tetrahydroindazoles.

TABLE IX. METABOLIC STABILITY AND MABA MIC VALUES FOR HITS OBTAINED FROM A HTS OF AN ASINEX DIVERSE LIBRARY.

Compound ID	Structure	Half life(min) (Mouse)	Half life(min) (Human)	MIC (μM)	Compound ID	Structure	Half life(min) (Mouse)	Half life(min) (Human)	MIC (μM)
BAS 17695625	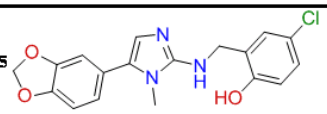	6.45	11.49	0.39	SYN 17217303	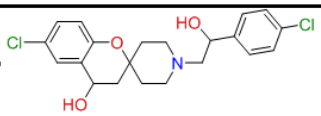	14.3	45.23	2.60
SYN 15580680	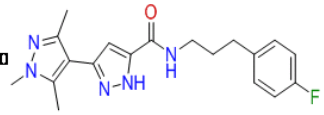	4.52	170.09	0.40	BAS 9867525	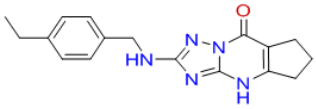	46.51	68.48	2.77
BAS 2140188	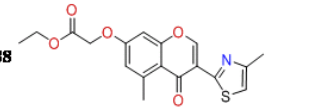	2.67	2.59	0.74	BAS 1862286	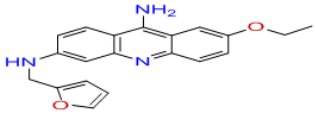	3.70	9.03	2.96
SYN 15601582	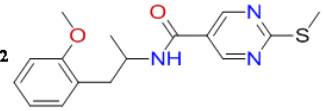	2.04	9.97	1.10	ASN 06579147	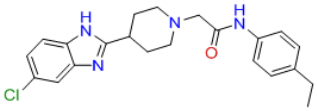	7.58	16.79	0.32
SYN 15446686	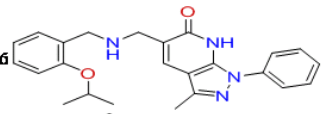	4.6	22.14	1.20	AOP 22094683	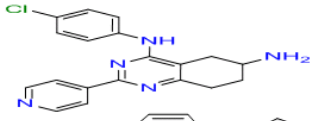	40.99	126.57	0.60
BAS 00888826	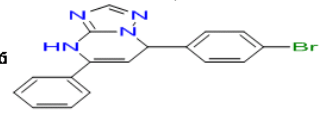	3.12	14.45	2.24	BAS 00363727	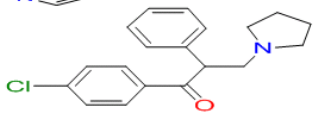	12.63	42.95	1.05
BAS 3655882	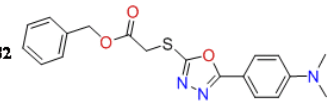	3.59	3.13	2.29	SYN 15557523	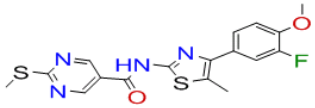	13.34	39.37	1.40
AOP 22296754	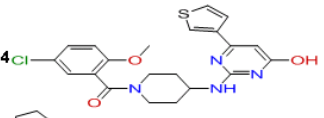	3.90	15.84	2.45	SYN 17217307	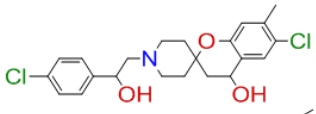	6.15	38.15	2.30
ASN 10814475	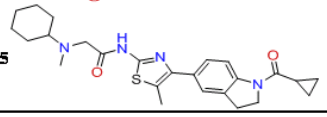	3.73	3.54	2.50	SYN 15560571	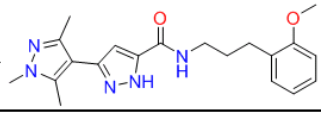	4.68	24.3	3.30

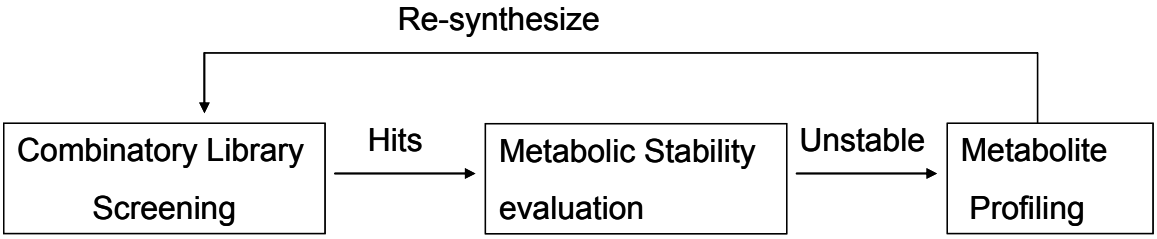

Figure 19. Scheme of metabolism-guided hit-to-lead optimization.

4.2. Materials and methods

4.2.1. Chemicals and reagents.

Reference compounds were synthesized in-house.

4.2.2. MABA

The *in vitro* potency of compounds against replicating *M. tuberculosis* was assessed by the MABA assay (*58*). The stock concentration of compounds was 12.8 mM. Two-fold dilutions of compounds were prepared in Middlebrook 7H12 medium (7H9 broth containing 0.1% w/v casitone, 5.6 µg/mL palmitic acid, 5 mg/mL bovine serum albumin, 4 mg/mL catalase, filter-sterilized) in a volume of 100 µL in 96-well microplates (black plates). 100 µL 7H12 medium containing 2×10^5 cfu/mL *M. tuberculosis* H37Rv was inoculated in the plates, yielding a final testing volume of 200 µL. The plates were incubated at 37 °C. On the 7th day of incubation 12.5 µL of 20% Tween 80 and 20 µL of alamar blue were added to the test plate. After incubation at 37

°C for 16-24 h, fluorescence of the wells was measured (ex 530, em 590 nm). The MICs were defined as the lowest concentration effecting a reduction in fluorescence of 90% relative to the mean of replicate bacteria-only controls. Reported MICs were an average of two individual measurements.

4.2.3. LORA

A low-oxygen adapted culture of recombinant H37Rv (pFCA-luxAB), expressing a *Vibrio harveyii* luciferase gene with an acetamidase promoter, was grown in a BiostatQ fermentor. Cells were collected, washed in PBS, and stored at -80 °C. Then ca.10^5 CFU/mL of thawed NRP cells were exposed to 2-fold serial dilutions of test compound in 7H12 medium in white 96-well plates, which were incubated 10 days anaerobically at 37 °C. Luminescence readings were obtained following a 28 h recovery in an aerobic environment (5% CO_2). The data were analyzed graphically, and the lowest concentration of test compound preventing metabolic recovery (90% reduction relative to untreated cultures) was determined as described previously (*73*).

4.2.4. Cytotoxicity Assay

Cytotoxicity was determined by exposing different concentrations of samples to Vero cells. Samples were dissolved at 12.8 mM in DMSO. Geometric 3-fold dilutions were performed in growth medium MEM (Gibco, Grand Island, NY) containing 10% fetal bovine serum (HyClone, Logan, UT), 25 mM N-(2-hydroxyethyl)-piperazine-N′-2-ethanesulfonic acid (HEPES, Gibco), 0.2% $NaHCO_3$ (Gibco), and 2 mM glutamine (Irvine Scientific, Santa Ana, CA). Final DMSO concentrations in assay did not exceed

1% v/v. Drug dilutions were distributed in duplicate in 96-well tissue culture plates (Becton Dickinson Labware, Lincoln Park, NJ) at a volume of 50 µL per well. An equal volume containing either 5 × 10^5 log phase Vero cells (CCL-81; ATCC, Rockville, MD) was added to each well and the cultures were incubated at 37 °C in an atmosphere containing 5% of CO_2. After 72 h, cell viability was measured using the CellTiter 96 aqueous nonradioactive cell proliferation assay (Promega Corp., Madison, WI) according to the manufacturer's instructions. Absorbance at 490 nm was read in a Victor2 multilabel reader (PerkinElmer). The IC_{50}s were determined using a curve-fitting program (*74-75*).

4.2.5. Macrophages and culture conditions

The J774A.1 mouse macrophage-like cell line, obtained from ATCC (TIB-67), was grown in Dulbecco's modified Eagle's medium (DMEM; Gibco-BRL Life Technologies, Gaithersburg, Md.) in 75-cm^2 flasks (Corning Costar Corp., Cambridge, Mass.). DMEM medium with 100 mM sodium pyruvate, 200 mM L-glutamine, 3.7 g of sodium bicarbonate (Sigma) per liter, and 10% fetal calf serum without any antibiotics. M.Tb was diluted with cell culture medium DMEM to final concentration at 1-3 x10^5 CFU/ml before tranfered into 24 well plates containing cover slips with 1 ml aliquot in each well. The macrophages were trypsinized and seeded to the same 24-well plates containing cover slips at a density of approximately (3-5 × 10^5) cells/ml for co-culture with bacteria overnight. The macrophages were incubated at 37 °C in 5% CO_2 atmosphere. The medium containing the bacteria was discarded, Macrophage monolayers were washed twice in phosphate buffered saline to remove the free

bacteria. Drugs were diluted to different concentrations with DMEM and then the cover slips with infected cells were transferred to these plates and incubated for 6-7 days in the 5% CO_2 incubator. *M. tuberculosis* from day 1 and day 7 infected, but untreated cultures and from day 7 treated cultures was enumerated by plating macrophage lysates on agar media. The monolayers that had been washed with phosphate buffered saline were lysed by adding 1 ml of water plus 0.05% sodium dodecyl sulfate for 5 min. The 1 ml of lysate was serially diluted, and 0.1 ml was plated onto Middlebrook 7H11 agar plates (Difco Laboratories). The numbers of CFU were read after 3 to 4 weeks. Analyses of EC_{90} & EC_{99} were performed by the program CurveExpert 1.3.

4.2.6. Time dependent and concentration dependent killing assay

The stock concentration of compounds was 10 mM. Four-fold dilutions of compounds were prepared in Middlebrook 7H12 medium in a volume of 100 µL in 96-well microplates (black plates). 100 µL 7H12 medium containing 2×10^5 cfu/mL *M. tuberculosis* H37Rv was inoculated in the plates, yielding a final testing volume of 200 µL. The plates were incubated at 37 °C. On day 1, 3, 7 and 14 of incubation, the culture medium at each individual concentration were collected and centrifuged at 10,000 g for 2 minutes. The resulting suspension was 10, 100 and 1000-fold diluted before being inoculated in the agar plates. The colonies on the agar plates were counted after three weeks. The percentage inhibition of compounds against *M. tuberculosis* was calculated compared to the drug free control.

4.2.7. Determination of MIC for single-drug-resistant strains of *M. tuberculosis*

The resistant strains of different established drugs were obtained from ATCC (r-KM (kanamycin): ATCC#36827; r-INH (isoniazid): ATCC#35822; r-RMP (rifampin): ATCC#35838; r-SM (streptomycin): ATCC#35820; r-CM (cycoserine): ATCC#35826). MIC determination was performed following the MABA protocol.

4.2.8. Mutation frequency

Twenty-four 10 ml cultures were prepared in 50 ml flasks containing Middlebrook 7H9 broth plus glycerol, casitone and OADC at an initial density of *M. tuberculosis* of less then 10^4/ml. Cultures were monitored for the presence of pre-existing resistant bacteria by plating 100 µL aliquots on media containing the test compound at 4× and 8× MIC, and was incubated for 2-3 weeks with shaking until absorbance at 570 nm was higher than 0.9. This was equivalent to approximately 2×10^9 cfu/ml. Four cultures were diluted and plated on drug-free 7H11 agar to determine actual CFU. One hundred microliter aliquots of undiluted and 1:10-diluted cultures (approx. 1×10^9 cfu/ml and 1×10^8 cfu/ml, respectively) of *M. tuberculosis* H37Rv were plated on 7H11 agar containing 2x, 4x, 8x and 16x the MIC. Each suspension was plated on 10 plates at each MIC multiple. Individual mutation frequencies were calculated for each of the 24 original cultures and the median value selected as representative. This minimized the effect of any jackpots that may be encountered (*76*).

4.2.9. Dosing and in vivo sample collection

Groups of twelve female BALB/c mice (20–22 g) were administered two oral doses of 75 mg/kg compounds **8a** at time 0 and 8h respectively. The dose was

formulated in 20% cyclodextrin. Whole blood samples (250 *μ*L) were collected aseptically from the retro orbital sinus at 0, 0.5, 1, 2, 4, 8, 8.5, 9, 11, and 24h hour postdose. Plasma was prepared from the whole blood by centrifugation at 2000 g for 30 minutes. Three volumes of acetonitrile containing the internal were added to each sample, and the samples were centrifuged at 4000 g for 30 minutes before LC-MS-MS analyses.

4.2.10. Pharmacokinetics of compound XIII

The formulation of compound XIII (2% NMP (N-methyl-2-pyrrolidone and 98% sesame oil, dosage of 100mg/kg) was modified from previous report (*48*).

4.2.11. Metabolite identification of compound 1

Compound stock solutions were prepared in DMSO. The final concentration of DMSO in the incubation media was 0.2% (v/v). 50 μM test compounds were co-incubated with 1 mg/ml mouse microsome and 1 mM NADPH for 60 minutes. The reaction was quenched with three-fold ice cold acetonitrile before centrifuge at 4000 g for 30 minutes. The supernatant was analyzed using LC-MS-MS.

Metabolite characterization of compound **1** was carried out with a Waters (Milford, MA) Q-TOF high resolution hybrid mass spectrometer SYNAPT™ Mass Spectrometry. Aliquots of 5 μL of each sample were analyzed using a Waters XTerra MS C18 (100 × 2.1 mm, 3.5 μm) reversed-phase column. A linear gradient from 0.1% formic acid in water (solvent A) to methanol (solvent B) was used as follows: 20-50% B for 5 min; isocratic 50% B for 5 minutes; 50-70% B for the next 20 min; and isocratic

90% B for 5 min. The flow rate was 0.2 mL/min. Positive ion electrospray was used for the detection of compound **1** and its metabolite. The column temperature was 40 °C, and the autosampler was maintained at 4 °C. Ionization was conducted in the positive ionization mode. The electrospray voltage was 4 kV, and the capillary temperature was 300 °C.

4.2.12. LC-MS-MS quantitation of isoxazole series

Quantitative analyses of compounds **1, 6o, and 8a** were carried out using LC-MS-MS with positive ion electrospray and SRM on a Thermo Finnigan TSQ quantum triple quadrupole mass spectrometer coupled with a Waters 2695 HPLC system using a Waters XTerra MS C18 (150 × 2.1 mm, 3.5 μm) reversed-phase column. A linear gradient from 0.1% formic acid in water (solvent A) to acetonitrile (solvent B) was used as follows: 30-45% B for 20 min; isocratic 90% B for the next 5 min; and isocratic 30% B for the next 12 min. Aliquots of 5 μL of each sample were analyzed. The flow rate was 0.2 mL/min. The SRM and retention times of the above compounds are listed in TABLE X.

TABLE X. SRMS AND RETENTION TIMES OF COMPOUNDS 1, 6o, 8a

Compd.	SRM ion pairs (m/z)	CE (eV)	Fragmentor	RT (min)
1	435-->250	23	103	11.33
6o	397-->212	26	91	10.57
8a	399-->212	26	91	11.04

Quantitative analysis of **compound 6g** was carried out using LC-MS-MS with an Agilent 1200 series HPLC system interfaced to Agilent 6410 triple quadrupole mass spectrometer with a Waters XTerra MS C18 (50 × 2.1 mm, 2.5 µm) reversed-phase column. A linear gradient from 0.1% formic acid in water (solvent A) to acetonitrile (solvent B) was used as follows: 30~70% B for 0.5 min; 30~70% B for 0.5 over the next 2.8 min. The flow rate was 0.5 mL/min. Aliquots of 5 µL of each sample were analyzed. Positive ion electrospray was used for the detection of compound **6g.** The and retention time of compound **6g** are listed in Table XI.

TABLE XI. SRMS AND RETENTION TIMES OF COMPOUND 6g

SRM ion pairs (m/z)	CE (eV)	Fragmentor	RT (min)
413.2-->228.1	25	140	1.76

4.2.13. Metabolite characterization of compound I from tetrahydroindazole series

Compound stock solutions were prepared in DMSO. The final concentration of DMSO in the incubation media was 0.2% (v/v). 50 µM test compounds were co-incubated with 1 mg/ml mouse microsome and 1 mM NADPH for 60 minutes. The reaction was quenched with three-fold ice cold acetonitrile before centrifugation at 4000 g for 30 minutes. The supernatant was analyzed using LC-MS-MS.

Metabolite identification of compound **I** was carried out with a Waters SYNAPT™ mass spectrometer. Aliquots of 5 µL of each sample were analyzed using a Waters

XTerra MS C18 (100 × 2.1 mm, 3.5 µm) reversed-phase column. A linear gradient from 0.1% formic acid in water (solvent A) to methanol (solvent B) was used as follows: 20-40% B for 5 min; 40-90% B for the next 15 min; and isocratic 90% B for the next 10 min. The flow rate was 0.2 mL/min. Positive ion ESI was used for the detection of compound its metabolite and I.

4.2.14. LC-MS-MS method for quantitation of tetrahydroindzole series

Quantitative analyses of compound analogs were carried out using LC-MS-MS with a Agilent 1200 series HPLC system interfaced to an Agilent 6410 triple quadrupole mass spectrometer. Aliquots of 5 µL of each sample were analyzed using a Waters XTerra MS C18 (50 × 2.1 mm, 2.5 µm) reversed-phase column. A linear gradient from 0.1% formic acid in water (solvent A) to acetonitrile (solvent B) was used for quantitative analysis of compound analogs: 50~70% B for 2.5 mins; 95% B over the next 2 mins. The flow rate was 0.5 mL/min. The column was re-equilibrated for 4 min between injections. The column temperature was 40 °C, and the autosampler was maintained at 4 °C. Ionization was conducted in the positive ionization mode. The electrospray voltage was 4 kV, and the capillary temperature was 300 °C. The gas flow was 6L/min and the nebulizer gas pressure was 25psi. The analogs were quantified using LC-MS-MS with SRM (TABLE XII).

TABLE XII. SELECTED REACTION MONITORING (SRM TRANSITIONS) AND RETENTION TIMES OF ANALOGS

Compd.	SRM ion pairs (m/z)	CE (eV)	Fragmentor	RT (min)
I	380.1-->323.2	30	160	2.08
II	252.2-->295.1	20	150	4.3
III	392.1-->315.1	28	145	3.96
IV	392.1-->265.1	36	150	4.26
V	392.1-->265.1	36	150	4.24
VI	342.1-->215.1	32	154	3.81
VII	402-->345	20	150	4.17
VIII	381.2-->324.2	24	155	3.57
IX	339.2-->282.1	20	135	1.97
X	354.2-->297.1	20	155	3.77
XI	369.1-->242.1	28	150	3.72
XII	449.2-->392.1	20	170	3.9
XIII	408.0-->351.2	25	140	1.45

4.3. Drug metabolism-guided hit-to-lead optimization of isoxazole series

. Approximately 50,000 compounds from a commercial library (ChemBridge 'NOVACore' library) were screened for growth innibition of *M. tuberculosis*. Several compounds containing an isoxazole core (typified by compound **1**) demonstrated submicromolar MICs against *M. tuberculosis* (Figure 20). Chemical modifications were focused on synthesizing analogs of compound **1** around the aryl group and amine group to investigate the structure-activity relationship (SAR) (TABLE XIII and TABLE XIV).

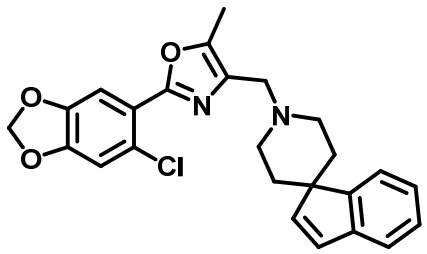

Figure 20. Structure of compound 1.

TABLE XIII. IN VITRO ACTIVITY (μM) OF ISOXAZOLE ANALOGS – ARYL MODIFICATIONS*

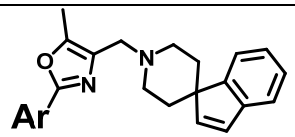

#	Ar	MIC		VERO cells IC_{50}	#	Ar	MIC		VERO Cells IC_{50}
		Replicating	NRP				Replicating	NRP	
1	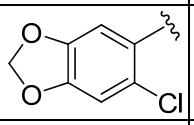	0.48	13.8	>128	6h	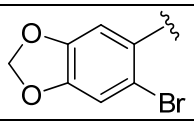	0.59	10.8	32.3
6a	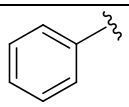	7.8	33.7	51.5	6i	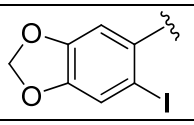	0.95	7.4	49.6
6b	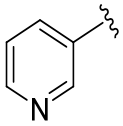	96.7	113	-	6j	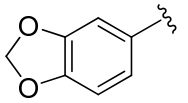	0.27	26.7	42.5
6c	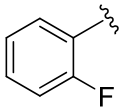	29.1	43.7	60.5	6k	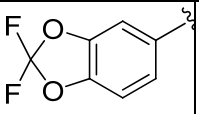	0.98	28.5	58.5
6d	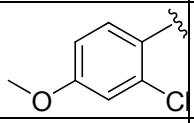	0.97	6.2	38.9	6l	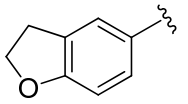	1.69	14.9	41.5
6e	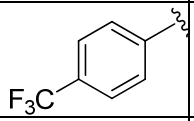	0.96	27.8	63.9	6m	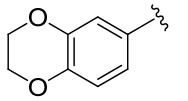	0.86	36.7	64.1
6f	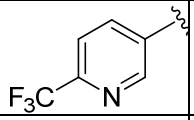	0.85	52.3	58.9	6n	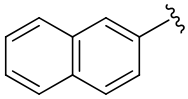	1.93	17.5	67.7
6g	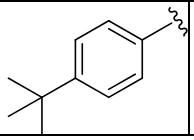	0.26	3.3	39.2	6o	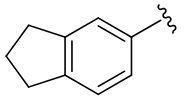	0.48	11.9	57.5

* MICs for replicating and NRP cultures were determined via MABA and LORA, respectively.

TABLE XIV. IN VITRO ACTIVITY (μM) OF ISOXAZOLE ANALOGS – AMINE MODIFICATIONS*

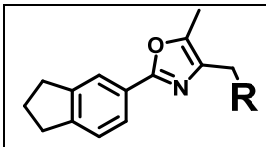

#	R	MIC		VERO cells IC_{50}
		Replicating	NRP	
8a	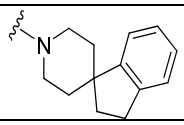	0.64	10.6	70.32
8b	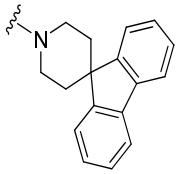	7.58	6.2	>128
8c	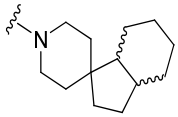	12.43	14.67	>128
8d	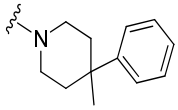	3.8	13.2	56.4
8e	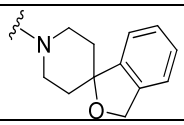	0.74	0.9	30.9
8f	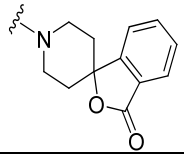	7.8	6.2	117.7

* MICs for replicating and NRP cultures were determined via MABA and LORA, respectively.

The MIC of all compounds against replicating and non-replicating *M. tuberculosis* was determined using MABA and LORA, respectively. Inhibition of the growth of the VERO cell line (green monkey kidney cells) was used to assess the potential for mammalian toxicity.

It was clear from the data in TABLE XIII that compounds containing the pendant aryl group without C-4 substituents lacked optimal anti-TB activity. Although the corresponding bromo and iodo analog to compound **1** were prepared and found to be similar in anti-TB activity, the more simple and accessible des-halo analog, **6j**, was also quite active. Other 4, 5-fused rings (compounds **6k-6o**) all exhibited reasonable activity with similar LORA activity and VERO cell toxicity. In light of the microsomal metabolism data of compound **1** to be described later, we focused on the assumedly more stable indano-core as in analog **6o**.

Changes to the amine moiety gave varied results (TABLE XIV). Spiro-indane **8a** was slightly less potent than **6o** but lacked a typical metabolic 'soft-spot', the indeno double bond, and was chosen as the best candidate from these analogs for further study. Modifications to the spiroindene ring system such as benz-fusion (**8b**), reduction (**8c**; mixture of cis-isomers is presumed), and ring opening (**8d**) all led to less active analogs. The spiroisobenzofurans **8e** and **8f** were interesting in that the carbonyl in the latter rendered the analog approximately 10-fold less potent. The LORA activity of both analogs, however, was notable and generally atypical of the series.

4.3.1. Metabolism of compound 1

As described above, compound **1** was selected for further study based upon its bioactivity and toxicity profile determined during our HTS campaign. To predict the in vivo oxidative clearance of potential lead compounds, selected bioactive analogs were incubated with mouse liver microsomes, and the disappearance of parent compound was measured over time using a well-stirred model. Compound **1** was rapidly degraded

with predicted hepatic plasma clearance ($Cl_{p,h}$) to be approximately 98.59% of the mouse liver plasma flow ($T_{1/2}$=1.9min) (Figure 21, TABLE XV). The high elimination rate of compound **1** indicated the importance of enhancing metabolic stability through chemical modification.

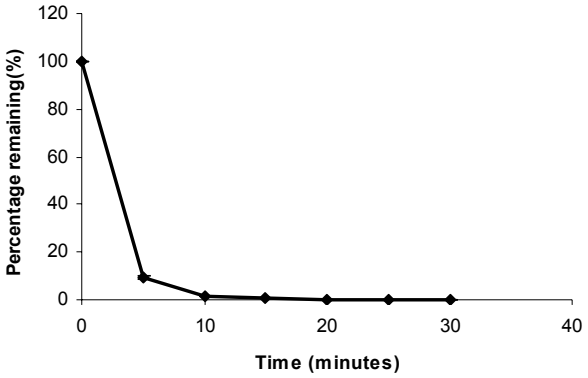

Figure 21. ***In vitro*** **metabolism of compound 1 by mouse liver microsomes.**

TABLE XV. METABOLIC STABILITY PARAMETERS OF COMPOUND 1 IN MOUSE MICROSOMES

Compd.	Half life $T_{1/2}$ (min)	C_{lint} (mL/min/kg)	Pred $Cl_{p,h}$ (mL/min/kg)	$Q_{p,h}$	$Q_{p,h}$%
1	1.9	2836.03	39.93	40.5	98.59

4.3.2. Major metabolites of compound 1

The major metabolites, **M1** and **M2**, of compound **1** were characterized by LC/MS and (Figure 22). The accurate mass measurements of compound **1**, **M1**, and **M2** were 435.1463, 423.1465 and 186.1298, respectively. The formula of **M1**, the most abundant metabolite of compound **1**, was determined to be $C_{24}H_{24}N_2O_3Cl$, indicating

loss of one carbon from the parent formula, based upon the elemental composition predicted from the accurate mass results. In a similar manner, the formula of **M2** was determined to be $C_{13}H_{16}N$ (TABLE XVI).

TABLE XVI. ACCURATE MASS OF COMP.1, M1, AND M2

	Mesured Mass	Formula	Calculated Mass	m Da	ppm	DBE
Comp. 1	435.1463	C25H24N2O3Cl	435.1475	-1.2	-2.8	14.5
M1	423.1465	C24H24N2O3Cl	423.1475	-1	-2.4	13.5
M2	186.1298	C13H16N	186.1283	1.5	8.1	6.5

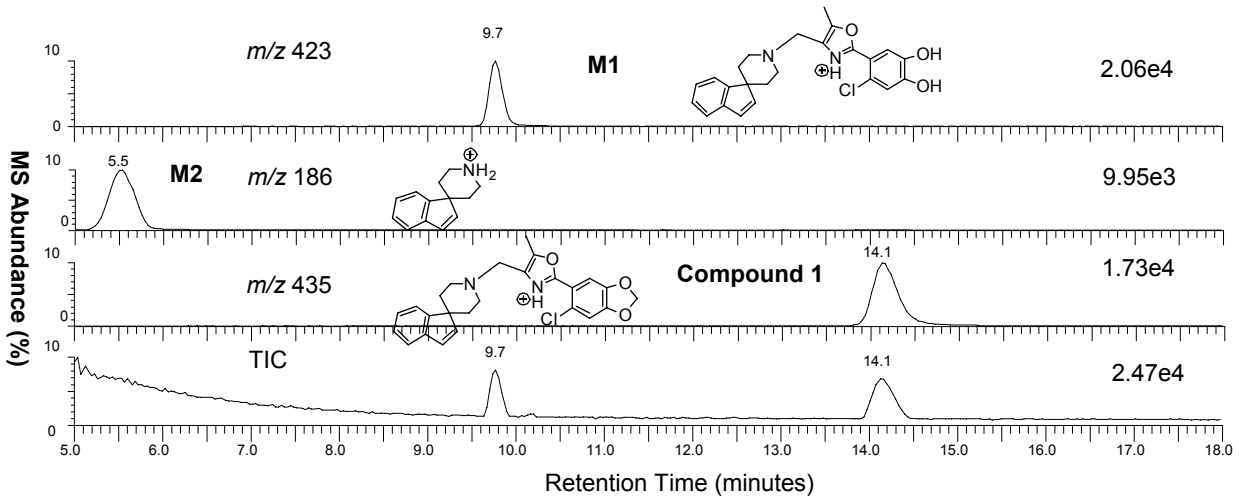

Figure 22. LC-MS chromatograms for the positive ion electrospray LC-MS analysis of metabolites of compound 1

Metabolites **M1, M2,** were identified as 4-chloro-5-(5-methyl-4-(spiro[indene-1,4'-piperidine]-1'-ylmethyl)oxazol-2-yl)benzene-1,2-diol and spiro[indene-1,4'-piperidine] respectively. TIC, Total Ion Chromatogram.

The structure of **M1** was proposed by using tandem mass spectrometry Figure 23 and Figure 24). The most abundant fragmentation reaction for compound **1** in the source

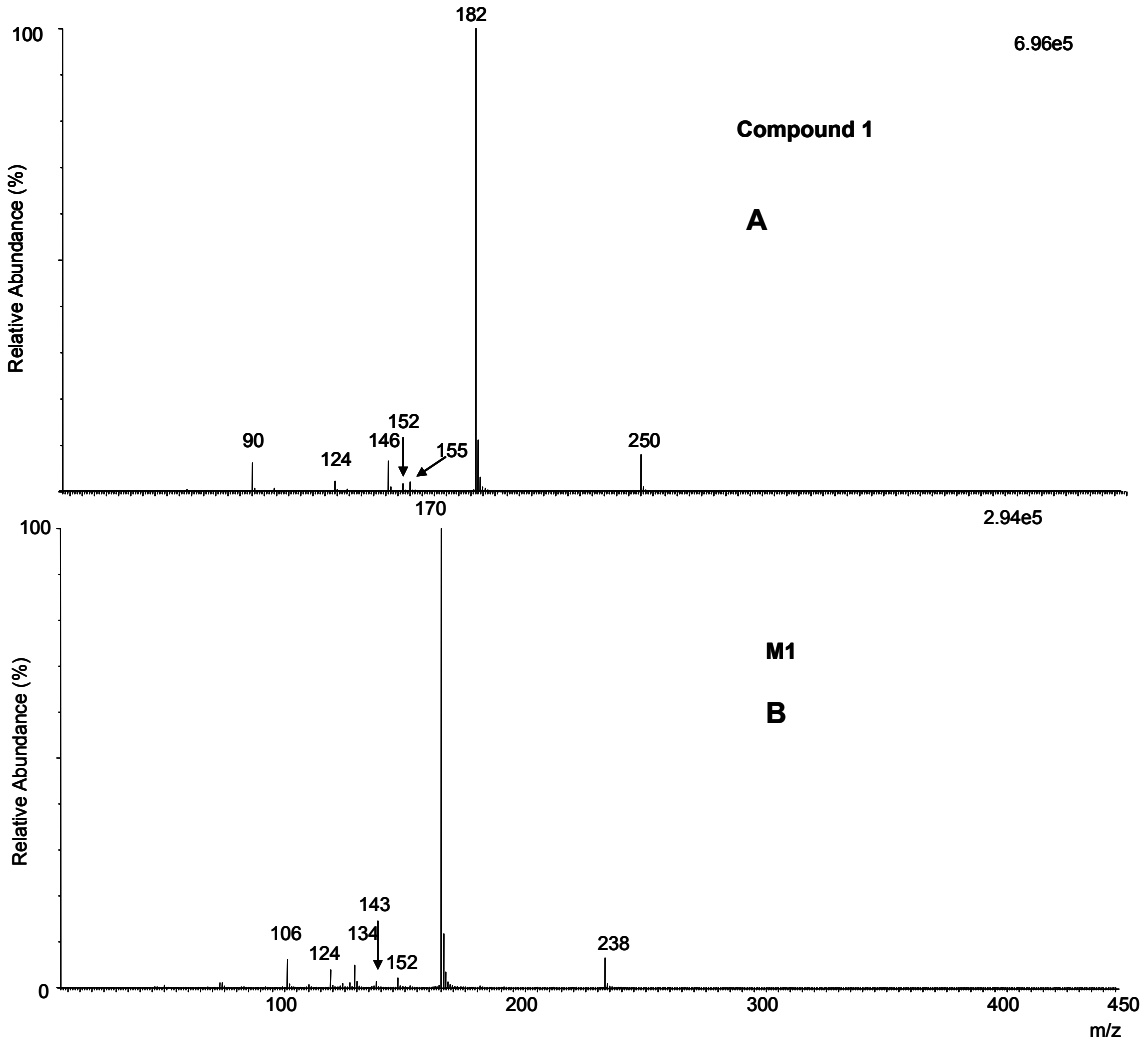

Figure 23. Tandem mass spectra of compound 1 (A) and M1 (B) under collision energy of 50eV.

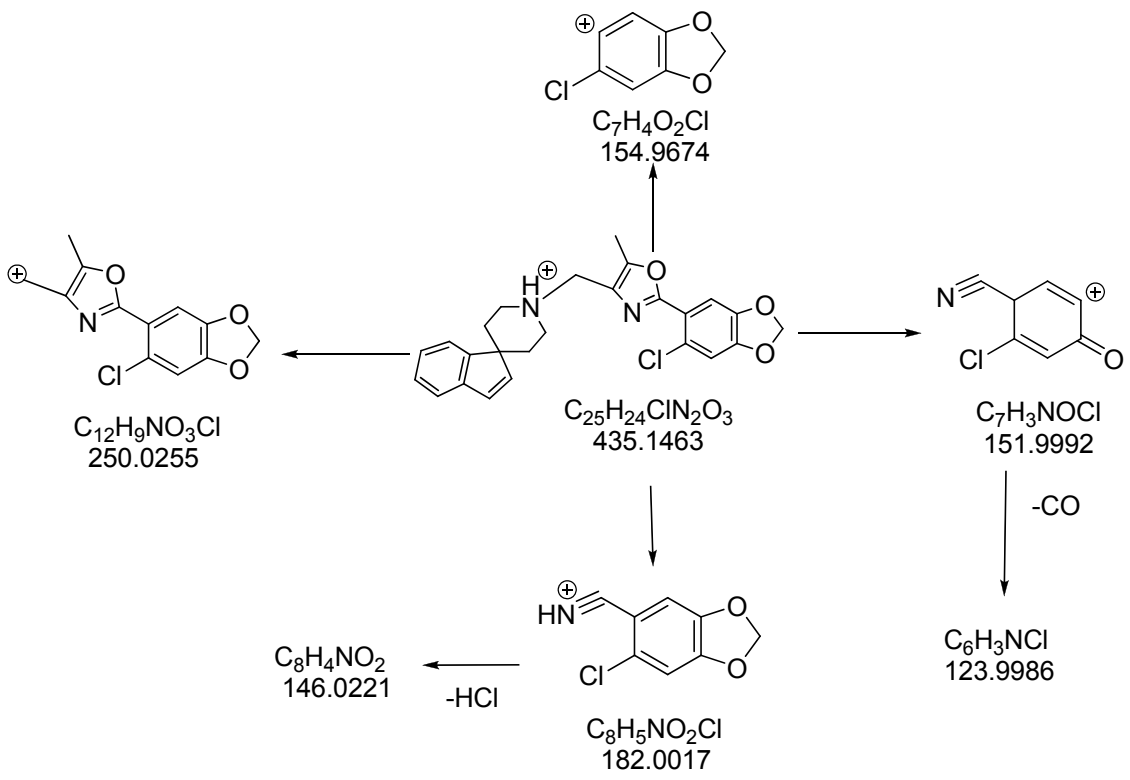

Figure 24. The proposed fragmentation pathway of compound 1.

was the dissociation of the “benzylic” linker between the piperidino group and the isoxazole core. This type of collision pattern is very helpful in determining if the metabolic biotransformation occurred on the aryl-isoxazole core (m/z 250.0255). The ion of the aryl-isoxazole core (m/z 250.0255) of compound **1** was then fragmented to key components weighing 182.0017, 154.9674, 151.9992, 123.9986, 146.0221 (Figure 23A). Comparing with that of compound **1**, in the spectrum of **M1** (Figure 23B), the fragment ion of 238.0260 indicated that the loss of carbon took place in the aryl-isoxazole core. The base peak of 170.0028 in the spectrum of **M1** eliminates the

possibility that the loss of carbon originates from a demethylation reaction on the isoxazole ring. The fragment ion of 142.9989 (loss of 12 mass units from the 6-chlorobenzo[d][1,3]dioxol (m/z 154.9674) fragment) further suggested that this fragmentation was derived exclusively from the 1,3-benzodioxole ring. The presence of a *m/z* 151.9992 fragment in the two spectra implied that the benzyl ring remained unmetabolized. The loss of carbon must therefore occur on the dioxole ring. The data thus suggested that the structure of **M1** was the corresponding catechol derivative arising from the loss of carbon from the dioxymethylene ring: 4-chloro-5-(5-methyl-4-(spiro[indene-1,4'-piperidine]-1'-ylmethyl)oxazol-2-yl)benzene-1,2-diol. The structure of **M2** was confirmed by comparison to the commercially available authentic standard spiro[indene-1,4'-piperidine] with a cleaved methylene linker.

4.3.3. Metabolite activity and toxicity

M1, as the proposed major metabolite, with a catechol substructure, is very easily converted by liver enzymes to benzoquinone which is reactive with electrophiles such as proteins and nucleosides, thereby raising safety concerns (*77*). The benzo[d][1,3]dioxole substructure (**1, 6h, 6i, 6j, 6k**) was thus avoided in selecting lead compounds from this class of analogs. Although **M2** appeared to be relatively abundant, it lacked both anti-TB and cytotoxic activity.

4.3.4. Selecting lead compounds based on metabolism profiles

Attempts at stabilizing the linker between the N-aryl group and the isoxazole ring (the metabolic soft spot of **M2**) by using longer spacer groups such as carbonyl and

ethyl linkers resulted in a complete loss of activity. The methylene linker thus is a possible crucial site for retaining the activity of this class of compounds. Based on this result, subsequent efforts focused more on replacing the dioxole ring with other functional groups to block the metabolism site of **M1**.

Overall, among the newly synthesized compounds substituting other functional groups for the 1,3-benzodioxole substructure (compounds **6b, 6c, 6d, 6e, 6f, 6g, 6i, 6m, 6n, 6o**;TABLE XIII), compounds **6g** and **6o** had the best potency and cytotoxicity profiles with in vitro metabolic half-lives approximately 5 and 10 times longer, respectively than compound **1**. The 2, 3-dihydro-1H-indene ring of compound **6o** was therefore considered as a better building block for future structural modification.

Among those compounds containing a 2,3-dihydro-1H-indene ring group and an amine group substitution (TABLE XIV), compounds **6o**, **8a**, **8e** were the most potent. These three compounds shared a very similar structure with a piperidine ring connected to a five member and six member fused ring system. The selectivity indices ($SI=IC_{50}/MIC$) of **6o** and **8a** were higher than that of compound **8e**. Although the half-lives of compounds **6o** and **8a** in mouse microsomes were similar, the former contained a labile unsaturated bond near the resonant ring system. Therefore compound **8a** was selected as the best compound for future optimization.

4.3.5. Metabolism study of compound 8a

By replacing the 1,3-dioxole ring with the cyclopentano-ring, the metabolic degradation which occured with **M1** was diminished as expected. Compound **8a** also contained the spiro-indanopiperidine rather than the indeno analog to avoid potential oxidation of the double bond; this substitution did not greatly affect the anti-TB activity of

the series. In fact, the in vitro half life ($T_{1/2}$) of **8a** in mouse liver microsomes was 19 min, a ten-fold enhancement relative to compound **1**, with predicted hepatic plasma clearance ($Q_{p,h}$) to be approximately 88% of the mouse liver plasma flow. The $T_{1/2}$ in human liver microsomes was 44 minutes with hepatic plasma clearance ($Q_{p,h}$) approximately 77% of the human liver plasma flow. The plasma protein binding of compound **8a** was 95.93±0.19% (TABLE XVII).

TABLE XVII. METABOLIC STABILITY PARAMETERS OF COMPOUND 8a IN MOUSE AND HUMAN MICROSOMES.

Species	Half life $T_{1/2}$ (min)	Cl_{int} (mL/min/kg)	Pred $Cl_{p,h}$ (mL/min/kg)	$Q_{p,h}$	$Q_{p,h}$%
Mouse	18.24	299.25	35.67	40.5	88.07
Human	44.47	36.46	8.63	11.30	76.34

4.3.6. Time dependent and concentration dependent killing effects of compound 8a

Effective *in vivo* growth inhibition or killing of *M. tuberculosis* requires that compound be present in plasma/tissue at some threshold concentration for a sufficient period of time. The bactericidal activity of compound **8a** in axenic medium was both concentration and time-dependent with maintenance of threshold concentrations of 0.39 uM and 1.56 uM required for static and cidal activities, respectively (Figure 25). In light of this result, the dosing regimen of compound **8a** for mice was designed to achieve a bactericidal exposure in vivo.

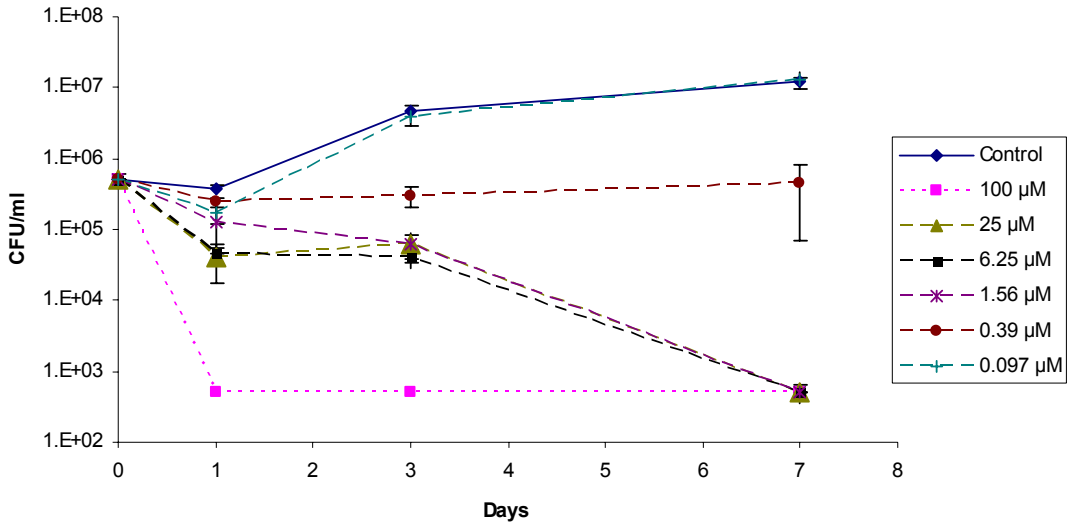

Figure 25. Time dependent and concentration dependent killing of *M. tuberculosis* by compound 8a.

4.3.7. Pharmacokinetics of compound 8a in mice

Guided by the in vitro metabolic stability data, the time/concentration dependant killing results and preliminary tolerance testing (data not shown), mice were dosed with compound **8a** at 75mg/kg twice/day (BID) with the intent of achieving maximum coverage of the MIC and preferably the MBC. On each day, the second dose was administered 8 hours after the first dose. After five days of BID dosing, there was an obvious accumulation of **8a** in both the systemic circulation (Figure 26) and in the lungs (Figure 27). Plasma C_{max} of **8a** was 0.25 hrs after the first dose and 0.5 hrs after the second dose (Figure 26). Concentrations of **8a** in lung tissue 24 hours after the first dose on day 1 and day 5 were 0.38 µg/ml and 2.73µg/ml, respectively, both of which

exceeded the MIC (Figure 27). The pharmacokinetic parameters of compound **8a** are summarized in TABLE XVIII.

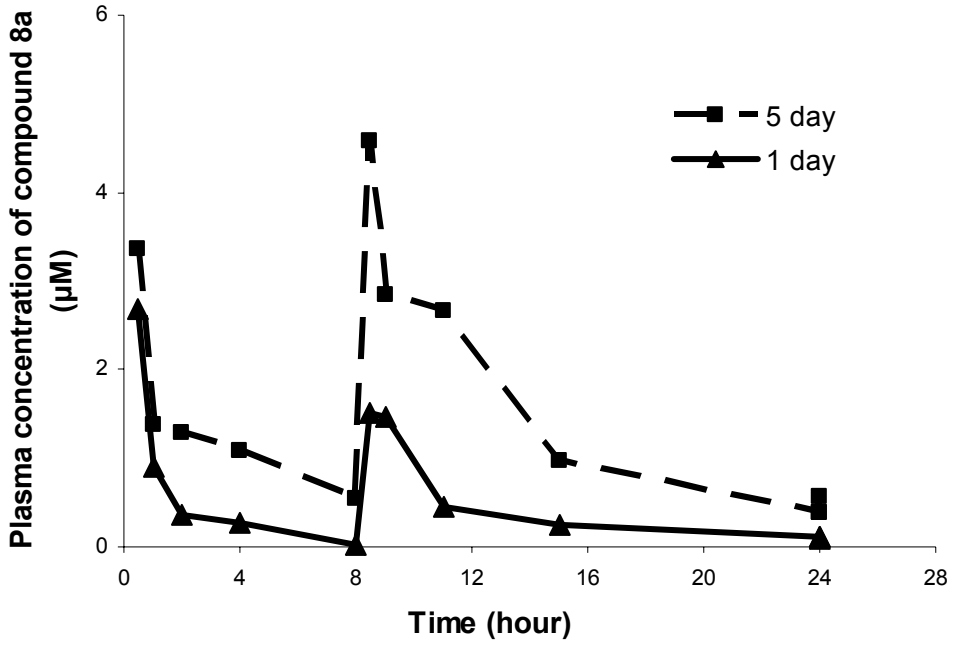

Figure 26. Pharmacokinetics of compound 8a in mice at 75mg/kg po (BID, second dose at 8 hours).
The dashed line represents pharmacokinetics profile after doing the animals in consequent five days with 75mg/kg BID. The solid line represents pharmacokinetics profile with BID dose at day one.

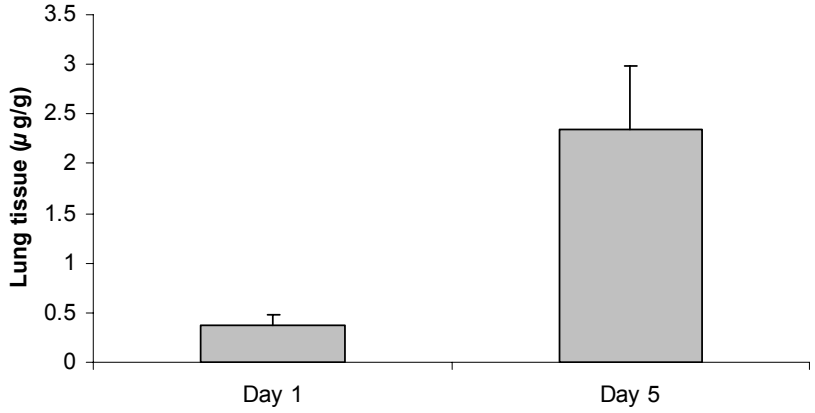

Figure 27. Lung tissue concentration of compound 8a at 16 hours after the second daily dose. The concentration of compound **8a** after 16hours dosing was 0.38 μg/ml on day one and 2.73μg/ml on the fifth day of treatment.

TABLE XVIII. PHARMACOKINETIC PARAMETERS OF COMPOUND 8a IN MICE.

	AUC_{8h}(mg-h/L)	C_{max8h}(μM)	T_{max8h}(hour)	C_{8h} (μM)	AUC_{24h}	$C_{8.5h}$ (μM)
Day 1	1.37	2.69	0.25	0.03	3.83	1.52
Day 5	3.56	3.37	0.25	0.53	12.34	4.58

4.3.8. Biological profiling of compound 8a

4.3.8.1. Confirmation of intracellular concentration of compound 8a (by Dr. Yuehong Wang)

M. tuberculosis resides both intra- and extra-cellularly in human lung tissue and mainly intracellularly in mouse lung tissue. Compound **8a** showed dramatic intracellular inhibition of *M. tuberculosis* in macrophage but without bacteriacidal activity at 0.4 μg/ml (0.92μM) (Figure 28).

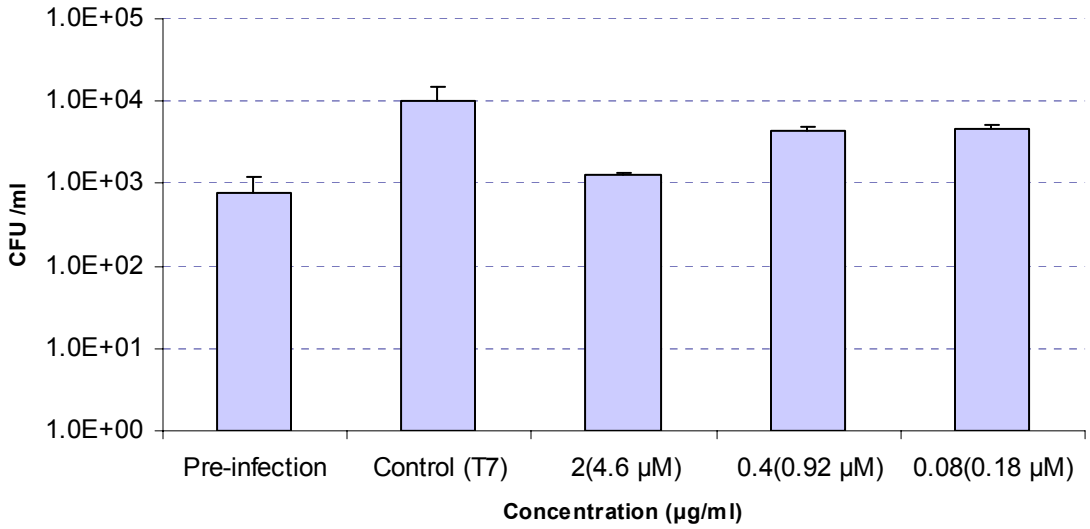

Figure 28. Compound 8a versus *M. tuberculosis* in J775A.1 macrophages.
There is approximately one log bacterial growth in untreated cultures (T0 to T7). The Y axis represents the desnity of *M. tuberculosis* in the macrophage culture. The X axis represents the concentration of compound **8a**.Micromolar concentrations are in Parentheses.

4.3.8.2. Mutation frequency of compound **8a** (by Dr. Sanghyun Cho)

The mutation frequency, the ratio of mutants to total bacteria in the population, was determined by plating aliquots of *M. tuberculosis* culture on media containing concentrations of the test compound that exceeded the MIC. The mutation frequency of *M. tuberculosis* to compound **8a** was 5.5×10^{-5} on 1X MIC plates. The mutation frequency to 8X MIC rifampin, determined in parallel, was 9.6×10^{-6}.

4.3.9. In vivo efficacy of compound 8a

Compound **1** was inactive in the acute mouse infection model (Figure 29), while compound **8a,** with higher metabolic stability, showed marginal efficacy in vivo at a 75mg/kg po dose (BID) (Figure 30).

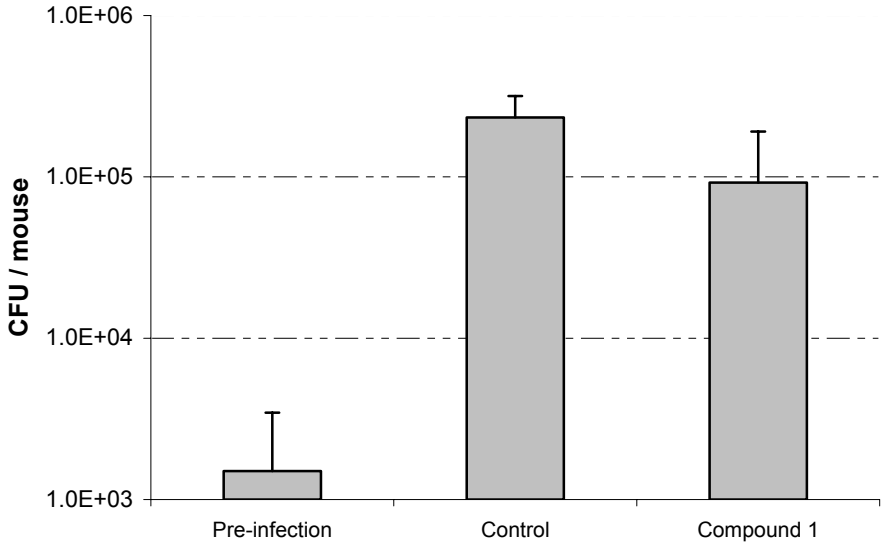

Figure 29. Compound 1 *vs. M. tuberculosis* Erdman in Balb/c mice
Dosage: 400mg/kg; formulation: CMCNa.

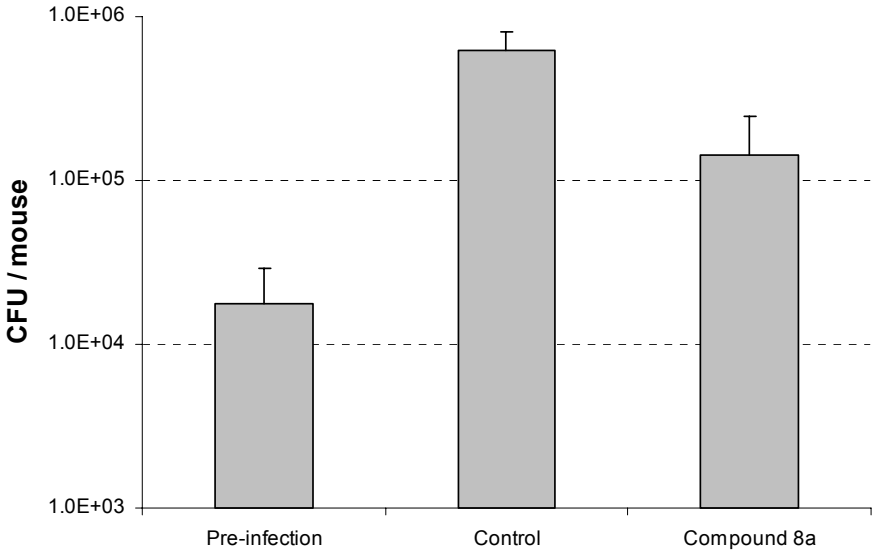

Figure 30. Compound 8a *vs M.tuberculosis* Erdman in Balb/c mice
Dosage: 75mg/kg; BID; formulation: 20% cyclodextrin

4.3.10. Discussion

The isoxazole derivatives described herein exhibit excellent in vitro inhibitory effects on replicating and non-replicating *M. tuberculosis* as well as against the bacteria within macrophage cells. However, analogs from this series of compounds were subject to extensive metabolism. Modification on the 'soft-spots' of metabolism typically led to detrimental effects on the anti-TB activity. The metabolism of compound **1**, compound **6g,** and compound **8a** was dose dependently inhibited by ketoconazole at micromolar concentration. This suggests that these analogs are substrates of CYP3A. Co-administration of ketoconazole with compound **8a** elongates the half-life and elevated the plasma concentration of the latter in mice.

Through chemical modification of hit compound **1**, a putative site for metabolic inactivation leading to a catechol metabolite was successfully blocked while a second metabolic cleavage site at a benzylic position was identified. To optimize the in vivo exposure, compound **8a** was dosed twice/day. At 75 mg/kg marginal efficacy of compound **8a** was observed in *M. tuberculosis*-infected mice. However at higher dosages (100 mg/kg) the mice exhibited signs of toxicity. While it is possible that this toxicity is species-specific (as the IC_{50} for the J774A.1 murine cell line was approximately one-third that for the VERO green monkey kidney cell line), it may be tissue/organ specific or represent more general off-target acitivity.

4.4. Tetrahydroindazole series

To distinguish from compounds in the previous section (section 4.3), all compounds discussed in this section are numbered by Roman numerals.

Compound **I** (N-(1-(4-tert-butylphenyl)-4,5,6,7-tetrahydro-1H-indazol-4-yl)-4-methyl-1,2,5-oxadiazole-3-carboxamide) (Figure 31) is a hit, found in a HTS of a commercial library (ChemBridge 'NOVACore' library), with good in vitro anti-TB activity (MIC = 1.7 μM in MABA). The chemical synthesis and biological activity of this series of compounds were reported in a previous publication, suggesting very promising features for tuberculosis treatment (*48*). However, the metabolite of compound **I** was not identified and the anti-TB activity of the metabolite remains unknown. The intracellular bacteria inhibition potency and activity against resistant strains, which are critical properties of a good anti-TB lead compound, also need to be investigated. Herein, we updated the progress of the metabolism and biological study of current lead compound **XIII**, and introduced a metabolism-guided discovery process for the tetrahydroindazole series.

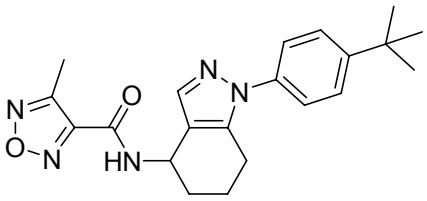

Figure 31. Structure of lead compound I.

4.4.1. Metabolism of compound I

To achieve sufficient plasma exposure, a good drug candidate needs to pass the metabolic stability filter. However, compound **I** was rapidly degraded in mouse microsomes (half life = 27 minutes). The predicted hepatic plasma clearance ($Q_{p,h}$) was approximately 83% of the mouse liver plasma flow (TABLE XIX). This high elimination rate addressed the importance of modifying the structure of compound **I** to enhance metabolic stability.

TABLE XIX. METABOLIC STABILITY PARAMETERS OF COMPOUND I IN MOUSE MICROSOMES.

Compd.	Half life $T_{1/2}$ (min)	Cl_{int} (mL/min/kg)	Pred $Cl_{p,h}$ (mL/min/kg)
I	27.34	199.59	33.67

4.4.2. Metabolite identification of compound I

The major metabolite of compound **I** following incubation in mouse liver microsomes, M1 (m/z 396), was detected by LC-MS (Figure 32). Using collision induced dissociation, the major product ions of compound **I** were found to be *m/z* 323.1879, 253.1702 and 197.1080 (Figure 33**,** Figure 34). The fragment ion of *m/z* 323.1879 was possibly formed by the dissociation of the oxadiazole ring. The fragment ion of *m/z* 253.1702 was formed by cleavage of the amine bond between the tetrahyroindazole core and the amide group. The fragment ion of *m/z* 197.1080 was a product ion of *m/z* 253.1702 after loss of the tert-butyl from the para position of the benzyl ring. The

tandem spectra of **M1** was then compared with that of compound **I** (Figure 33). Fragment m/z 197 without the tert-butyl group is the only product ion that is common to both compound **I** and **M1**. All the other **M1** fragments with the tert-butyl group (m/z 339.1827, 269.1659) were 16 mass units higer than the corresponding fragments of compound **I**. The hydroxylation was thus proposed to occur on the tert-butyl substituent. This proposed metabolite structure was then confirmed by comparing the tandem mass spectra to that of the synthesized compound N-(1-(4-(1-hydroxy-2-methylpropan-2-yl)phenyl)-4,5,6,7-tetrahydro-1H-indazol-4-yl)-4-methyl-1,2,5-oxadiazole-3-carboxamide.

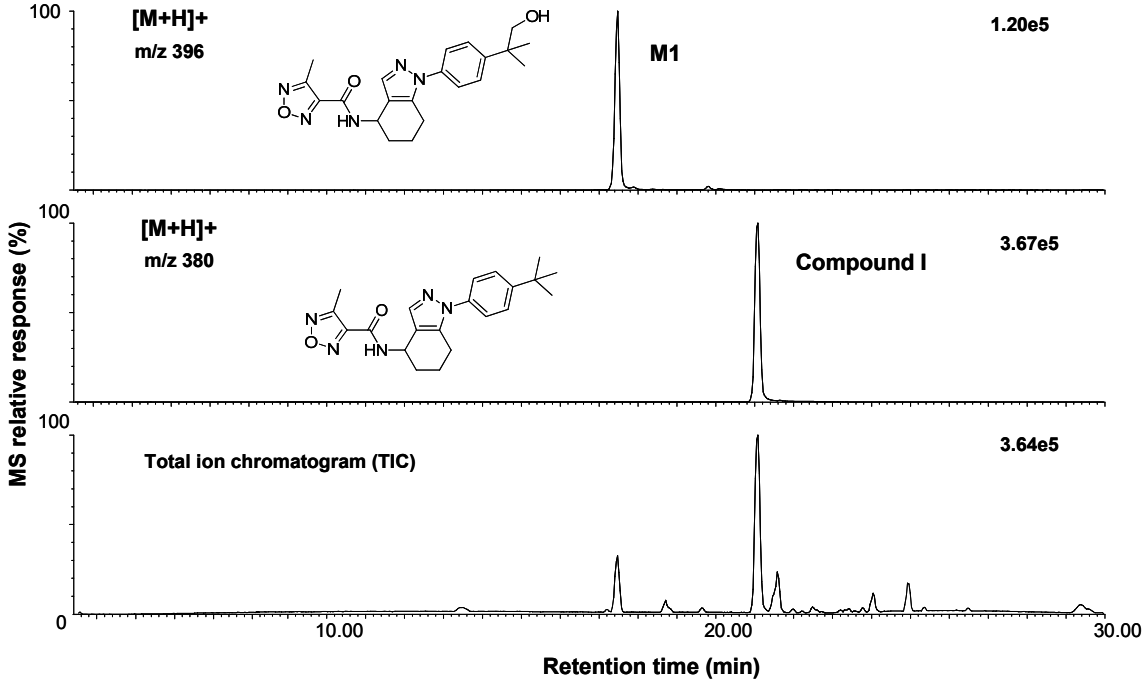

Figure 32. LC-MS chromatograms for the positive ion electrospray LC-MS analysis of metabolites of compound I.
Metabolite **M1** was identified as N-(1-(4-(1-hydroxy-2-methylpropan-2-yl)phenyl)-4,5,6,7-tetrahydro-1H-indazol-4-yl)-4-methyl-1,2,5-oxadiazole-3-carboxamide by comparing with synthetic standard. TIC, total ion chromatogram.

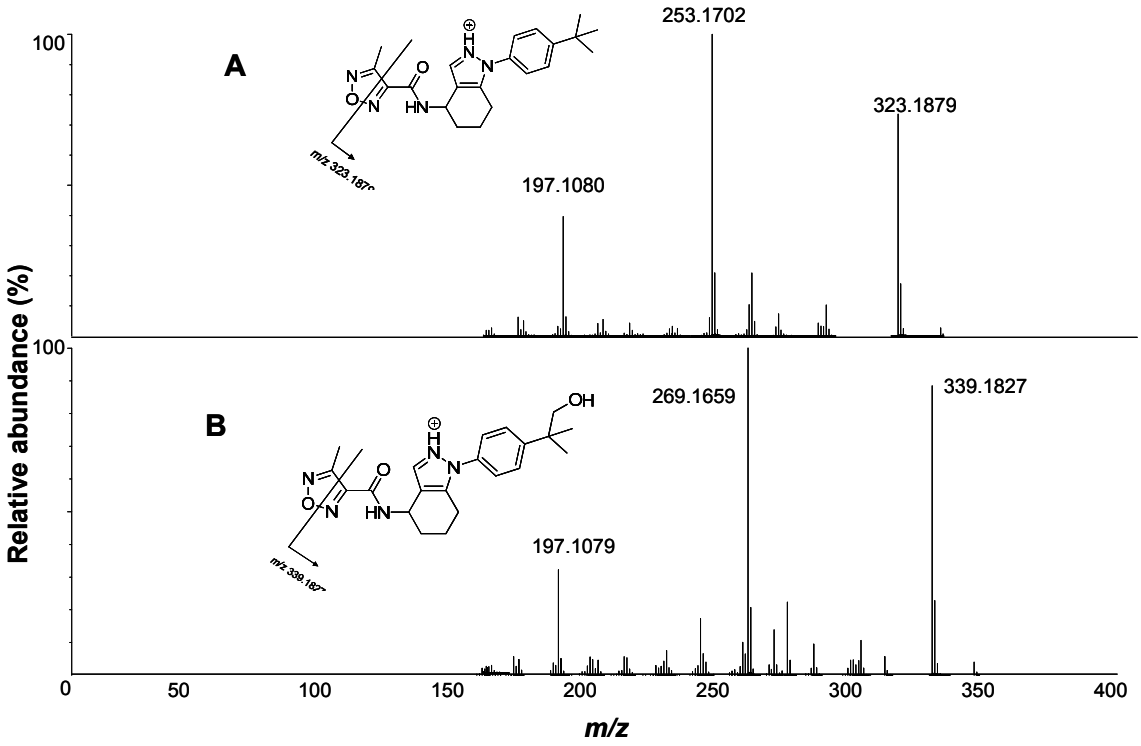

Figure 33. Positive ion electrospray product ion tandem mass spectra of protonated molecules of compound I (A) and M1 (B) of *m/z* 380 and *m/z* 396.

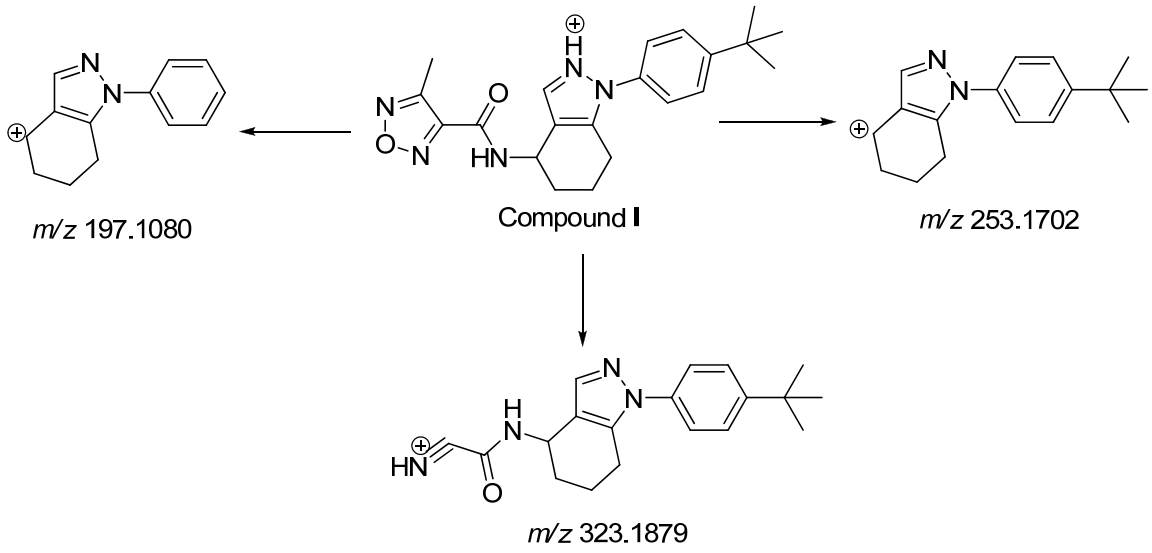

Figure 34. Proposed fragmentation pattern of compound I.

4.4.3. Anti-TB activity of M1

The MIC of **M1** against *M. tuberculosis* was higher than 200 *μ*M.

4.4.4. Metabolism of synthesized analogs

With the primary goal of improving metabolic stability, a series of analogs were synthesized with modifications of the tert-butyl substituent in the para position of the N-aryl group (*48*) (TABLE XX). Compounds **I** and **II,** bearing alkyl branches on the benzyl ring, were susceptible to hydroxylation with half-lives of 27.34 and 3.28 minutes, respectively. With respect to anti-TB activity, the presence of a para substituent on the N-aryl group, rather than ortho or meta substitution, might best improve potency (*48*). However from the perspective of metabolic stability, substitution at the meta position (as in compound **IV**) of the N- aryl substituent appeared superior to the ortho (compound **III**) or para (compound **V**) positions. It was thus hypothesized that hydroxylation on the

TABLE XX. METABOLIC STABILITY AND IN VITRO ANTI-TB ACTIVITY OF TETRAHYDROINDAZOLE SERIES.

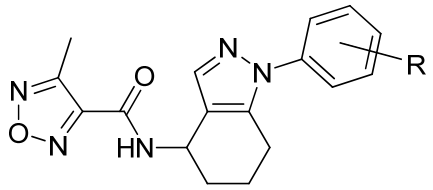

Compound	R	MIC(μM)	Half life(min)	$Q_{p,h}$%
I	4-$C(CH_3)_3$	1.7	42	83
II	3,5-CH_3,CH_3	>128	3	98
III	2-CF_3	>128	6	96
IV	3-CF_3	15.4	191	41
V	4-CF_3	1.9	63	68
VI	4-F	30.7	23	86
VII	4-Br	64.6	16	90
VIII	4-$NHCH(CH_3)_2$	>128	stable	stable
VIIII	4-NH_2	>128	12	92
X	4-OCH_3	>128	10	93
XI	4-NO_2	>128	108	56
XII	4-NHCO-(3-CH_3)-furazan	44.9	806	14
XIII	4-OCF_3	1.9	102	57

***** $Q_{p,h}$%: The percentage of hepatic plasma clearance ($Cl_{h,p}$) to mouse liver plasma flow

meta site was another major competing metabolism reaction for this series of compounds. According to the hydrogen rebound theory for cytochrome P450-mediated metabolism, electron withdrawing groups on the para position of the N-aryl group would impart some degree of metabolic stabilization. The metabolic stability of compounds **V, VI, VII, IX, X, XI, XIII,** was positively correlated with the electron withdrawing strength of their para substituents. Conversely compounds **VIII** and **XII,** with 4-$NHCH(CH_3)_2$, and 4-NHCO-(3-CH_3)-furazan substituents, respectively, were stabilized by these electron

donating groups possibly due to steric hindrance with respect to access of the active pocket of cytochrome P450. Finally, compound **XIII,** bearing a trifluoromethoxy group, was selected for further study due to the combination of favorable potency and five-fold higher stability to microsomes compared to compound **I**.

4.4.5. Pharmacokinetics of compound XIII

When formulated with sesame oil and NMP, compound **XIII** formed a stable suspension, even after addition to simulated gastric fluid, in contrast to the precipitation observed with a PEG400/NMP formulation used in previous study (*48*). A single oral dose of compound **XIII** at 100 mg/kg in the NMP/sesame oil formulation resulted in plasma concentrations that exceeded the MIC for more than 24 hours (Figure 35,TABLE XXI). The AUC was enhanced by more than five-fold relative to the AUC obtained using the PEG400/NMP formulation.

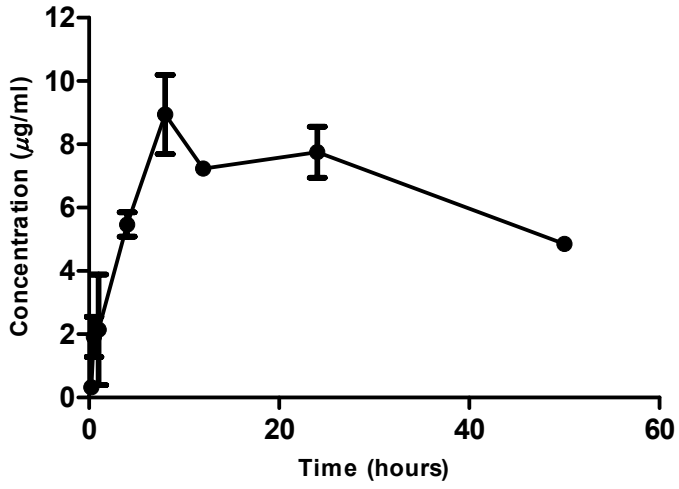

Figure 35. Plasma concentrations of compound XIII in Balb/c mice following a single oral dose of 100mg/kg (N=3)

TABLE XXI. PHARMACOKINETIC PARAMETERS OF COMPOUND XIII AT A DOSAGE OF 100MG/KG*

C_{max} (μg/ml)	T_{max}(h)	$AUC_{(0-t)}$ (μg·h/ml)	$AUC_{(0-\infty)}$(μg·h/ml)
8.94	8	327.8	598.1

*C_{max}: The peak serum concentration of a therapeutic drug; T_{max}: The amount of time that a drug is present at the maximum concentration in serum; AUC (0~t): The area under the curve from time zero to 48 hour; AUC (0~∞): The area under the curve from time zero to infinity.

4.4.6. Intracellular anti-TB activity determination of compound XIII (by DR. Yuehong Wang)

M. tuberculosis resides both intracellularly and extracellularly in human lung tissue and mostly intracellularly in mouse lung tissue. Through co-incubating compound **XIII** with J774.1 cells (a murine macrophage cell line), the intracellular inhibitory (but not cidal) potency of compound **XIII** was verified at concentrations of 2 *μ*g/ml and 0.4 *μ*g/ml which was lower than the C_{min} (Figure 36).

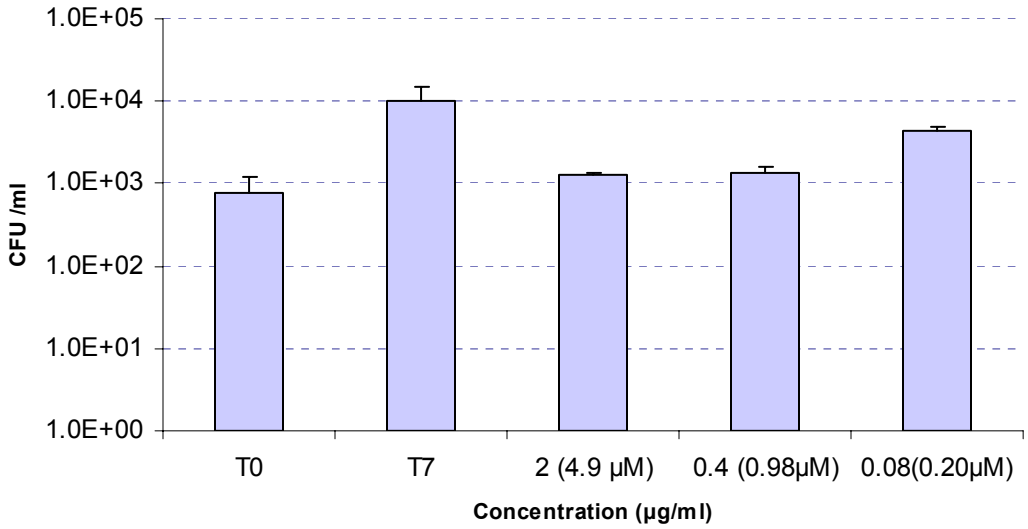

Figure 36. Compound XIII versus *M. tuberculosis* in J774.2 macrophages.
There was approximately one log bacterial growth in untreated controls (Control (T0) to Control (T7)). Micromolar concentrations are in Parentheses.

4.4.7. Activity of compound XIII against single-drug-resistant strains of *M. tuberculosis* and against non-mycobacteria (by Dr. Sanghyun Cho)

With a MIC of >50 uM against *Escherichia coli, Staphylococcus aureus, and Candida albicans,* compound **XIII** appeared to have a relatively narrow spectrum of activity (TABLE XXII). With a novel structure, compound **XIII** was, as expected, active against a panel of five single-drug-resistant *M. tuberculosis* isolates. The MICs obtained for single-drug-resistant strains of *M. tuberculosis*, including those resistant to isoniazid (INH), rifampin, streptomycin, kanamycin and cycloserine ranged from 1.44 to 5.17µM (TABLE XXIII).

TABLE XXII. COMPARATIVE MICS (*μ*M) OF COMPOUND XIII *

E. coli	*S. aureus*	*C. albicans*	*M. smegmatis*	*M. tuberculosis*
>50	>50	>50	23.8	1.51

* The assays were performed against each bacteria strain under various culture conditions.

TABLE XXIII. MIC (*μ*M) OF COMPOUND XIII AGAINST *M. TUBERCULOSIS* STRAINS RESISTANT TO SINGLE TB DRUGS*

rCS	rINH	rKM	rRMP	rSM
5.17	4.93	1.51	1.44	3.68

* MIC determined by MABA. r-KM (kanamycin), r-INH (isoniazid), r-RMP (rifampin), r-SM (streptomycin), r-CS (cycoserine).

4.5. Discussion

Reports of the synthesis and biological activity of tetrahydroindazole-based compounds date back to the 1960s. Compounds with this core structure were reported to be HMG-CoA reductase inhibitors (*78*), bacterial type II topoisomerase inhibitors (*79-80*), anticancer agents (*81*), HSP-90 inhibitor (*82*), mitotic motor protein modulator (*83*), *etc*. This study confirms and extends the recently reported anti-TB activity of tetrahydroindizoles.

Compound **XIII**, an analog of compound **I** with enhanced stability to liver microsomes, demonstrates a favorable activity profile. With an improved formulation, the exposure of compound **XIII** in mice has been significantly increased to make possible once daily dosing. Compound **XIII** inhibits the growth of *M. tuberculosis* strains resistant to existing TB drugs, suggesting a unique molecular target but is not broadly antimicrobial which is an asset for long-term treatment. The compound also restricts growth of *M. tuberculosis* in macrophages. As a compound series emanating from a phenotypic screen, the further optimization of tetrahydroindazoles as anti-TB agents should be facilitated by elucidation of the molecular target.

5. HARNESSING HepaRG CELLS FOR CYTOCHROME P450 INDUCTION STUDIES

5.1. Introduction

As reviewed in section 1.3, liver enzyme induction is one major drawback of existing anti-TB drugs. Liver enzyme induction can cause undesirable drug-drug interactions as well as drug metabolite-induced liver toxicity. Anti-TB drugs are usually used in combinations with each other or with antiviral drugs for the treatment of HIV/TB co-infection. Liver enzyme induction caused by anti-TB drugs can increase the activity of CYP P450 enzymes and increase the metabolism of other drugs. This often results in decreasing the efficacy of other drugs. Faliure to detect such activity in the discovery stage might result in treatment failure or drug resistance in phase IIb or later TB clinical trials..

HepaRG is a new human liver immortalized cell line that has a long life-span and shows expression of key drug metabolism enzymes comparable to those of primary hepatocytes. As a hepatoma cell line with almost unlimited resources and consistent CYP enzyme expression, HepaRG cells show great potential for drug metabolism and toxicity studies (*84-87*). As an induction model, the HepaRG cell model is more consistent than models using primary hepatocytes which have significant inter-donor differences. The published results (*87*) using this cell line in CYP induction and toxicity studies have been confirmed in our lab (chapter 2).

Despite all of the advantages of the HepaRG cell model mentioned above, there are still three major drawbacks that limit the wide application of the HepaRG cell model in drug discovery programs. First, maintaining CYP P450 expression of HepaRG cells requires growing the cell line in a commercial medium for 4 weeks. This medium is

expensive ($500/500ml) compared to common culture media, limiting the application of this cell model in screening large numbers of compounds. Secondly, HepaRG cells need to be cultured for at least four weeks before they can be used for induction assay, which limits the throughput. Thirdly, DMSO, which is included in the medium to differentiate the cells, inhibits cytochrome P450 enzyme activity and also causes cell death at the concentration that is required for CYP enzyme expression. To overcome the above limitations, new studies were carried out in this chapter to investigate time course and each ingredient in the medium to come up with a shorter and more cost-effective method for liver enzyme induction study. Our optimization focused on the elimination of DMSO from the differentiation medium in order to reduce cell death and interference on CYP enzyme activity. The development and validation of a HepaRG cell-based assay to study the toxicity of test compounds has been described in section 2.10. Therefore, this chapter will focus on the development and validation of using HepaRG cells for a CYP enzyme induction assay.

5.2. Materials and methods

5.2.1. Chemicals and reagents.

Williams' E medium was purchased from Invitrogen (Carlsbad, CA). Human insulin, hydrocortisone, DMSO, rifampin, 3-MC, CITCO and other chemicals were purchased from Sigma-Altrich (St Louis, MO). Fetal calf serum (FCS) was purchased from Lonza (Switzerland).

5.2.2. Culturing of HepaRG cells in customized medium for induction study

The cell culture protocol of HepaRG cells is outlined in Figure 37. For general maintenance of the cell culture, HepaRG cells were seeded in 25 cm^2 flasks with a starting density of 2.6×10^4 cells/cm^2 in DMSO-free medium. The medium composition was Williams' E medium supplemented with 10% FCS, 100 units/ml penicillin, 100 µg/ml streptomycin, 5 µg/ml insulin, 2 mM glutamine, and 5×10^{-5} M hydrocortisone. The medium was replenished every two or three days. Cells continued proliferating until reaching confluence. The cells were then trypsinized and passaged.

For induction assay, the cells were cultured according to the general maintenance protocol except that they were seeded in 12/96 well supports and cultured for two weeks. The inducers were dissolved in Williams' E medium without DMSO and phenol red and supplemented with 2% FCS, 100 units/ml penicillin, 100 µg/ml streptomycin, 0.5 µg/ml insulin, 2 mM glutamine, and 5×10^{-5}M hydrocortisone. This medium was added to the culture for 48 hours before real-time reverse transcriptase-quantitive PCR (RT-qRCR) analysis or 72 hours before functional assay.

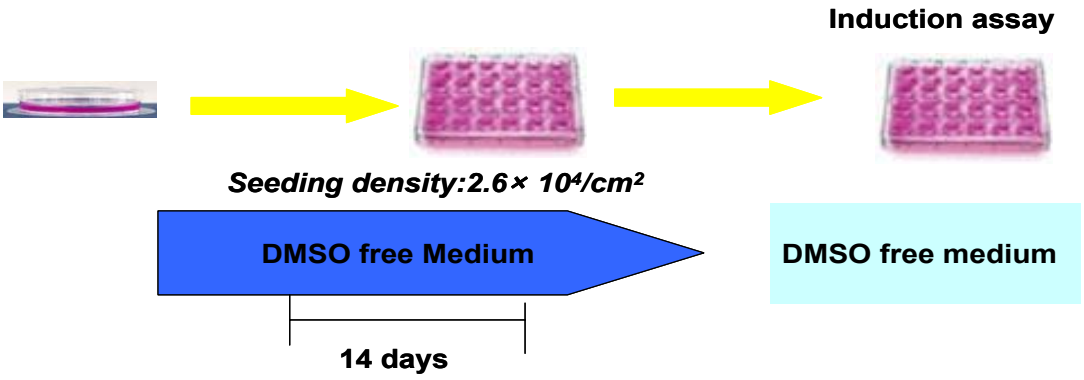

Figure 37. Cell culture of HepaRG cells in customized medium.

5.2.3. Establish methods to evaluate CYP activity and expression in HepaRG cells.

To quickly and accurately measure CYP activity and expression in HepaRG cells for induction study, functional assays and RT-qRCR assays were established. Functional assay using mass spectrometry to measure the relative metabolite concentration from each CYP substrate is faster and less complicated than RT-qPCR method. Furthermore, a functional assay directly measures liver enzyme activity, which is the fundmental factor affecting the clearance of drug, thus providing an advantage relative to indirect methods such as RT-qPCR. However, for compounds which have both inhibition and induction effects on liver enzymes, assays based on mRNA levels would be the only means of detecting induction.

5.2.3.1. Functional assay

The assay protocol is described in section **2.6.**

5.2.3.2. RT-qPCR method

Total RNA was extracted from 10^6 HepaRG cells using the SV total RNA isolation system (Promega, Madison, WI). RNAs were reverse-transcribed into cDNA using a high-capacity cDNA Archive kit (Applied Biosystems, Foster City, CA). Real-time quantitative PCR for all genes (TABLE XXIV) was performed using SYBR Green PCR Master Mix (Applied Biosystems, Foster City, CA) on an ABI Prism 7000 thermocycler (Applied Biosystems, Fsoter City, CA). The amplification curves were measured by ABI Prism 7000 SDS software using the comparative cycle threshold algorithm. The relative quantification of steady-state mRNA levels was calculated after normalization over total reference cDNA (β-actin RNA and albumin RNA). Furthermore, a dissociation curve was performed after PCR to verify the specificity of the amplification.

TABLE XXIV. PRIMER PAIRS FOR EACH TRANSCRIPT.

Albumin-F	TGCTTGAATGTGCTGATGACAGG
Albumin-R	AAGGCAAGTCAGCAGGCATCTCATC
β-Actin-F	ATCCTGGCCTCGCTGTCC
β-Actin-R	CTCCTGCTTGCTGATCCACAT
AhR-F	ACATCACCTACGCCAGTCGC
AhR-R	TCTATGCCGCTTGGAAGGAT
CAR-F	TGATCAGCTGCAAGAGGAGA
CAR-R	AGGCCTAGCAACTTCGCATA
PXR-F	CCAGGACATACACCCCTTTG
PXR-R	CTACCTGTGATGCCGAACAA
CYP1A2-F	TGGAGACCTTCCGACACTCCT
CYP1A2-R	CGTTGTGTCCCTTGTTGTGC
CYP2B6-F	TTCCTACTGCTTCCGTCTATCAAA
CYP2B6-R	GTGCAGAATCCCACAGCTCA
CYP2C9-F	GGACAGAGACGACAAGCACA
CYP2C9-R	AATGGACATGAACAACCCTCA
CYP2E1-F	TTGAAGCCTCTCGTTGACCC
CYP2E1-R	CGTGGTGGGATACAGCCAA
CYP3A4-F	CTTCATCCAATGGACTGCATAAAT
CYP3A4-R	TCCCAAGTATAACACTCTACACAGACAA
CYP1A1-F	TCCAGAGACAACAGGTAAAACA
CYP1A1-R	AGGAAGGGCAGAGGAATGTGAT
CYP2C8-F	AGATCAGAATTTTCTCACCC
CYP2C8-R	AACTTCGTGTAAGAGCAACA
CYP2C19-F	TTGAATGAAAACATCAGGATTG
CYP2C19-R	GAGGGTTGTTGATGTCCATC
CYP2D6-F	GGTGTGACCCATATGACATC
CYP2D6-R	CTCCCCGAGGCATGCACG
CYP3A5-F	AGTGTTCTTTCCTTCACTTTA
CYP3A5-R	TTCAACATCTTTCTTGCAAGT

5.2.4. Time course of cytochrome P450 induction by rifampin

Cells were seeded as per section 5.2.2 in 12-well plate supports. The cells were tested for induction potential after each week for four weeks. Three concentrations (10

μM, 1 μM, 0.1 μM) of rifampin were dissolved in low serum medium and incubated with the cells for three days before evaluating the cytochrome P450 activity by functional assays.

5.2.5. Method to assess effect of medium composition on CYP activity

HepaRG cells were seeded in 12-well plates with a density of 10^5 cells /well. The medium was changed every two or three days. After two weeks CYP enzyme activity was evaluated by functional assay. To investigate DMSO effects, the cells were cultured in DMSO-free medium for 2 weeks before changing to media containing various concentrations of DMSO (0, 0.25, 0.5, 1, 2%). After an additional two weeks of culture, CYP activity was assessed by functional assay. DMSO-free, William's E media contained various concentrations of hydrocortisone (0, 2, 10, 50, 250 μM), insulin (0, 0.2, 1.5, 2, 5 μg/ml), and FCS (10%, 20%).

5.2.6. Medium composition effect on CYP induction potential by rifampin

HepaRG cells were seeded in 12-well plates with a density of 10^5 cells/well. The medium was changed every two or three days. After two weeks culture, 1 ml phenol red-free medium with/without 10 μM rifampin was added to cultures for 3 days before CYP enzyme activity was evaluated by functional assay. DMSO-free William's E media contained various concentrations of hydrocortisone (0, 2, 10, 50, 250 μM), insulin (0, 0.2, 1, 5, 25 μg/ml) and FCS (10%, 20%).

5.2.7. Effect of DMSO on CYP induction

1% DMSO culturing protocol: HepaRG cells were seeded in 12-well plates at a density of 10^5 /well in DMSO-free medium. After one week of culture, the cells were incubated in medium containing 1% DMSO for another week prior to the induction assays.

DMSO free culturing protocol: as per section 5.2.2.

5.2.8. Assay validation using benchmark inducers

HepaRG cells were cultured as described in section 5.2.2. The following inducers were dissolved in low serum medium at the following concentrations: nifedipine, 62.5 μM; omeprazole, 40 μM; 3-MC, 1 μM; trogolitazone, 6.25 μM; Phenobarbital, 200 μM; dexamethasone, 250 μM; carbamazepine, 250 μM.

CYP P450 enzyme activity and mRNA experession were evaluated by functional assay and RT-qPCR, respectively, as described in section 5.2.3.

5.3. Results

5.3.1. Effects of DMSO on CYP expression

Previous research has shown that a four week culture is required for HepaRG cells to show robust responses to benchmark inducers (*88*). In the first two weeks, HepaRG cells were grown in DMSO-free medium. The following two weeks, HepaRG cells were grown in medium containing 2% DMSO which is essential to differentiate the cells to express cytochrome P450 enzymes (*88-89*). In an attempt to reproduce the effect of 2% DMSO on the CYP expression in HepaRG cells reported in the published literature, we observed numberous floating cells, presumably due to cytotoxicity of 2% DMSO. Next we investigated the effect of various concentrations of DMSO (0 to 2%) on CYP activity using the published 4-week protocol. The activity of each of the 5 CYP enzymes showed a bell shaped relationship with respect to DMSO concentration, being positively correlated with DMSO concentration up to 1% and decreasing at 2% (Figure 38). For example, the activity of CYP2B6 at 1% DMSO was 16 times higher than its activity at either 0% or 2% DMSO. Furthermore, no significant floating cells were observed at 1% DMSO. Therefore, 1% was chosen as the optimal DMSO concentration for maximum level of CYP activity.

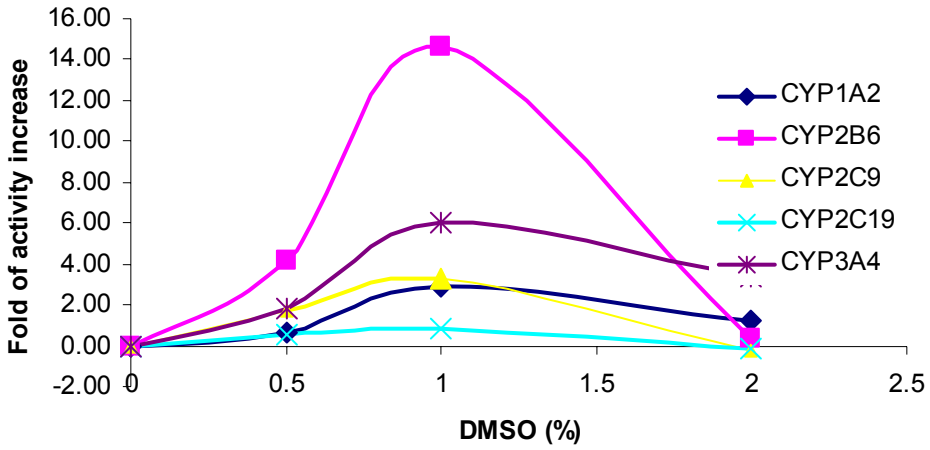

Figure 38. Effects of DMSO on CYP P450 activity of HepaRG cells.

5.3.2. Effect of DMSO on CYP induction

DMSO was reported to be essential for maintaining HepaRG culture for induction studies. As both an induction and differentiation reagent, DMSO could both inhibit cell proliferation and enhance cytochrome P450 enzyme expression (*90-91*).

In section 5.3.1, we observed that 1% DMSO was optimal for CYP activity in HepaRG cells without evidence of significant cytotoxicity. Here we wanted to test the effects of DMSO on the induction of CYP enzymes in these cells. HepaRG cells were grown in DMSO-free medium for one week and switched to medium in the presence and absence of 1% DMSO for an additional week. Following two weeks of culture (for rationale for using two weeks culture instead of four weeks, see section 5.3.3), cells received fresh DMSO-free media containing inducers at various concentrations. After 48 hours, RT-qPCR was used measure the induction potential of rifampin, 3-MC, and CITCO on CYP3A4, CYP1A2, and CYP2B6, respectively. After 72 hours incubation,

induction was assessed by means of functional assays. The mRNA of CYP1A2 and CYP3A4 in the absence of DMSO was equivalent to or greater than that observed in the presence of 1% DMSO (Figure 39), indicating that DMSO is not essential for the differention of cells to an inducible phenotype (*88-89*). 3-MC, CITCO and rifampin are specific inducers of CYP1A2, 2B6 and 3A4 enzymes through activation of AhR, CAR and PXR receptors, respectively. These results also validated the induction potential of hepaRG cells in DMSO-free medium. By eliminating DMSO in the media used for culture, it is not necessary to then change to a DMSO-free medium for three days to decrease the basal level of CYP activity prior to induction.

mRNA expression appears to be more sensitive to these three inducers than enzyme activity (Figure 39). The mRNA level of CYP1A2 showed a 70 to 100-fold increase after induction by 3-MC while less than a 2-fold increase was observed in the metabolism of melatonin, regardless of the presence or absence of 1% DMSO. There are a few possible reasons for the incongruity between mRNA and enzyme activity readouts. First, some factor is missing in the translation from mRNA to protein for CYP1A2 in HepaRG cells. Second, the enzyme activity determined by functional assay is highly dependent on the choice and concentration of the cocktail of probe substrates. The alternate substrate phenacetin was applied in the functional assay for CYP 1A2 in section 5.3.6.

Based on the above observations, we conclude that 1% DMSO seemed to be unnecessary for the induction potential of HepaGR cells. Therefore, the remaining optimization experiments were performed in DMSO-free medium.

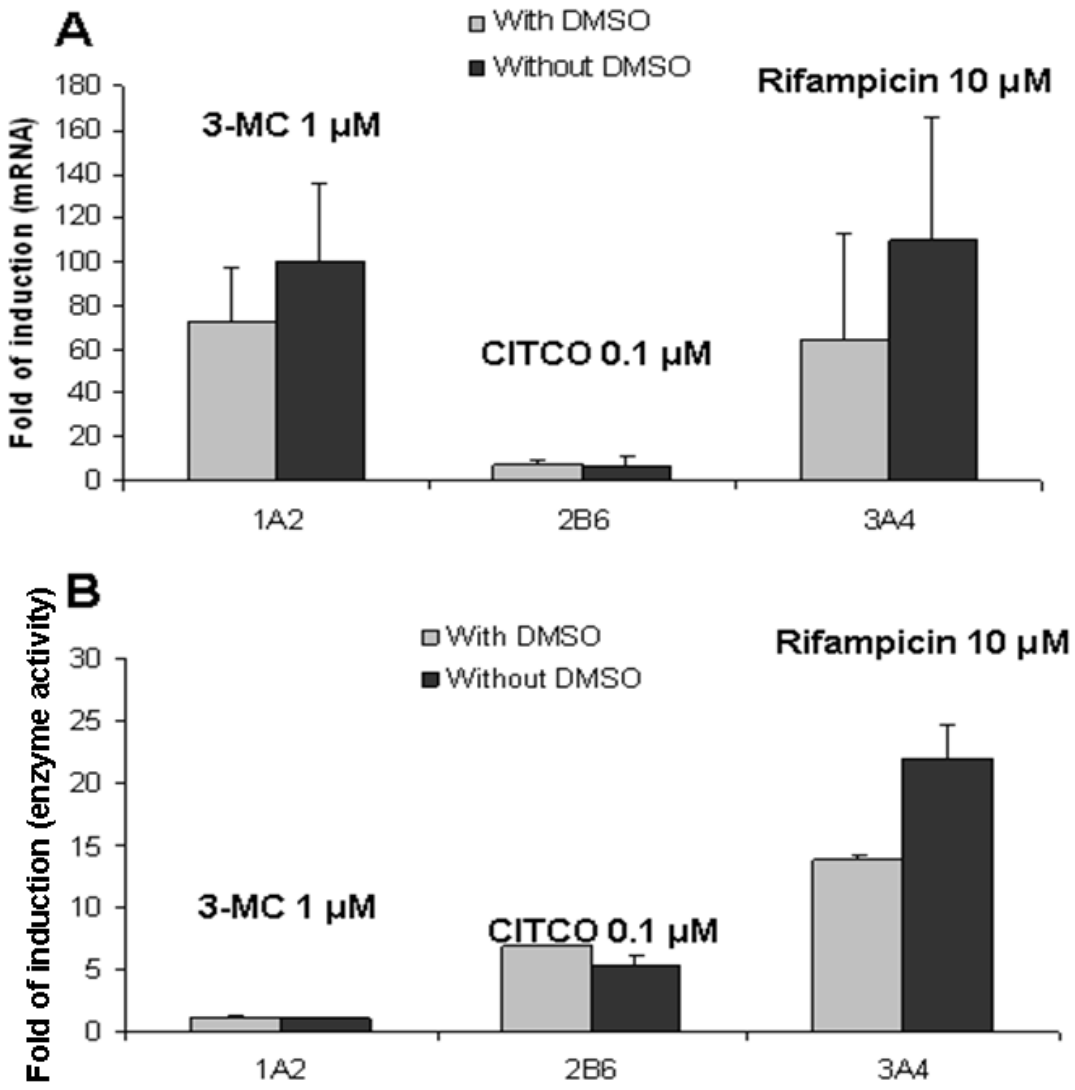

Figure 39. The induction potential of three inducers on CYP enzymes of HepaRG cells in the presence and absence of 1% DMSO.
The fold induction was determined using both RT-qPCR (A) and functional assay (B).

5.3.3. Kinetics of CYP P450 induction by rifampin

Previous published research has shown that a four week culture is required for HepaRG cells to show robust responses to benchmark inducers (*88*). In the first two weeks, HepaRG cells are grown in DMSO free medium. The following two weeks, HepaRG cells were grown in medium containing 2% DMSO. For our high-throughput application of HepaRG cells, we prefer to use HepaRG cells after a shorter culture time, e.g. 2 weeks. Therefore, it was necessary to perform a time course study on the responsiveness of HepaRG cells to inducers over a 4 week period and determine whether 2 weeks was sufficient for induction. The induction potential of benchmark inducer rifampin for major CYPs was evaluated over four weeks to determine the optimal culture time. Based on the results obtained in section 5.3.2, DMSO-free medium was used in this time course study. The induction potential of rifampin was measured using the functional assay described in section 2.6. A dose-dependent increase in actigity for all three CYP enzymes tested (CYP3A4, CYP2B6 and CYP1A2) was observed when rifampin concentrations varied from 0.1 μM to 10 μM, regardless of culture time (Figure 40). At 10 μM rifampin, the induction kinetics varied among different CYP enzymes.. For example, activities of CYP3A4 and CYP2B6 peaked at week three and started to decrease slightly at week four. For CYP1A2, activity was maximal at week 1 and decreased from week two to week four (Figure 40). In summary, the results suggested that activity (induction) maxima are observed between week two and three. In order to increase throughput, two weeks culture time was chosen as the starting point for the following optimization.

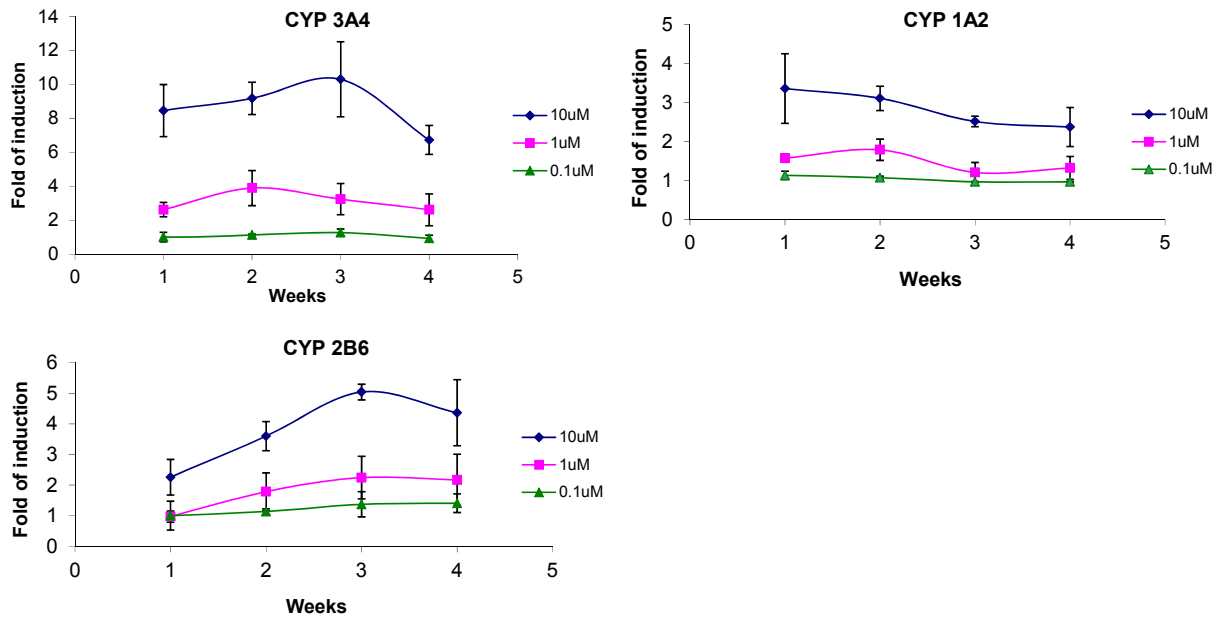

Figure 40. Time course of CYP P450 induction by rifampin using HepaRG cell model.

5.3.4. Optimization of culture medium for maximum CYP P450 expression.

The previous experiment in section 2.8 was performed using commercial medium specifically designed for high expression of CYP enzymes in HepaRG cells. However,the high cost of the medium limits its utility. Previous studies have shown that four components are critical for optimal CYP expression in HepaRG cells: hydrocortisone, insulin, DMSO and FCS, however the concentration dependence was not evaluated. Our results in section 5.3.2 showed that DMSO had little effect on the induction potential of HepaRG cells, therefore, this study focused on the effects of the other three components on the CYP expression level and induction potential by varying the concentration of one component at fixed concentrations of the others. The purpose was to determine an optimal formula to prepare an in-house medium that yields optimal

expression of CYP enzymes in HepaRG cells. All the cell culture media used in this study were made in-house and used with a two week culture protocol. The initial concentrations of the above four key components were based on published data (concentrations of hydrocortisone, insulin, FCS were 50 μM, 5 μg/ml and 10%, respectively) (*88*).

5.3.4.1. Effects of hydrocortisone on CYP P450 expression

In this experiment, the effect of hydrocortisone concentration on CYP enzyme activity was tested in DMSO-free medium. The insulin concentration was fixed at 5 μg/ml and FCS at 10%. The expression of four out of five CYP enzymes increased with increasing hydrocortisone concentration (0 to 250 μM) in a dose dependent manner (Figure 41). CYP2C8 expression was maximal at 10 μM hydrocortisone and significantly lower at higher hydrocortisone concentrations. This finding was consistent with a literature report that hormones such as hydrocortisone are essential for most CYP expression in primary hepatocytes (*88*). Based on these results, a hydrocortisone concentration of 50 μM was chosen.

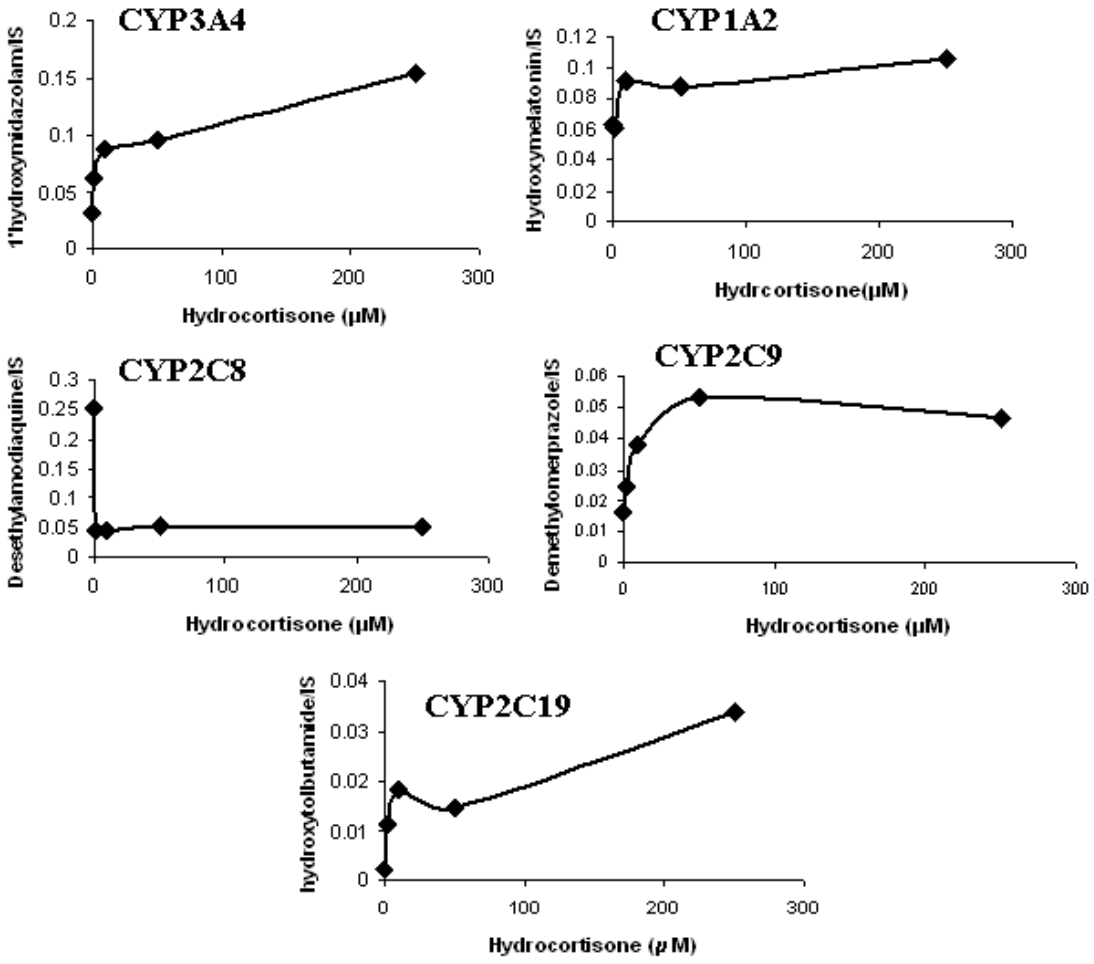

Figure 41. Effects of hydrocortisone on CYP P450 activity of HepaRG cells.

5.3.4.2. Effects of hydrocortisone on induction potential

Although the previous experiment showed CYP activity was enhanced with increasing hydrocortisone concentration, it was not the same case for induction potential. A concentration of 2 μM hydrocortisone showed the highest induction potential for CYP3A4, 1A2, 2C9 and 2C19 (TABLE XXV). However, 2 μM hydrocortisone was not enough to support healthy cell growth and a significant number of floating dead cells

was observed. A concentration of 50 μM hydrocortisone showed slightly lower induction potential of CYP enzymes compared to 2 μM. Furthermore, there were no significant floating cells observed at 50 μM hydrocortisone. From both induction potential and cell viability perspectives, the optimized hydrocortisone concentration was determined to be 50 μM.

TABLE XXV. HYDROCORTISONE CONCENTRATION-DEPENDENCE OF CYP ENZYME INDUCTION IN HEPARG CELLS.

Concentration (μM)		0	2	10	50	250
Fold of induction	CYP3A4	5.80	10.36	7.49	8.40	6.28
	CYP1A2	1.40	3.26	2.06	2.58	2.99
	CYP2C8	0.68	0.77	0.70	0.51	0.94
	CYP2C9	1.31	2.07	1.52	1.21	1.54
	CYP2C19	1.43	1.56	1.13	1.55	0.97

5.3.4.3. Effects of human insulin on CYP P450 expression

To study the effect of insulin on CYP expression in DMSO-free medium, hydrocortisone and FCS were held fixed at 50 μM at 10%, respectively. No clear dose-response relationship was observed between insulin concentration and CYP enzyme activity (Figure 42). For CYP2C8, 2C9 and 2C19, 0.2-1 μg/mL insulin supported the highest activity. For CYP2C8 and CYP2C9, concentrations higher than 1 μg/mL insulin resulted in decreased activity. For CYP3A4, 0.2 μg/mL insulin supported the highest activity while higher concentrations decreased activity. For CYP1A2, the response showed a complex pattern and it was not possible to discern a single concentration of insulin supporting optimal activity. Microscopic observation revealed, floating cells when

the insulin concentration was below 5 µg/mL. Therefore, an insulin concentration 5 µg/mL was chosen in order to avoid cell death.

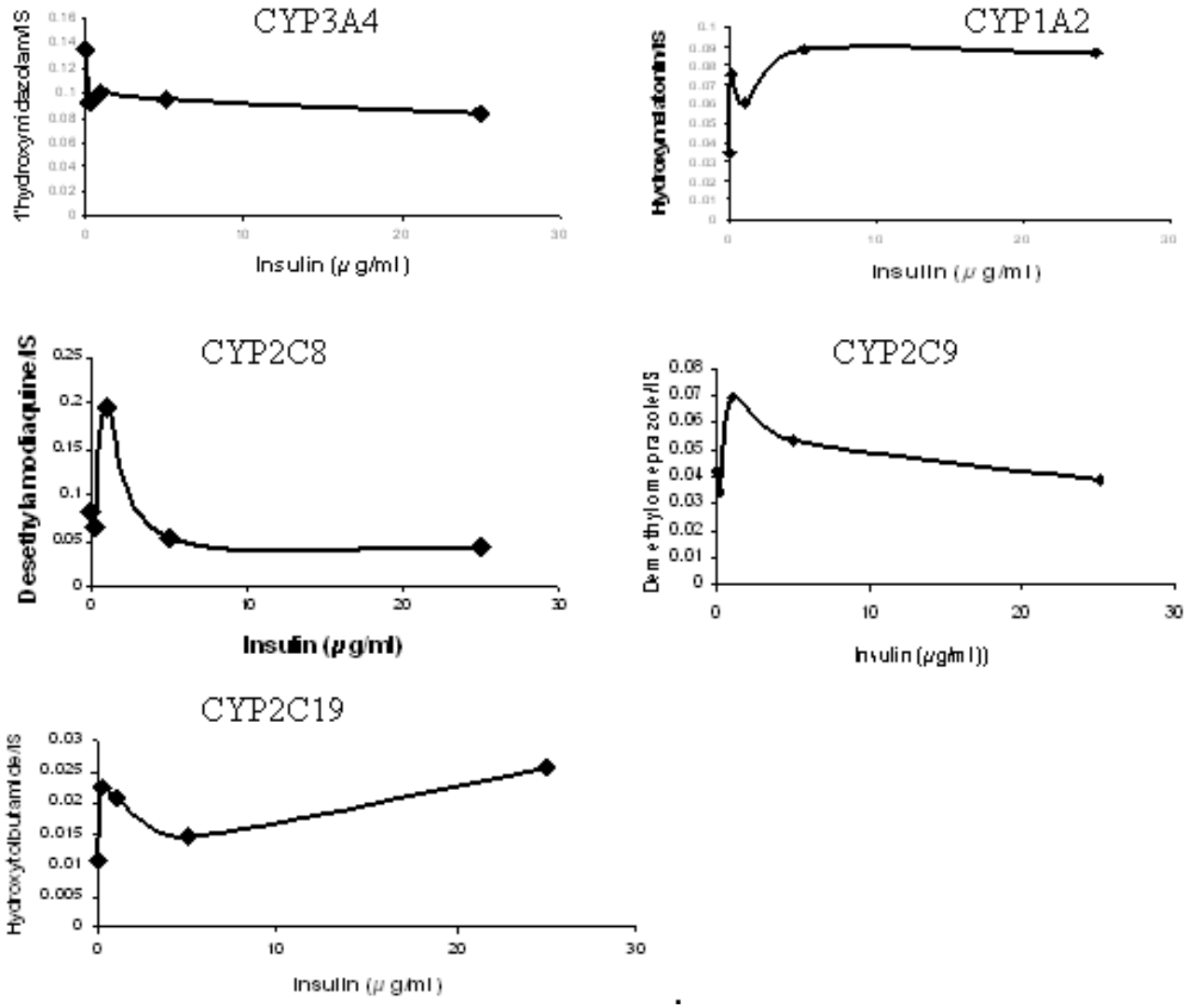

Figure 42. Effects of insulin concentration on CYP activity of HepaRG cells.

5.3.4.4. Effects of insulin on induction potential

Insulin showed a similar induction trend as hydrocortisone. Among tested concentrations, 0.2 µg/ml insulin supported the highest induction of CYP3A4, 1A2, 2C9, and 2C19 (TABLE XXVI)**.** However, less than 5 µg/mL insulin was not enough to support healthy cell growth. An increase was not observed at 25 ug/ml insulin, therefore, the optimized insulin concentration was 5 µg/ml.

TABLE XXVI. EFFECT OF INSULIN CONCENTRATION ON INDUCTION OF CYP ENZYMES IN HepaRG CELLS.

CYP enzyme fold induction at different insulin concentration (µg/ml)						
Concentration (*µg/ml*)		**0**	**0.2**	**1**	**5**	**25**
Fold of induction	**CYP3A4**	6.39	10.35	8.89	8.40	8.40
	CYP1A2	3.91	3.61	2.90	2.58	2.36
	CYP2C8	1.54	1.00	0.47	0.51	0.87
	CYP2C9	1.65	2.36	1.36	1.21	1.71
	CYP2C19	1.23	1.61	1.13	1.55	1.04

5.3.4.5. Effect of FCS concentration on CYP expression

The effect of 10% and 20% FCS on CYP enzyme expression was determined in DMSO-free medium at fixed concentrations of hydrocortisone (50 µM) and insulin (5 µg/ml). An inverse correlation was observed between FCS concentration and CYP enzyme activity (TABLE XXVII). At 5% FCS, HepaRG cells grew very slowly (data not shown). Therefore, 10% FCS was chosen as an optimal FCS concentration.

TABLE XXVII. EFFECT OF FCS CONCENTRATION ON CYP ACTIVITY OF HepaRG CELLS

FCS concentration on enzyme activity			
FCS percentage		**10%**	**20%**
Relative activity (Substrate/IS)	**CYP3A4**	0.095	0.032
	CYP1A2	0.088	0.075
	CYP2C8	0.053	0.027
	CYP2C9	0.053	0.021
	CYP2C19	0.015	0.005

5.3.4.6. Effect of FCS on CYP induction potential

10% FCS showed higher induction potential than 20% FCS. Since HepaRG cells grew very slow at 5% FCS, 10% FCS was chosen for induction experiments (TABLE XXVIII).

TABLE XXVIII. EFFECT OF FCS CONCENTRATION ON INDUCTION OF CYP ENZYMES IN HepaRG CELLS

FCS percentage on fold of induction			
FCS percentage		**10%**	**20%**
Fold of induction	**CYP3A4**	8.40	6.28
	CYP1A2	2.58	1.30
	CYP2C8	0.51	0.60
	CYP2C9	1.21	1.40
	CYP2C19	1.55	1.23

5.3.5. Optimized culture medium for CYP induction assay using HepaRG cells

In summary, we have found that DMSO is not absolutely required for the induction of CYP enzymes in HepaRG cells. In DMSO-free medium, hormones such as

hydrocortisone are essential for expression of most CYP enzymes in HepaRG cells while there is no clear dose-response relationship between insulin concentration and CYP enzyme activity. However, super-maximal levels of CYP expression with high concentration of hydrocortisone and insulin result in a decrease in the dynamic range of the induction response. Considering the assay sensitivity and cell viability, the optimized medium composition is: Williams' E medium supplemented with 10% FCS, 100units/ml penicillin, 100 µg/ml streptomycin, 5 µg/ml insulin, 2 mM glutamine, and 5×10^{-5} M hydrocortisone. Furthermore, the optimal growth period for CYP expression and induction in HepaRG cells is two weeks.

5.3.6. Induction assay validation by benchmark inducers

A total of six benchmark inducers were tested on HepaRG cells in DMSO-free medium. The induction potentials of these inducers were tested on CYP3A, 2B6 and 1A2 in HepaRG cells using both functional assays and RT-qPRC (Figure 43, Figure 44). The six drugs showed a similar induction rank order across 3A4 and 2B6 by both functional assay and RT-qPCR measurements which is not suprising considering that the compounds are all ligands for PXR, the upstream nuclear receptor for 3A4 and 2B6 enzyme expression. 3-MC is the ligand of AhR in hepatocytes which showed highest induction of 1A2 mRNA among the panel of inducers. Interestingly, the high induction of CYP1A2 mRNA level did not result in high CYP1A2 activity in the cells using phenacetin as substrate (Figure 43 and Figure 44).

Overall, the induction potentials measured by both functional assay and RT-qPCR were comparable to literature reported values (*88, 92-93*). We conclude that the induction assay protocol presented here was validated.

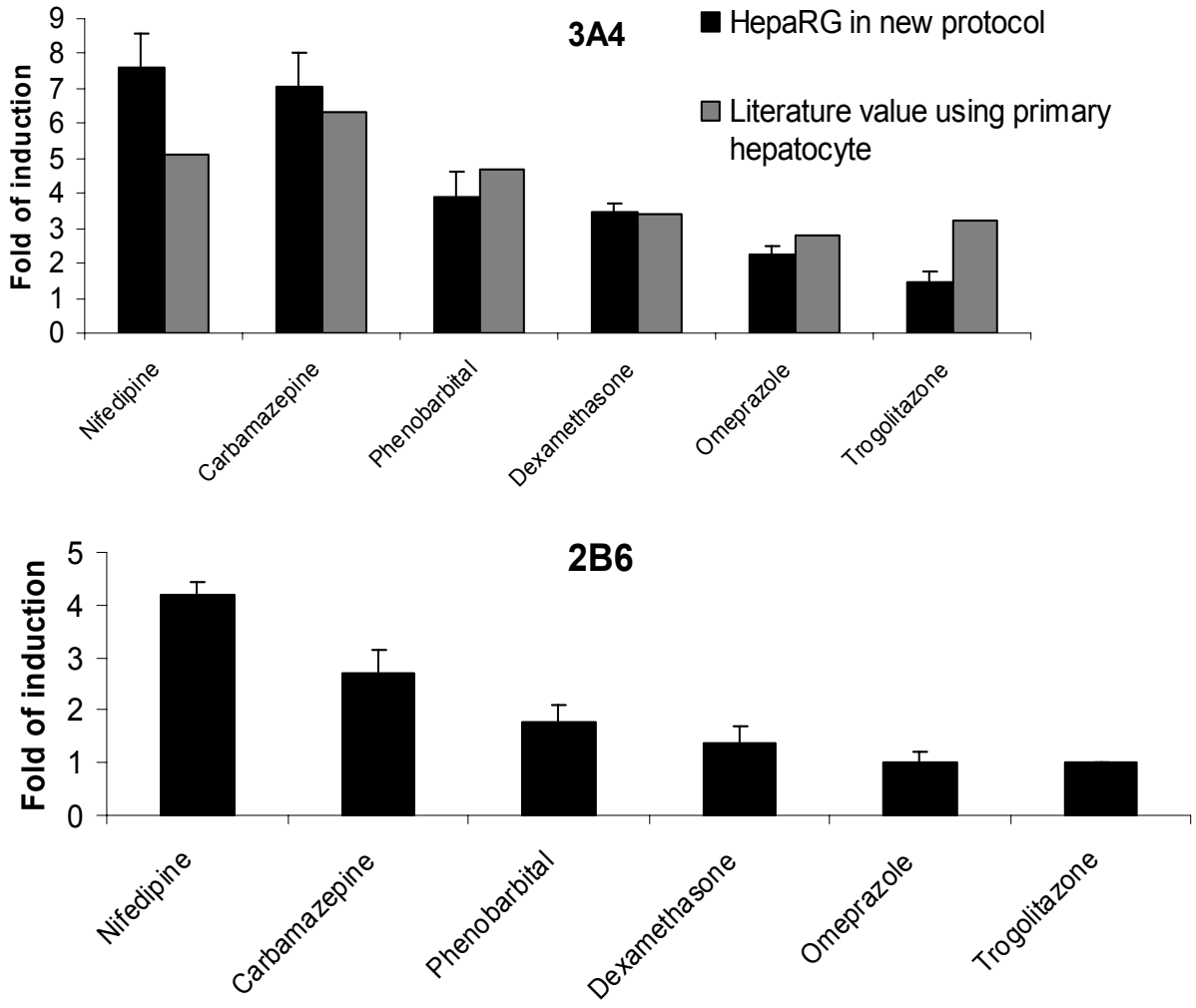

Figure 43. CYP induction by multiple inducers using functional assay readouts.
nifedipine: 62.5μM, omeprazole: 40μM, trogolitazone: 6.25μM, phenobarbital: 200μM, dexamethasone: 250μM, carbamazepine: 250μM.

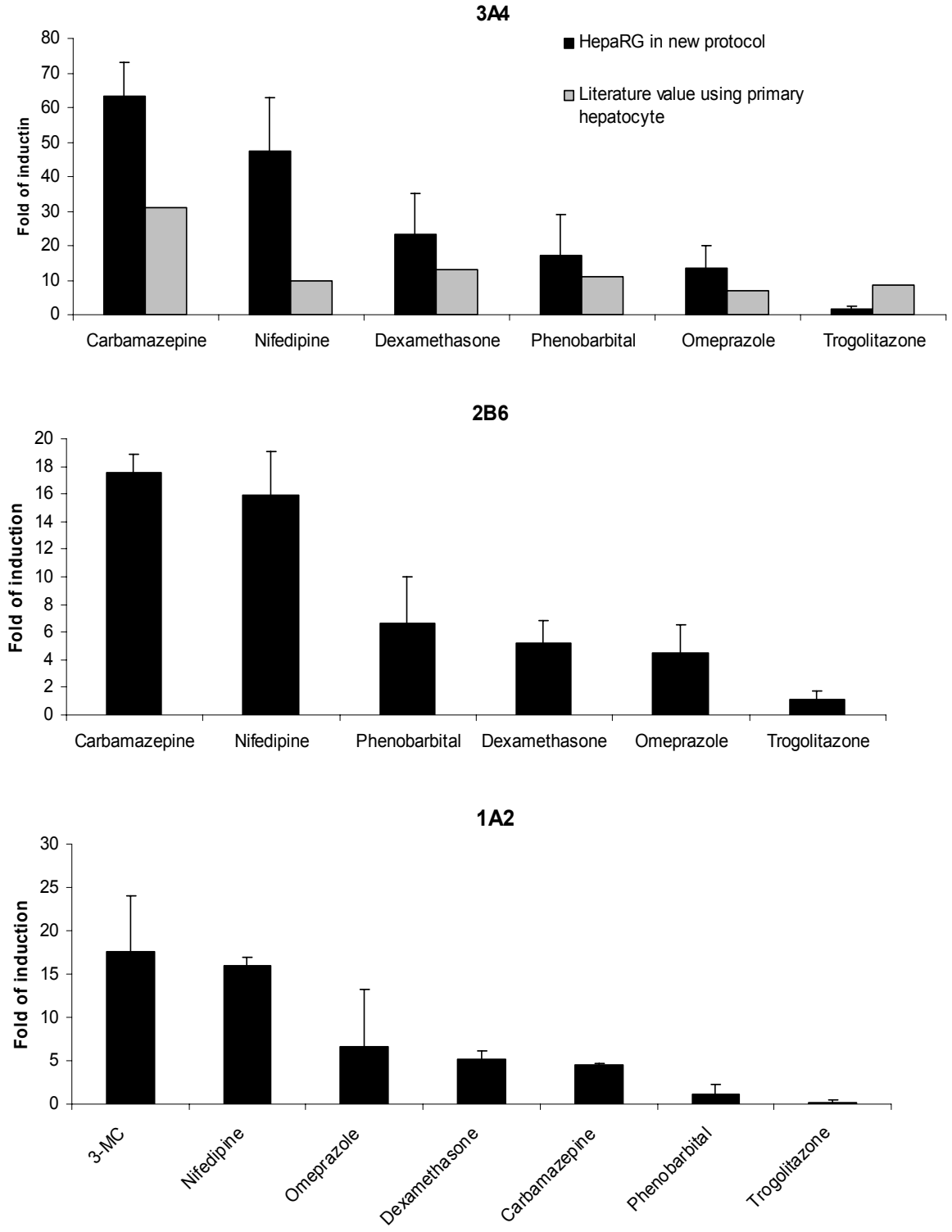

Figure 44. CYP induction by multiple inducers using mRNA readout.
Concentration: nifedipine: 62.5μM, omeprazole: 40μM, 3-MC:1μM, trogolitazone:6.25μM, phenobarbital:200μM, dexamethasone:250μM ,carbamazepine:250μM.

5.3.7. Concentration-dependent induction of CYPs by rifampin in DMSO-free medium

EC_{50} and E_{max} are two widely used parameters in the modeling of in vitro-in vivo correlation of induction potentials. The validated in vitro CYP induction assay mentioned above will be mainly used to deternmine the EC_{50} and E_{max} of test compounds. In a proof of concept experiment, the induction potential of rifampin on CYP3A4 was measured at multiple concentrations of rifampin using a functional assay (Figure 45). Dose response analysis showed an EC_{50} value of 1.9 μM (with a E_{max} of 6-fold of induction). This EC_{50} value was consistent with the literature reported EC_{50} of 0.6 uM using primary hepatocytes (*56, 92*).

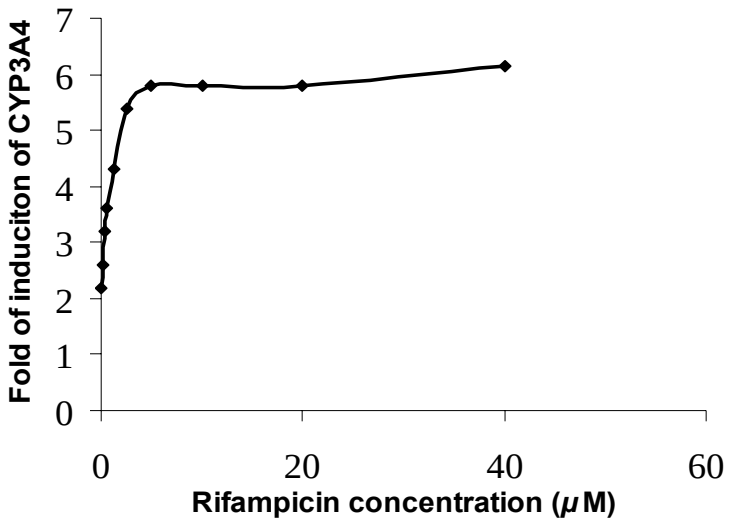

Figure 45. Rifampin concentration-dependent induction on CYP3A4 in HepaRG cells grown in customized DMSO-free medium.

5.4. Discussion

Due to expression of a complete set of CYP enzyme at levels close to those observed in human primary hepatocytes, HepaRG is an excellent cell line for measuring liver enzyme induction potentials of drug candidates. However, there were two chanllenges preventing use of this cell line in high-throughput screening of a large number of compounds for induction potential: 4 week incubation for differentiation to a phenotype capable of expression of high level of CYP enzymes and the high cost of commercial medium for cell culture and differentiation. The current studies focused on overcoming these two challenges.

The published induction protocol required two weeks of HepaRG cell growth in DMSO free-medium followed by another two weeks of growth in medium containing 2% DMSO. In an attempt to set up a HepaRG-based induction assay using this published protocol, significant cell death was observed in medium containing 2% DMSO. Further studies suggested that the effect of DMSO on the induction potential of CYP enzymes was negligible or even detrimental. Based on this finding, a new DMSO-free medium was optimized and validated for measuring the induction potential of various inducers in HepaRG cells. A time course study suggested that two weeks culture in the customized DMSO free medium was sufficient for a robust response to inducers in HepaRG cells.

Based on these findings, a new induction protocol was established with a significantly shorter turnaround time than published method. Multiple inducers were tested in this cellular model with consistent results achieved for CYP P450 1A2, 2B6, 3A4 mRNA levels. The cost for the new assay was 50-fold lower than that using primary hepatocytes and 8-fold lower than when using HepaRG cells with the published protocol

and commercial medium. The shorter total assay time and lower cost makes this a superior model for large scale CYP enzyme induction screening in the early stages of drug discovery.

However, for CYP1A2 induction, there was a discrepancy between the results from the functional assay and RT-qPCR. Using western blot assay to quantify induced CYP1A2 can provide insights to explain the observed discrepancy. If there is in fact an elevated level of CYP1A2 in the induced cells, the observed discrepancy could possibly be due to the presence of the other substrates in the cocktail. This possibility could be examined by comparing activity with a single substrate vs. the substrate cocktail.

Ultimately the value of in vitro models is determined by the extent to which they correlate with in vivo observations. To establish a predictive model, both parameters of EC_{50} and E_{max} from the induction dose response curves are to be included in the modeling(*85*). The dose response of rifampin has been tentativelhy established using this HepaRG-based induction assay with excellent agreement with literature reported values. More inducers are to be included in this study for functional assay and RT-qPCR evaluation. The EC_{50} and E_{max} of those inducers would be applied to extrapolate to the clinical AUC change through mathematical modeling.

Compared with the use of preimary hepatocytes, the HepaRG immortalized cell line could be used to generate more consistent data with less interbatch variation which makes it more suitable for SAR studies in the early drug discovery stage, thus decreasing the chance of encountering undesired drug-drug interactions in later clinical development. With the modified protocol and customized medium, the assay cost is dramatically lowered which makes possible high-throughput screeing applications. With

the in vitro-in vivo correlation established, this assay was validated to replace the hepatocyte model to predict the induction potential of compounds in humans. However, there are still hurdles that prevent wider applications of this induction model. First, as described above, the discrepancy between mRNA level and enzyme activity of CYP1A2 needs to be solved. Second, since HepaRG is a single donor cell line, how well this cell line could accurately predict the average induction in humans still needs to be determined with more inducers.

After establishment of the HepaRG cell culture platform in our lab, further studies using HepaRG cells included cytochrome P450 inhibition, cytotoxicity, and uptake transporters. An economic and consistent cellular model is expected to be established and applied in an academic setting to serve anti-TB drug discovery.

6. DEVELOPMENT OF ACTIVE METABOLITE-BASED BIOASSAY SYSTEM TO STUDY ANTI-TB ACTIVITY OF COMPOUND METABOLITE

6.1. Introduction

Current algorithms for HTS-based drug discovery for antimicrobial agents fail to account for the possibility of active metabolites early in the drug discovery process. In order to overcome this drawback in our screening efforts for novel anti-TB drugs, we propose to establish an in vitro assay to rapidly detect the anti-TB activity of liver enzyme-derived metabolites. These TB-active metabolite assays (TAMA) can obviate the need for metabolite ID and synthesis to confirm the presence or absence of an active metabolite. A novel method to evaluate metabolite activity was developed by combining a liver enzyme metabolite generation system (MGS) with an anti-TB assay. For detection of prodrugs (type 4 compounds; inactive parent compound with active metabolites, Figure 46), a single point “one pot” assay was established. This can serve to increase compound library chemical diversity and give consideration to revisiting previously screened libraries. The ability to detect active metabolites by this method early in the drug discovery process will allow for the further progression of some active (type 3) compounds with poor metabolic stability that otherwise would be deprioritized using only LC-MS based stability assays. The above methodology is to be developed using established and modified control compounds and then applied to a HTS with hit to lead follow up.

	Type 1	Type 2	Type 3	Type 4 prodrug
Parent	active	active	active	inactive
Stability	high	low	low	low
Metabolite	NA	inactive	**active**	**active**

Figure 46. Four types of compounds with metabolites.

6.1.1. Deficiencies in contemporary drug discovery algorithms

Drug discovery efforts often begin with the screening of focused or diverse compound libraries initially against either molecular targets or whole cells and hits identified. Compounds that are inactive in such screens but which might be converted to active metabolites in vivo by liver enzymes go undetected. (Such prodrugs are occaisionally designed later in the drug discovery scheme only when a clinical candidate requires chemical modification to improve ADME properties). Among those hits that do emerge from initial screens, many will be subjected to a number of in vitro filters in the hit to lead phase prior to choosing a small number for scale up synthesis and evaluation of pharmacokinetics and/or efficacy in animal models (*94-95*). Compounds with poor stability in the presence of liver enzymes (as determined by LC-MS) are typically not progressed to in vivo evaluation of pharmacokinetics or efficacy. In our own experience, liver microsome instability is the most commonly encountered deficit among selective anti-TB hits. In cases where the compound is deemed to be of sufficient interest, identification of the major metabolite(s) is determined in order to guide analog synthesis toward more stable compounds. To assess whether such metabolites might possess activity equal or greater than that of the parent compound, the metabolite need not only to be identified but to be synthesized as well. Because of

the amount of effort involved, this is usually part of the more downstream lead optimization process and only performed on compounds which already have some degree of metabolic stability.

6.1.2. Importance of pharmacologically active metabolite(s)

As the product of metabolism and detoxification, active metabolites usually have lower drug-drug interactions and improved physicochemical (e.g, solubility), pharmacokinetic and overall safety profiles than the parent drug (*96-98*).

Examples of clinical drugs in the market that were developed from active metabolites include sulfanilamide (parent drug: prontosil), acetaminophen (parent drug: phenacetin), digoxin (parent drug: parent drug: β-methyldigoxin), fexofenadine (parent drug: terfenadine), mesoridazine (parent drug: thioridazine) and morphine (parent drug: codeine) (*99*).

Some existing and experimental anti-TB drugs also have known or suspected active metabolites (*25*) (TABLE XXIX). For example, the experimental compounds SQ-109 and LL3858 (Chapter 3) are reported to be active *in vivo*, but are not stable in the presence of liver microsom*es(30, 100-102)*. These findings highlight the need to develop early-stage methods for evaluating parent compounds *and* their metabolites.

TABLE XXIX. CLINICAL AND EXPERIMENTAL ANTI-TB DRUGS WITH KNOWN OR SUSPECTED ACTIVE METABOLITES.

Drugs	Active metabolites
Rifampicin	25-deacetylrifampicin
Pyrazinamide	pyrazonic acid
Ethionamide	S-oxide ethionamide
Clarithromycin	14-OH clarithromycin
SQ-109	Unstable, possibly has active metabolits
LL3858	Unstable, possibly has active metabolits

6.1.3. Novelty of this approach

The idea of evaluating the biological activity of compounds in vitro following metabolism by liver enzymes is not in itself novel as this is routine in the Ames mutagenicity assay. We are not aware, however, of any attempt to use this approach in the identification of new anti-infectives or any other drug in the early stages of drug discovery.

6.2. Materials and methods

6.2.1. Materials

Mouse microsomes were purchased from Xenotech, LLC, (Lenexa, Kansas), NADPH was purchased from Sigma. Alamar blue dye was purchased from AbD serotec (Raleigh, NC).

6.2.2. Interference of Microsomes and NADPH on MABA

This study focused on the effect of various concentrations of microsomes and NADPH on MABA readout. The experiment was performed in the absence of *M. tuberculosis* in the culture medium. Different concentrations of fresh mouse microsomes and NADPH were mixed with 7H12 medium before adding 20 µl 10x alamar blue dye and 12.5 µl 20% Tween-80 into the wells for 16 to 24 hours. Fluorescence of alamar blue was measured (ex 530nm, em 590nm) in fluorescence unit using a fluorescence plate reader (PerkinElmer, Fremont, CA). The increment ratio is calculated using the following equation:

$$\text{Increment Ratio} = \frac{\text{MABA Readout(test)} - \text{MABA Readout(medium control)}}{\text{MABA(medium control)}} \qquad (6)$$

6.2.3. Microsome and NADPH effects on *M. tuberculosis* growth

Measuring *M. tuberculosis* growth by colony counting: *M. tuberculosis* strain H37Rv was incubated with different concentrations of microsomes or NADPH in 7H12 medium for 7 days before spotting 50uL aliquots of serial 10-fold dilutions onto 7H11

agar plates (Collins and Franzblau 1997) and counting colonies after 21 days incubation. Bacteria viability relative to untreated controls was calculated by the following equation:

$$\text{Bacteria viability (\%)} = \frac{(\text{CFU}_{\text{test}} - \text{CFU}_{\text{control}})}{\text{CFU}_{\text{control}}} \times 100\,\% \qquad (7)$$

6.2.4. Eliminating interference from microsomes and NADPH in the assay

Acidic precipitation. HCl (1 µl of 1N solution) was added into the microsome and NADPH mixture to adjust the pH to 2 and the mixture incubated at 37C for 24 hours. After the protein was denatured, another 1 µl 1N NaOH was added to neutralize the acid prior to the addition of *M. tuberculosis*..

Physical removal. Microsomes were removed either by centrifugation of the mixture at 10000 rpm for 30 minutes or by filtration through a 10KD centrifugal filter. The supernatant and filtrate, respectively were added to the bacterial culture.

Filtration method. The microsome and NADPH mixture was added into 10KD filter tube and centrifuged. The filtrate was added into the bacteria culture.

The bacterial viability after the above methods was determined by the MABA.

6.3. Results

The development and validation of TAMA is outlined in Figure 47.

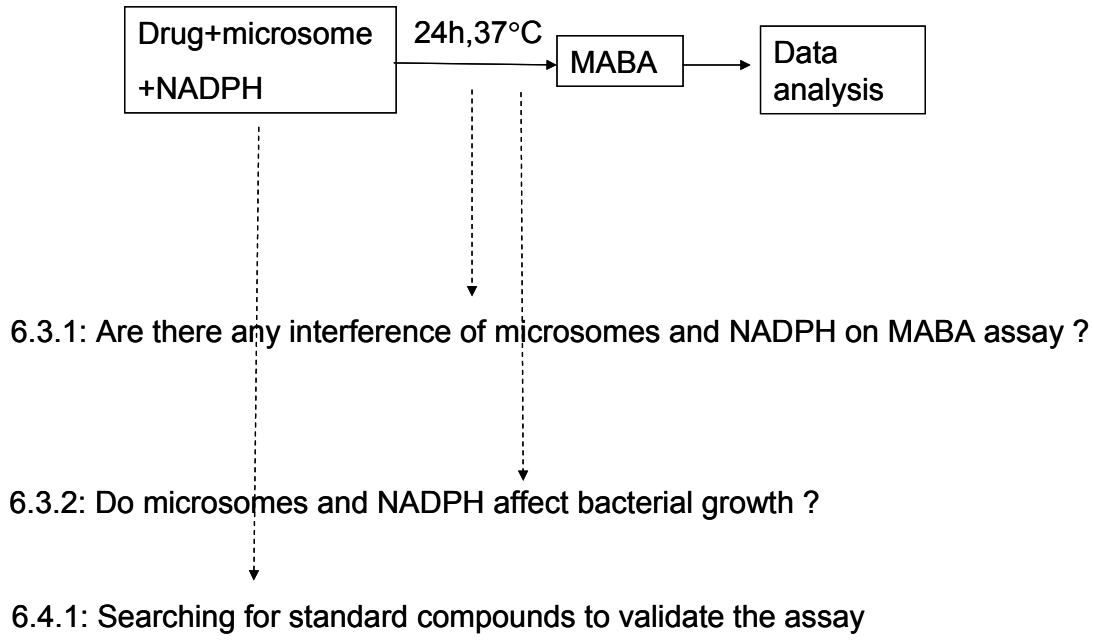

Figure 47. Optimization of TAMA

6.3.1. Interference of Microsome and NADPH on MABA

The ideal assay for anti-TB activity determination should be compatible with the microsome reaction mixture. Therefore the effect of microsomes and NADPH on the MABA readout was determined. A linear increase of fluorescence was observed in response to increasing concentrations of NADPH and microsomes (Figure 48). This is presumably due to ring-like structures present in NADPH and microsome, which

generate fluorescence signals when excited at 530 nm. The fluorescence signal generated from NADPH and microsomes in control incubations can be subtracted as background.

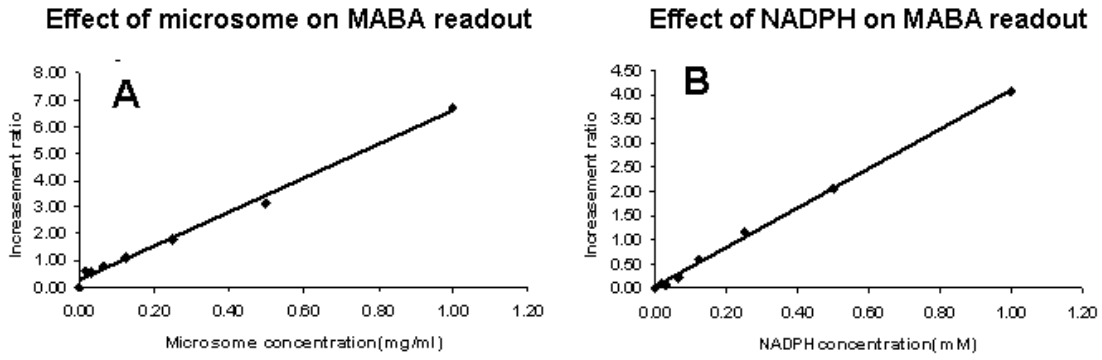

Figure 48. Interference of microsome (A) and NADPH (B) on MABA readout.

6.3.2. Effects of microsome and NADPH on the growth of *M. tuberculosis*

To determine if a “one-pot” assay was feasible, the effects of microsomes and NADPH on *M. tuberculosis* growth/viability was determined following incubation for one week by determining colony forming units (*58*).

Mouse microsomes showed an inhibitory effect on *M. tuberculosis* growth at high concentration (0.5, 1 mg/ml), and were slightly growth stimulating at lower concentration (0.125, 0.25 mg/ml). NADPH effected a slight dose-dependent stimulation of growth over the entire concentration range (Figure 49).

The bacterial growth stimulation effects of microsomes at 0.25 mg/ml and NADPH can be accommodated via normalization to develop a “one-pot” methodology. For anti-TB compounds with relatively low MIC (e.g. 2.5 μM), corresponding low concentrations of test compound can be used with low concentrations of microsomes.

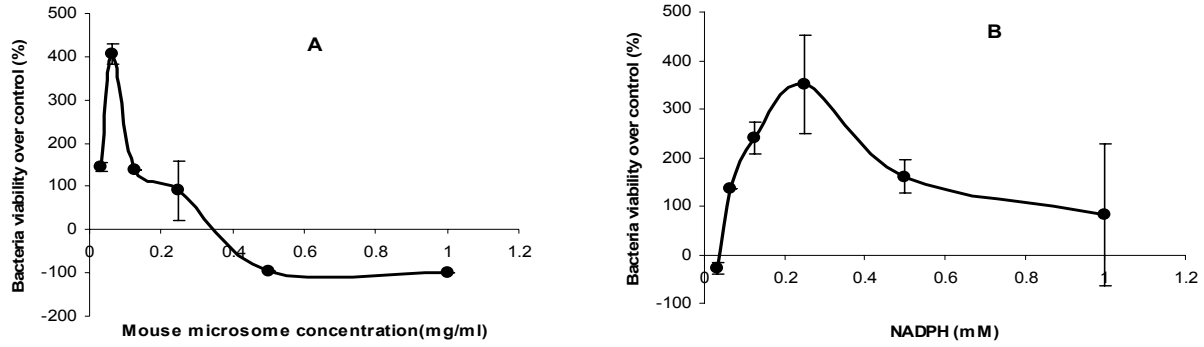

Figure 49. Effect of liver microsomes and NADPH on *M. tuberculosis* growth/viability as determined by cfu.
The line above the x axis represents growth stimulation effects while the line below represents growth inhibition effects in this concentration range. From day 0 to day 7, the bacterial control increased from $1.7x10^4$ to $1.34x10^5$ cfu/ml.

6.3.3. A pilot experiment with metabolically stable and unstable compounds

As a proof of concept we evaluated ITR306, an experimental anti-TB compound with good potency (MIC=0.37μM) and low metabolic stability (<20% parent compound remaining after incubating with mouse microsomes for 30 minutes) and PA-824 (MIC=0.85 μM), a relatively stable drug in microsomes (86% and 92% percent remaining after 30 minutes incubation with mouse and human microsomes respectively) (*103*).

Because the microsome reaction mixture (microsome + NADPH + test compound) was pre-incubated for 24 hrs prior to being diluted 4x into the *M. tuberculosis* culture, the concentration of microsomes and NADPH can be 4x higher during this pre-incubation. Since 0.25 mg/ml was the highest microsome concentration showing no inhibition of *M. tuberculosis* growth, in this particular experiment a concentration of 1 mg/ml microsome and 1 mM NADPH (sufficient to saturate the system (*94*)) was used for compound incubation, resulting in final concentrations of 0.25 mg/ml microsomes and 0.25 mM NADPH after addition of the *M. tuberculosis* culture.

In order to normalize the interferences of microsome assay on MABA readout and the growth rate of *M. tuberculosis*, several control experiments were set up to provide background assay signals (Figure 50). The experiment demonstrated no significant reduction in the inhibition of *M. tuberculosis* growth after PA-824 was pre-incubated with a complete microsome reaction (microsome + NADPH) compared to incubations without either microsomes or NADPH (Figure 51). This suggested that PA-824 retained most of its anti-TB activity in this system, which was consistent with its previously established metabolic stability. In contrast, a significant reduction in activity was observed for ITR306 when comparing the complete reaction mixture with the incomplete reactions. This suggested that ITR306 was rapidly metabolized to one or

Complete (test):	10*u*M compound+1mg/ml mouse microsome+1mM NADPH (total volume 50*μ*l)	*Complete(bacground control):*	1mg/ml mouse microsome+1mM NADPH (total volume 50*μ*l)
Control 1(test):	10*u*M compound+ 1mg/ml microsome (total volume 50μl)	*Control 1(background):*	1mg/ml microsome (total volume 50μl)
Control2(test):	10*u*M compound+ 1mM NADPH (total volume 50μl)	*Control 2(background):*	1mM NADPH (total volume 50μl)

Pre-incubated for 24 hour in 37°C

50μl 2X concentrated medium
100μl H37Rv bacteria

Final concentration:
microsome:0.25mg/ml
NADPH:0.25mM
Compound:2.5μM

Incubate for 7days in 37°C

Add 20μl 10 fold alamar blue dye and 12.5μl 20% Tween80

Incubate for 24hour in 37°C

Measure fluorecence reasout (ex 530nm, em 590nm)

Calculate percentage inhibition as equation (1)

$$\text{Percentage inhibition}(\%) = \frac{\text{MABA readout(background)} - \text{MABA readout(test)}}{\text{MABA readout(background)}} \times 100\% \quad (1)$$

Figure 50. Work flow of pilot experiments

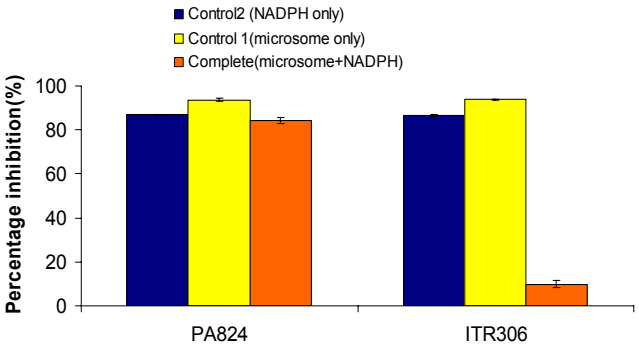

Figure 51. Comparison of bacterial growth inhibition effects of PA824, ITR306 between reaction and control groups.

more compounds devoid of significant anti-TB activity. This was consistent with data obtained in our attempts at developing this compound series.

This pilot experiment suggested that the current assay system could identify compounds that were metabolically unstable and had inactive metabolites. However, we still require a benchmark anti-TB compound which is metabolically unstable but has active metabolites to validate the assay to screen for active metabolites.

6.4. Discussion

6.4.1. Searching for control compounds with active metabolites to validate the assay

Several anti-infective drugs that were designed or discovered later to be prodrugs represent a potential source of compounds with active metabolite(s) to be used for assay validation (TABLE XXX, Figure 52). Prontosil is a potent antibacterial drug however, its metabolite, sulfanilamide, has very limited anti-tuberculosis activity. Thioridazine is a known anti-tuberculosis compound *in vitro* and *in vivo* (*104*). However, one of its two metabolites,

TABLE XXX. ANTI-INFECTIVE DRUGS TESTED AND THEIR METABOLITE(S)

Prodrug	Active metabolite	Problem
Prontosil	Sulfanilamide (>200μM)	Hard to get commercial available prodrug
Prulifloxacin (1.5μM)	Ulifloxacin (1.9 μM)	Fail to convert in liver microsome
Thioridazine (12μM)	Mesoridazine(195.9μM)	Metabolite not active
Compound I (0.9μM)	Hydroxylation metabolite (>200μM)	Metabolite not active
Ciprofloxacin methyl ester (99.6 μM)	Ciprofloxacin (1.2 μM)	Fail to convert in liver microsome

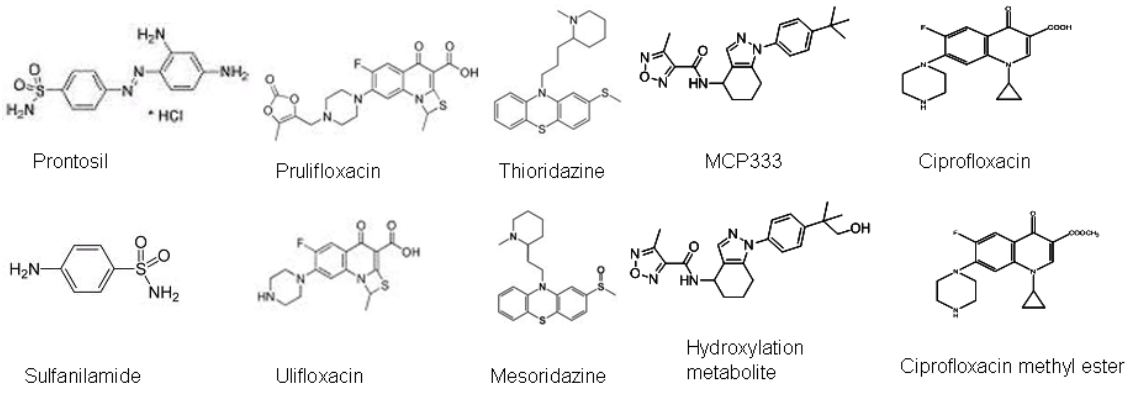

Figure 52. Candidate Type 3 or Type 4 controls and their metabolites

mesoridazine, has very limited anti-tuberculosis activity. Sulforidazine, the other metabolite of thioridazine, remains to be tested for its anti-tuberculosis activity. Prulifloxacin and ulifoxacin were previously used for the treatment of urinary tract and respiratory tract infections (*105*). Prulifloxacin is metabolized to ulifloxacin by paraoxonase which is present in serum and liver microsomes. Since both prulifloxacin and ulifloxacin have potent anti-tuberculosis activity, the former can be used as a benchmark compound for this assay. However, this biotransformation failed in liver microsomes while the conversion is high in subcellular fraction of S9. Compound **I** is the lead compound from the tetrahyroindazole series. The major metabolite of this lead compound was identified and confirmed (see Chapter 3.1 for details) but is inactive against M. tuberculosis. The ethyl ester of ciprofloxacin was synthesized in our lab as a prodrug of the active form. But conversion back to the carboxylic acid was also not observed in the microsome system.

In this case and in that of prulifloxacin other metabolite generation systems such as S9 or HepaRG cells would be considered to be included in the futher studies and perhaps argues that these more complete MGS be favored over isolated liver microsomes, assuming they are compatible with at least one type of anti-TB assay.

In the event that none of these approaches is successful and we find ourselves in the catch-22 of not being able to validate the assay with respect to identification of type 3 and type 4 compounds because none are currently known/available, then the assays will necessarily be developed based on conditions that validate use with type 2

compounds in section 6.3.3. Active metabolites identified from the screening (section 6.4.3) would then be used to fine tune the assay retrospectively.

6.4.2. Eliminating interference from microsomes and NADPH

To enhance the assay compability with higher test compound concentrations (which requires correspondingly higher concentrations of microsomes), different methods were investigated to eliminate the interference of NADPH and microsomes on the assay system. Acidic precipitation could eliminate the readout enhancement effects of microsomes when used at low concentrations. After centrifugation at 10000 rpm, the growth inhibition by microsomes was eliminated while filtration could significantly eliminate both microsome-mediated enhancement and inhibition. However, the activity of the residual compounds could not be detected in MABA, presumably due to the non-specific binding of the compounds to the filtration membrane. Similarly when using centrifugation, the presumed non-specific binding led to a decrease of the final compound concentration in the culture. For this reason, currently, there is still no effective method available to limit the interference of microsomes in the assay. Thus, the hightest compound concentration in the microsome and NADPH mixture would be 10 μM, resulting in a final concentration in the bacterial culture of 2.5 μM. This approximates the threshold used in selecting hits from high throughput screening against *M. tuberculosis*.

6.4.3. Development of HTS assay to identify prodrugs (Type 4 compounds)

A single concentration, HTS-compatible workflow is to be developed based on preliminary data obtained from the scheme in Figure 50. Only confirmed inactive parent compounds are included in the assay. The results of Type 4 compounds with active metabolites would be similar to the projected results in Figure 53.

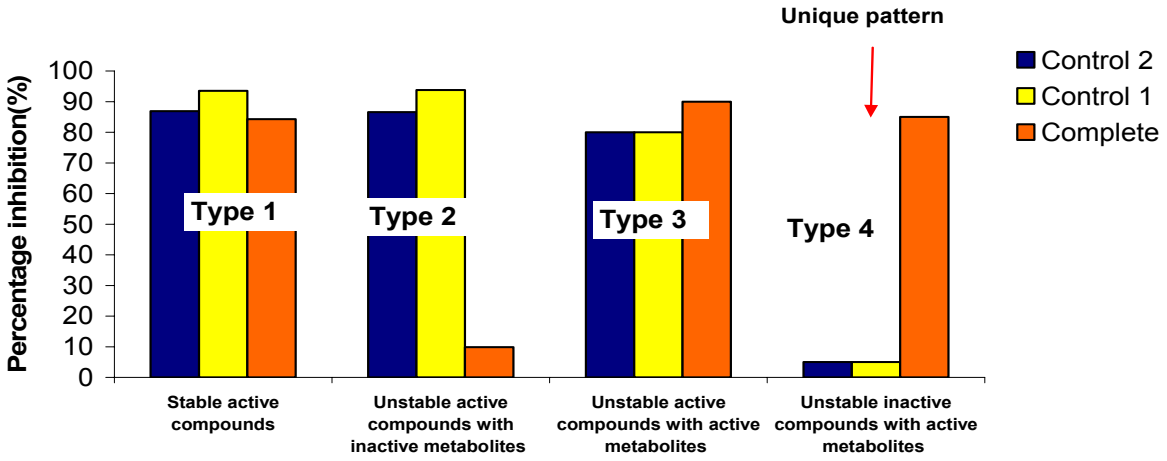

Figure 53. Projected data scheme of TAMA.

Overall, for futher application of this method for active metabolite identification, a 100,000 compound library will be screened against *M. tuberculosis* with and without MGS to generate metabolites. Compounds active only in the TAMA assay with MGS will be evaluated for function as prodrugs. This will not only provide a rough estimation of the hit rate of type 4 compounds but also possibly identify the type 4 compounds to further validate the assay.

CITED LITERATURE

1. Bloom, B. R. (1992) Tuberculosis. Back to a frightening future, *Nature 358*, 538-539.

2. Cole, S. T. (2002) Comparative and functional genomics of the *Mycobacterium tuberculosis* complex, *Microbiology 148*, 2919-2928.

3. Neyrolles, O., and Guilhot, C. (2011) Recent advances in deciphering the contribution of Mycobacterium tuberculosis lipids to pathogenesis, *Tuberculosis (Edinburgh, Scotland) 91*, 187-195.

4. Rook, G. A., and Zumla, A. (2001) Advances in the immunopathogenesis of pulmonary tuberculosis, *Curr Opin Pulm Med 7*, 116-123.

5. Smith, I. (2003) Mycobacterium tuberculosis pathogenesis and molecular determinants of virulence, *Clin Microbiol Rev 16*, 463-496.

6. Raviglione, M. C., and Uplekar, M. W. (2006) WHO's new Stop TB Strategy, *Lancet 367*, 952-955.

7. Tripathi, R. P., Tewari, N., Dwivedi, N., and Tiwari, V. K. (2005) Fighting tuberculosis: an old disease with new challenges, *Med Res Rev 25*, 93-131.

8. Glaziou, P., Floyd, K., and Raviglione, M. (2009) Global burden and epidemiology of tuberculosis, *Clin Chest Med 30*, 621-636, vii.

9. Zhang, Y. (2005) The magic bullets and tuberculosis drug targets, *Annu Rev Pharmacol Toxicol 45*, 529-564.

10. Organization, W. H. (2003) The World Health Organization Global Tuberculosis Program.

11. Donald, P. R., and van Helden, P. D. (2009) The global burden of tuberculosis--combating drug resistance in difficult times, *N Engl J Med. 360*, 2393-2395.

12. Migliori, G. B., Sotgiu, G., Lange, C., and Centis, R. (2010) Extensively drug-resistant tuberculosis: back to the future, *Eur Respir J 36*, 475-477.

13. Crabb, C. (2002) Global Alliance at full steam for new TB drugs, *Bull World Health Organ 80*, 517.

14. Pessayre, D., and Mazel, P. (1976) Induction and inhibition of hepatic drug metabolizing enzymes by rifampin, *Biochemical pharmacology 25*, 943-949.

15. Desta, Z., Soukhova, N. V., and Flockhart, D. A. (2001) Inhibition of cytochrome P450 (CYP450) isoforms by isoniazid: potent inhibition of CYP2C19 and CYP3A, *Antimicrob Agents Chemother 45*, 382-392.

16. Nwaka, S., and Hudson, A. (2006) Innovative lead discovery strategies for tropical diseases, *Nature reviews 5*, 941-955.

17. Vasudeva, R., and Woods, B. (1997) Isoniazid-related hepatitis, *Dig Dis 15*, 357-367.

18. Burman, W. J., and Reves, R. R. (2001) Hepatotoxicity from rifampin plus pyrazinamide: lessons for policymakers and messages for care providers, *Am J Respir Crit Care Med 164*, 1112-1113.

19. Karakoc, E., Sahinalp, S. C., and Cherkasov, A. (2006) Comparative QSAR- and fragments distribution analysis of drugs, druglikes, metabolic substances, and antimicrobial compounds, *J Chem Inf Model 46*, 2167-2182.

20. Dobson, P. D., Patel, Y., and Kell, D. B. (2009) 'Metabolite-likeness' as a criterion in the design and selection of pharmaceutical drug libraries, *Drug Discov Today 14*, 31-40.

21. Yee, D., Valiquette, C., Pelletier, M., Parisien, I., Rocher, I., and Menzies, D. (2003) Incidence of serious side effects from first-line antituberculosis drugs among patients treated for active tuberculosis, *Am J Respir Crit Care Med 167*, 1472-1477.

22. Schaberg, T., Rebhan, K., and Lode, H. (1996) Risk factors for side-effects of isoniazid, rifampin and pyrazinamide in patients hospitalized for pulmonary tuberculosis, *Eur Respir J 9*, 2026-2030.

23. Budha, N. R., Lee, R. E., and Meibohm, B. (2008) Biopharmaceutics, pharmacokinetics and pharmacodynamics of antituberculosis drugs, *Curr Med Chem 15*, 809-825.

24. Preziosi, P. (2007) Isoniazid: metabolic aspects and toxicological correlates, *Curr Drug Metab 8*, 839-851.

25. (2008) Handbook of anti-tuberculosis agents. Introduction, *Tuberculosis (Edinb) 88*, 85-86.

26. Henderson, M. C., Siddens, L. K., Morre, J. T., Krueger, S. K., and Williams, D. E. (2008) Metabolism of the anti-tuberculosis drug ethionamide by mouse and human FMO1, FMO2 and FMO3 and mouse and human lung microsomes, *Toxicol Appl Pharmacol. 233*, 420-427.

27. Matsumoto, M., Hashizume, H., Tomishige, T., Kawasaki, M., Tsubouchi, H., Sasaki, H., Shimokawa, Y., and Komatsu, M. (2006) OPC-67683, a nitro-dihydro-imidazooxazole derivative with promising action against tuberculosis in vitro and in mice, *PLoS Med 3*, e466.

28. Daniel, W. A., Syrek, M., Haduch, A., and Wojcikowski, J. (2000) Pharmacokinetics and metabolism of thioridazine during co-administration of tricyclic antidepressants, *Br J Pharmacol 131*, 287-295.

29. Diacon, A. H., Pym, A., Grobusch, M., Patientia, R., Rustomjee, R., Page-Shipp, L., Pistorius, C., Krause, R., Bogoshi, M., Churchyard, G., Venter, A., Allen, J., Palomino, J. C., De Marez, T., van Heeswijk, R. P., Lounis, N., Meyvisch, P., Verbeeck, J., Parys, W.,

de Beule, K., Andries, K., and Mc Neeley, D. F. (2009) The diarylquinoline TMC207 for multidrug-resistant tuberculosis, *N Engl J Med 360*, 2397-2405.

30. Jia, L., Noker, P. E., Coward, L., Gorman, G. S., Protopopova, M., and Tomaszewski, J. E. (2006) Interspecies pharmacokinetics and in vitro metabolism of SQ109, *Br J Pharmacol 147*, 476-485.

31. Prasad, B., and Singh, S. (2009) In vitro and in vivo investigation of metabolic fate of rifampicin using an optimized sample preparation approach and modern tools of liquid chromatography-mass spectrometry, *J Pharm Biomed Anal 50*, 475-490.

32. Yamamoto, T., Moriwaki, Y., Takahashi, S., Hada, T., and Higashino, K. (1987) Study of the metabolism of pyrazinamide using a high-performance liquid chromatographic analysis of urine samples, *Anal Biochem 160*, 346-349.

33. Shen, C., Meng, Q., Zhang, G., and Hu, W. (2008) Rifampicin exacerbates isoniazid-induced toxicity in human but not in rat hepatocytes in tissue-like cultures, *British journal of pharmacology 153*, 784-791.

34. Kopanoff, D. E., Snider, D. E., Jr., and Caras, G. J. (1978) Isoniazid-related hepatitis: a U.S. Public Health Service cooperative surveillance study, *Am Rev Respir Dis 117*, 991-1001.

35. Nishimura, Y., Kurata, N., Sakurai, E., and Yasuhara, H. (2004) Inhibitory effect of antituberculosis drugs on human cytochrome P450-mediated activities, *J Pharmacol Sci 96*, 293-300.

36. Black, H. R., Griffith, R. S., and Peabody, A. M. (1966) Absorption, excretion and metabolism of capreomycin in normal and diseased states, *Ann N Y Acad Sci 135*, 974-982.

37. Pieroni, M., Tipparaju, S. K., Lun, S., Song, Y., Sturm, A. W., Bishai, W. R., and Kozikowski, A. P. Pyrido[1,2-a]benzimidazole-Based Agents Active Against Tuberculosis (TB), Multidrug-Resistant (MDR) TB and Extensively Drug-Resistant (XDR) TB, *ChemMedChem*.

38. Moise, P. A., Birmingham, M. C., and Schentag, J. J. (2000) Pharmacokinetics and metabolism of moxifloxacin, *Drugs Today (Barc) 36*, 229-244.

39. Feng, P. C., Fenselau, C. C., and Jacobson, R. R. (1981) Metabolism of clofazimine in leprosy patients, *Drug Metab Dispos*. *9*, 521-524.

40. Ferrero, J. L., Bopp, B. A., Marsh, K. C., Quigley, S. C., Johnson, M. J., Anderson, D. J., Lamm, J. E., Tolman, K. G., Sanders, S. W., Cavanaugh, J. H., and et al. (1990) Metabolism and disposition of clarithromycin in man, *Drug Metab Dispos*. *18*, 441-446.

41. Charalampous, K. D., Johnson, P. C., and Estevez, V. (1974) Absorption and excretion of thioridazine and mesoridazine in man, *Dis Nerv Syst 35*, 494-496.

42. M.C. Rouan, K. A., M. Vermeir , F. Cuyckens, G. Mannens, J. Verbeeck, A. Raoof. (2006) Preclinical Pharmacokinetics, Metabolism and Distribution of TMC207, a Novel Anti-Tuberculosis Agent, In *ISSX meeting*, Manchester, UK.

43. Jia, L., Tomaszewski, J. E., Hanrahan, C., Coward, L., Noker, P., Gorman, G., Nikonenko, B., and Protopopova, M. (2005) Pharmacodynamics and pharmacokinetics of SQ109, a new diamine-based antitubercular drug, *Br J Pharmacol 144*, 80-87.

44. Falzari, K., Zhu, Z., Pan, D., Liu, H., Hongmanee, P., and Franzblau, S. G. (2005) In vitro and in vivo activities of macrolide derivatives against *Mycobacterium tuberculosis*, *Antimicrob Agents Chemother 49*, 1447-1454.

45. Zhu, Z. J., Krasnykh, O., Pan, D., Petukhova, V., Yu, G., Liu, Y., Liu, H., Hong, S., Wang, Y., Wan, B., Liang, W., and Franzblau, S. G. (2008) Structure-activity relationships of macrolides against *Mycobacterium tuberculosis*, *Tuberculosis (Edinburgh, Scotland) 88 Suppl 1*, S49-63.

46. Byrne, S. T., Gu, P., Zhou, J., Denkin, S. M., Chong, C., Sullivan, D., Liu, J. O., and Zhang, Y. (2007) Pyrrolidine dithiocarbamate and diethyldithiocarbamate are active against growing and nongrowing persister Mycobacterium tuberculosis, *Antimicrob Agents Chemother 51*, 4495-4497.

47. Mao, J., Yuan, H., Wang, Y., Wan, B., Pak, D., He, R., and Franzblau, S. G. (2010) Synthesis and antituberculosis activity of novel mefloquine-isoxazole carboxylic esters as prodrugs, *Bioorg Med Chem Lett 20*, 1263-1268.

48. Guo, S., Song, Y., Huang, Q., Yuan, H., Wan, B., Wang, Y., He, R., Beconi, M. G., Franzblau, S. G., and Kozikowski, A. P. (2010) Identification, synthesis, and pharmacological evaluation of tetrahydroindazole based ligands as novel antituberculosis agents, *J Med Chem 53*, 649-659.

49. Di, L., Kerns, E. H., Hong, Y., Kleintop, T. A., McConnell, O. J., and Huryn, D. M. (2003) Optimization of a higher throughput microsomal stability screening assay for profiling drug discovery candidates, *J Biomol Screen. 8*, 453-462.

50. Zacharis, C. K., Theodoridis, G. A., Podgornik, A., and Voulgaropoulos, A. N. (2006) Incorporation of a monolithic column into sequential injection system for drug-protein binding studies, *J Chromatogr A 1121*, 46-54.

51. Obach, R. S., Walsky, R. L., Venkatakrishnan, K., Gaman, E. A., Houston, J. B., and Tremaine, L. M. (2006) The utility of in vitro cytochrome P450 inhibition data in the prediction of drug-drug interactions, *J Pharmacol Exp Ther. 316*, 336-348.

52. Walsky, R. L., and Obach, R. S. (2004) Validated assays for human cytochrome P450 activities, *Drug Metab Dispos*. *32*, 647-660.

53. Tompkins, L. M., and Wallace, A. D. (2007) Mechanisms of cytochrome P450 induction, *J Biochem Mol Toxicol 21*, 176-181.

54. Jana, S., and Paliwal, J. (2007) Molecular mechanisms of cytochrome p450 induction: potential for drug-drug interactions, *Curr Protein Pept Sci 8*, 619-628.

55. Hewitt, N. J., Lecluyse, E. L., and Ferguson, S. S. (2007) Induction of hepatic cytochrome P450 enzymes: methods, mechanisms, recommendations, and in vitro-in vivo correlations, *Xenobiotica 37*, 1196-1224.

56. Andersson, T. B. (2010) The application of HepRG cells in evaluation of cytochrome P450 induction properties of drug compounds, *Methods Mol Biol. 640*, 375-387.

57. Todd P. Primm, S. G. F. (2007) Recent advances in methodologies for the discovery of antimycobacterial drugs, *Curr Bioact Compd. 3*, 8.

58. Collins, L., and Franzblau, S. G. (1997) Microplate alamar blue assay versus BACTEC 460 system for high-throughput screening of compounds against Mycobacterium tuberculosis and Mycobacterium avium, *Antimicrob Agents Chemother 41*, 1004-1009.

59. Franzblau, S. G., Witzig, R. S., McLaughlin, J. C., Torres, P., Madico, G., Hernandez, A., Degnan, M. T., Cook, M. B., Quenzer, V. K., Ferguson, R. M., and Gilman, R. H. (1998) Rapid, low-technology MIC determination with clinical Mycobacterium tuberculosis isolates by using the microplate Alamar Blue assay, *J Clin Microbiol 36*, 362-366.

60. Arain, T. M., Resconi, A. E., Hickey, M. J., and Stover, C. K. (1996) Bioluminescence screening in vitro (Bio-Siv) assays for high-volume antimycobacterial drug discovery, *Antimicrob Agents Chemother 40*, 1536-1541.

61. Changsen, C., Franzblau, S. G., and Palittapongarnpim, P. (2003) Improved green fluorescent protein reporter gene-based microplate screening for antituberculosis compounds by utilizing an acetamidase promoter, *Antimicrob Agents Chemother 47*, 3682-3687.

62. Petty, R. D., Sutherland, L. A., Hunter, E. M., and Cree, I. A. (1995) Comparison of MTT and ATP-based assays for the measurement of viable cell number, *J Biolumin Chemilumin 10*, 29-34.

63. Di, L., Kerns, E. H., Gao, N., Li, S. Q., Huang, Y., Bourassa, J. L., and Huryn, D. M. (2004) Experimental design on single-time-point high-throughput microsomal stability assay, *J Pharm Sci 93*, 1537-1544.

64. Zhao, S. X., Forman, D., Wallace, N., Smith, B. J., Meyer, D., Kazolias, D., Gao, F., Soglia, J., Cole, M., and Nettleton, D. (2005) Simple strategies for reducing sample loads in in vitro metabolic stability high-throughput screening experiments: a comparison between traditional, two-time-point and pooled sample analyses, *J Pharm Sci 94*, 38-45.

65. Pang, K. S., and Rowland, M. (1977) Hepatic clearance of drugs. I. Theoretical considerations of a "well-stirred" model and a "parallel tube" model. Influence of hepatic blood flow, plasma and blood cell binding, and the hepatocellular enzymatic activity on hepatic drug clearance, *J Pharmacokinet Biopharm 5*, 625-653.

66. Rowland, M., Benet, L. Z., and Graham, G. G. (1973) Clearance concepts in pharmacokinetics, *J Pharmacokinet Biopharm 1*, 123-136.

67. Liu, L., and Pang, K. S. (2006) An integrated approach to model hepatic drug clearance, *Eur J Pharm Sci 29*, 215-230.

68. Kelly, J. G., and McDevitt, D. G. (1978) Plasma protein binding of propranolol and isoprenaline in hyperthyroidism and hypothyroidism, *Br J Clin Pharmacol 6*, 123-127.

69. Mace, K., Aguilar, F., Wang, J. S., Vautravers, P., Gomez-Lechon, M., Gonzalez, F. J., Groopman, J., Harris, C. C., and Pfeifer, A. M. (1997) Aflatoxin B1-induced DNA adduct formation and p53 mutations in CYP450-expressing human liver cell lines, *Carcinogenesis 18*, 1291-1297.

70. Chen, X., Song, B., Jiang, H., Yu, K., and Zhong, D. (2005) A liquid chromatography/tandem mass spectrometry method for the simultaneous quantification of isoniazid and ethambutol in human plasma, *Rapid Commun Mass Spectrom 19*, 2591-2596.

71. Song, S. H., Jun, S. H., Park, K. U., Yoon, Y., Lee, J. H., Kim, J. Q., and Song, J. (2007) Simultaneous determination of first-line anti-tuberculosis drugs and their major metabolic ratios by liquid chromatography/tandem mass spectrometry, *Rapid Commun Mass Spectrom 21*, 1331-1338.

72. U.S. Department of Health and Human Services, F. a. D. A. (2001) Guidance for Industry Bioanalytical Method Validation.

73. Cho, S. H., Warit, S., Wan, B., Hwang, C. H., Pauli, G. F., and Franzblau, S. G. (2007) Low-oxygen-recovery assay for high-throughput screening of compounds against nonreplicating Mycobacterium tuberculosis, *Antimicrob Agents Chemother. 51*, 1380-1385.

74. Mangalindan, G. C., Talaue, M. T., Cruz, L. J., Franzblau, S. G., Adams, L. B., Richardson, A. D., Ireland, C. M., and Concepcion, G. P. (2000) Agelasine F from a Philippine Agelas sp. sponge exhibits in vitro antituberculosis activity, *Planta Med 66*, 364-365.

75. Cantrell, C. L., Lu, T., Fronczek, F. R., Fischer, N. H., Adams, L. B., and Franzblau, S. G. (1996) Antimycobacterial cycloartanes from Borrichia frutescens, *J Nat Prod 59*, 1131-1136.

76. Luria, S. E., and Delbruck, M. (1943) Mutations of Bacteria from Virus Sensitivity to Virus Resistance, *Genetics 28*, 491-511.

77. Monks, T. J., Hanzlik, R. P., Cohen, G. M., Ross, D., and Graham, D. G. (1992) Quinone chemistry and toxicity, *Toxicol Appl Pharmacol 112*, 2-16.

78. Connolly, P. J., Westin, C. D., Loughney, D. A., and Minor, L. K. (1993) HMG-CoA reductase inhibitors: design, synthesis, and biological activity of tetrahydroindazole-substituted 3,5-dihydroxy-6-heptenoic acid sodium salts, *J Med Chem 36*, 3674-3685.

79. Gomez, L., Hack, M. D., Wu, J., Wiener, J. J., Venkatesan, H., Santillan, A., Jr., Pippel, D. J., Mani, N., Morrow, B. J., Motley, S. T., Shaw, K. J., Wolin, R., Grice, C. A., and Jones, T. K. (2007) Novel pyrazole derivatives as potent inhibitors of type II topoisomerases. Part 1: synthesis and preliminary SAR analysis, *Bioorg Med Chem Lett 17*, 2723-2727.

80. Wiener, J. J., Gomez, L., Venkatesan, H., Santillan, A., Jr., Allison, B. D., Schwarz, K. L., Shinde, S., Tang, L., Hack, M. D., Morrow, B. J., Motley, S. T., Goldschmidt, R. M., Shaw, K. J., Jones, T. K., and Grice, C. A. (2007) Tetrahydroindazole inhibitors of bacterial type II topoisomerases. Part 2: SAR development and potency against multidrug-resistant strains, *Bioorg Med Chem Lett 17*, 2718-2722.

81. Xia M, Z. T., Wang YF, Xing GW. Tetrahydroindole derivatives and tetrahydroindazole derivatives, and use thereof, In *PCT international patent application*.

82. Qian CG, C. X., Zhai HX. (2009) Tetrahydroindole and tetrahydroindazole as HSP90 inhibitors containing a zinc binding moiety, In *PCT International Patent Application* US.

83. Schiemann K, F. D., Zenke F. Tetrahydrobenzoisoxazole and tetrahydroindazole derivatives as modulators of the mitotic motor protein, Patent, WO2008080455.

84. Turpeinen, M., Tolonen, A., Chesne, C., Guillouzo, A., Uusitalo, J., and Pelkonen, O. (2009) Functional expression, inhibition and induction of CYP enzymes in HepaRG cells, *Toxicol In Vitro 23*, 748-753.

85. Kanebratt, K. P., and Andersson, T. B. (2008) HepaRG cells as an in vitro model for evaluation of cytochrome P450 induction in humans, *Drug Metab Dispos 36*, 137-145.

86. Josse, R., Aninat, C., Glaise, D., Dumont, J., Fessard, V., Morel, F., Poul, J. M., Guguen-Guillouzo, C., and Guillouzo, A. (2008) Long-term functional stability of human HepaRG hepatocytes and use for chronic toxicity and genotoxicity studies, *Drug Metab Dispos 36*, 1111-1118.

87. Aninat, C., Piton, A., Glaise, D., Le Charpentier, T., Langouet, S., Morel, F., Guguen-Guillouzo, C., and Guillouzo, A. (2006) Expression of cytochromes P450, conjugating enzymes and nuclear receptors in human hepatoma HepaRG cells, *Drug Metab Dispos 34*, 75-83.

88. Antherieu, S., Chesne, C., Li, R., Camus, S., Lahoz, A., Picazo, L., Turpeinen, M., Tolonen, A., Uusitalo, J., Guguen-Guillouzo, C., and Guillouzo, A. Stable expression, activity, and inducibility of cytochromes P450 in differentiated HepaRG cells, *Drug Metab Dispos*. *38*, 516-525.

89. Guillouzo, A., Corlu, A., Aninat, C., Glaise, D., Morel, F., and Guguen-Guillouzo, C. (2007) The human hepatoma HepaRG cells: a highly differentiated model for studies of liver metabolism and toxicity of xenobiotics, *Chem-Biol Interact 168*, 66-73.

90. Sumida, K., Igarashi, Y., Toritsuka, N., Matsushita, T., Abe-Tomizawa, K., Aoki, M., Urushidani, T., Yamada, H., and Ohno, Y. Effects of DMSO on gene expression in human and rat hepatocytes, *Hum Exp Toxicol*.

91. Choi, S., Sainz, B., Jr., Corcoran, P., Uprichard, S., and Jeong, H. (2009) Characterization of increased drug metabolism activity in dimethyl sulfoxide (DMSO)-treated Huh7 hepatoma cells, *Xenobiotic 39*, 205-217.

92. McGinnity, D. F., Zhang, G., Kenny, J. R., Hamilton, G. A., Otmani, S., Stams, K. R., Haney, S., Brassil, P., Stresser, D. M., and Riley, R. J. (2009) Evaluation of multiple in

vitro systems for assessment of CYP3A4 induction in drug discovery: human hepatocytes, pregnane X receptor reporter gene, and Fa2N-4 and HepaRG cells, *Drug metabolism and disposition: the biological fate of chemicals 37*, 1259-1268.

93. Rhodes, S. P., Otten, J. N., Hingorani, G. P., Hartley, D. P., and Franklin, R. B. Simultaneous assessment of cytochrome P450 activity in cultured human hepatocytes for compound-mediated induction of CYP3A4, CYP2B6, and CYP1A2, *J Pharmacol Toxicol Methods 63*, 223-226.

94. Di, L., Kerns, E. H., Hong, Y., Kleintop, T. A., McConnell, O. J., and Huryn, D. M. (2003) Optimization of a higher throughput microsomal stability screening assay for profiling drug discovery candidates, *J Biomol Screen 8*, 453-462.

95. Thompson, T. N. (2001) Optimization of metabolic stability as a goal of modern drug design, *Med Res Rev 21*, 412-449.

96. Fura, A., Shu, Y. Z., Zhu, M., Hanson, R. L., Roongta, V., and Humphreys, W. G. (2004) Discovering drugs through biological transformation: role of pharmacologically active metabolites in drug discovery, *J Med Chem 47*, 4339-4351.

97. Fura, A. (2006) Role of pharmacologically active metabolites in drug discovery and development, *Drug Discov Today 11*, 133-142.

98. Humphreys, W. G., and Unger, S. E. (2006) Safety assessment of drug metabolites: Characterization of chemically stable metabolites, *Chem Res Toxicol 19*, 1564-1569.

99. Van Heek, M., France, C. F., Compton, D. S., McLeod, R. L., Yumibe, N. P., Alton, K. B., Sybertz, E. J., and Davis, H. R., Jr. (1997) In vivo metabolism-based discovery of a potent cholesterol absorption inhibitor, SCH58235, in the rat and rhesus monkey through the identification of the active metabolites of SCH48461, *J Pharmacol Exp Ther 283*, 157-163.

100. Meng, Q., Luo, H., Liu, Y., Li, W., Zhang, W., and Yao, Q. (2009) Synthesis and evaluation of carbamate prodrugs of SQ109 as antituberculosis agents, *Bioorg Med Chem Lett 19*, 2808-2810.

101. (2008) Ll-3858, *Tuberculosis (Edinb) 88*, 126.

102. Barry, P. J., and O'Connor, T. M. (2007) Novel agents in the management of Mycobacterium tuberculosis disease, *Curr Med Chem 14*, 2000-2008.

103. Ginsberg, A. M., Laurenzi, M. W., Rouse, D. J., Whitney, K. D., and Spigelman, M. K. (2009) Assessment of the effects of the nitroimidazo-oxazine PA-824 on renal function in healthy subjects, *Antimicrob Agents Chemother 53*, 3726-3733.

104. Martins, M., Viveiros, M., Kristiansen, J. E., Molnar, J., and Amaral, L. (2007) The curative activity of thioridazine on mice infected with Mycobacterium tuberculosis, *In Vivo 21*, 771-775.

105. Giannarini, G., Tascini, C., and Selli, C. (2009) Prulifloxacin: clinical studies of a broad-spectrum quinolone agent, *Future Microbiol 4*, 13-24.

VITA

Yang Song

EDUCATION

2006-present Ph.D. candidate in Pharmacognosy, Institute for Tuberculosis Research, College of Pharmacy, UIC
2003-2006 M. S. in Pharmacognosy, Peking Union Medical College, China
1998-2003 B. S. in Pharmacology, China Pharmaceutical University

AWARDS

Chancellor's Graduate Research Fellowship, University of Illinois at Chicago, 2011
Paul Sang Award for Academic Excellence, College of Pharmacy, UIC, 2010

PRESENTATION

LC-MS-MS quantitative analysis and metabolism studies of current anti-tuberculosis drugs. ASMS Conference on Mass Spectrometry and Allied Topics, Hot Topics in LC-MS Instrumentation Trouble Shooting, Denver, Co, June,2011.

PUBLICATIONS

Yang Song, Valentina Petukhova, Zhaohai Zhu, Yongmao Sun, Xiangyang Lei, Nan Zhang, Richard B. van Breemen , Baojie Wan, Yuehong Wang, Larry L. Klein, Scott G. Franzblau. Synthesis, pharmacological, metabolism and pharmacokinetics evaluation of Oxazole derivatives as novel anti-tuberculosis agents. *J Med Chem* (Submitted)

Yang Song, Guo S, Richard B. van Breemen , Baojie Wan, Yuehong Wang, Scott G. Franzblau. Metabolism and pharmacokinetics guided discovery of tetrahydroindazole based ligands as novel antituberculosis agents. *Tuberculosis* (submitted)

Guo S, **Song Y**, Huang Q, Yuan H, Wan B, Wang Y, He R, Beconi MG, Franzblau SG, Kozikowski AP. Identification, synthesis, and pharmacological evaluation of tetrahydroindazole based ligands as novel antituberculosis agents. *J Med Chem*. 2010, 53(2):649-59.

Run-Lan Cai, Meng Li ,Su-Hua Xie, **Yang Song**, Zhong-Mei Zou, Chun-Yan Zhu, Yun Qi. Antihypertensive effect of total flavone extracts from Puerariae Radix. *J Ethnopharmacol,* 2011, 133, 177–183

Pieroni M, Tipparaju SK, Lun S, **Song Y**, Sturm AW, Bishai WR, Kozikowski AP. Pyrido[1,2-a]benzimidazole-Based Agents Active Against Tuberculosis (TB), Multidrug-Resistant (MDR) TB and Extensively Drug-Resistant (XDR) TB. *ChemMedChem*,2011, 6(2):334-42.